SANDIA REPORT
SAND2012-8193
Unlimited Release
Printed September 2012

International Benchmark Calculations of Field Experiments at the Asse Salt Mine

J. Guadalupe Argüello, John F. Holland, and James E. Bean

Prepared by
Sandia National Laboratories
Albuquerque, New Mexico 87185 and Livermore, California 94550

Sandia National Laboratories is a multi-program laboratory managed and operated by Sandia Corporation, a wholly owned subsidiary of Lockheed Martin Corporation, for the U.S. Department of Energy's National Nuclear Security Administration under contract DE-AC04-94AL85000.

Approved for public release; further dissemination unlimited.

Sandia National Laboratories

Issued by Sandia National Laboratories, operated for the United States Department of Energy by Sandia Corporation.

NOTICE: This report was prepared as an account of work sponsored by an agency of the United States Government. Neither the United States Government, nor any agency thereof, nor any of their employees, nor any of their contractors, subcontractors, or their employees, make any warranty, express or implied, or assume any legal liability or responsibility for the accuracy, completeness, or usefulness of any information, apparatus, product, or process disclosed, or represent that its use would not infringe privately owned rights. Reference herein to any specific commercial product, process, or service by trade name, trademark, manufacturer, or otherwise, does not necessarily constitute or imply its endorsement, recommendation, or favoring by the United States Government, any agency thereof, or any of their contractors or subcontractors. The views and opinions expressed herein do not necessarily state or reflect those of the United States Government, any agency thereof, or any of their contractors.

Printed in the United States of America. This report has been reproduced directly from the best available copy.

Available to DOE and DOE contractors from
U.S. Department of Energy
Office of Scientific and Technical Information
P.O. Box 62
Oak Ridge, TN 37831

Telephone: (865) 576-8401
Facsimile: (865) 576-5728
E-Mail: reports@adonis.osti.gov
Online ordering: http://www.osti.gov/bridge

Available to the public from
U.S. Department of Commerce
National Technical Information Service
5285 Port Royal Rd.
Springfield, VA 22161

Telephone: (800) 553-6847
Facsimile: (703) 605-6900
E-Mail: orders@ntis.fedworld.gov
Online order: http://www.ntis.gov/help/ordermethods.asp?loc=7-4-0#online

SAND2012-8193
Unlimited Release
Printed September 2012

International Benchmark Calculations of Field Experiments at the Asse Salt Mine

J. Guadalupe Argüello, John F. Holland, and James E. Bean
Computational Structural Mechanics & Applications
Sandia National Laboratories
P.O. Box 5800
Albuquerque, New Mexico 87185-MS0840

Abstract

The geomechanical modeling efforts and results for two benchmark calculations performed by Sandia National Laboratories (Sandia) under the third phase of an overall joint project investigating the behavior of advanced geomechanical constitutive models for rock salt are described and discussed in this report. Sandia recently joined the third phase of the project and is a contributing partner to this U.S./German joint effort entitled "Comparison of current constitutive models and simulation procedures on the basis of model calculations of the thermo-mechanical behavior and healing of rock salt". The geomechanical models, corresponding results, and their comparison to the in-situ data associated with both the so-called Isothermal Free Convergence (IFC) and Heated Free Convergence Probe (HFCP) borehole experiments conducted by the Netherlands Energy Research Foundation, ECN, at the Asse Mine (Germany) in the mid-80's are detailed herein.

ACKNOWLEDGMENTS

The authors wish to acknowledge Andrew J. Giesler for his efforts on the study, through the Summer Intern Program (SIP), during the summer of 2012. The authors also wish to acknowledge Jonathan S. Rath for his technical review and editorial contribution to this report. This work was supported by the U.S. Department of Energy (DOE), Office of Nuclear Energy (NE), Fuel Cycle Research and Development (FCR&D) Program.

CONTENTS

1. Introduction 9
   1.1. Project Objectives 9
   1.2. Previous Work (Phases I & II) 9
   1.3. Description & Goals of Phase III Effort 10

2. Description of the Experiments for the IFC & HFCP benchmarks 13
   2.1. General Description 13
   2.2. Isothermal Free Convergence (IFC) 13
   2.3. Heated Free Convergence Probe (HFCP) 15

3. IFC Benchmark Calculation 17
   3.1. Idealized Configuration 17
   3.2. SIERRA Mechanics 18
      3.2.1. Aria 18
      3.2.2. Adagio 18
   3.3. Multi-mechanism Deformation (MD) Creep Constitutive Model 19
   3.4. IFC Computational Model 21
      3.4.1. 5° Slice Model 21
      3.5.2. Quarter-Borehole Model 23
   3.5. Secondary Creep Parameter (A_2) Fitting 24
   3.6. Results 27
      3.6.1. 5° Slice Model 27
      3.6.2. Quarter-Borehole Model 30

4. HFCP Benchmark Calculation 33
   4.1. Idealized Configuration 33
      4.1.1 Mechanical Initial/Boundary Conditions 34
      4.1.2 Thermal Initial/Boundary Conditions 34
   4.2 Simulation Tools 35
   4.3 Temperature-Dependence in MD Model 35
   4.4 HFCP Computational Model 36
   4.5 Results 38
      4.5.1 Thermal 38
      4.52. Mechanical 44

5. Summary & Conclusions 73

6. References 75

Appendix A: Specification of Benchmark Problems 77

Appendix B: Description Asse Speisesalz Lab Data 85

Appendix C: RESPEC Memorandum on MD Creep Model Parameter Estimation 97

Distribution 117

FIGURES

Figure 1. Schematic Showing Locations of Experiments (Lowe & Knowles 1989) 14
Figure 2. Schematic of Heated Free Convergence Probe (HFCP) Make-Up (Lowe & Knowles 1989) 16
Figure 3. Idealized Configuration for IFC Benchmark Problem 17
Figure 4. "Baseline" Computational Mesh Used for 5° Slice Model (Overall Mesh on Top & Progressively Zoomed-In Views on Bottom) 22
Figure 5. Computational Mesh Used for Quarter-Borehole Model (Overall Mesh on Top & Progressively Zoomed-In Views on Bottom) 24
Figure 6. A2 Fitting of Radial Displacements - Isothermal Model 26
Figure 7. A2 Fitting Early Times - Isothermal Model 27
Figure 8. Comparison of Radial Displacement with Varying Model Thickness for the 5° Slice Model 28
Figure 9. Comparison of Radial Displacement with Varying Number of Elements Through-the-Thickness (TTT) for the 5° Slice Model 29
Figure 10. Comparison of Radial Displacement with Varying Number of Elements in the Radial Direction for the 5° Slice Model 30
Figure 11. Comparison of Radial Displacement Results from Baseline 5° Slice Model to those from Quarter-Borehole Model 31
Figure 12. Comparison of Quarter-Borehole Model Results with Measured Convergence Data and Results from the Baseline 5° Slice Model 32
Figure 13. Idealized Configuration for HFCP Benchmark Problem 33
Figure 14. Computational Mesh Used for HFCP Model (Overall Mesh on Left & Zoomed-In View on Right) 36
Figure 15. Central Portion of Computational Mesh Used for HFCP Model (Overall Mesh on Top & Progressively Zoomed-In Views Clockwise from There) 37
Figure 16. Time History Locations 39
Figure 17. Temperature Histories for Points A, B, C, L, and M 40
Figure 18. Temperature Histories for Points A, D, E, and F 41
Figure 19. Temperature Histories for Points G, H, J, and K 42
Figure 20. Horizontal Temperature Profiles 43
Figure 21. Vertical Temperature Profiles 44
Figure 22. Radial Displacement History at Heater Mid-Plane 45
Figure 23. Principal Stress Histories at Heater Mid-Plane (In Geomechanics Notation) 46
Figure 24. Equivalent Creep Strain History at Heater Mid-Plane 47
Figure 25. Creep Strain Rate History at Heater Mid-Plane 48
Figure 26. Horizontal Profiles of Radial Displacement at Heater Mid-Plane 49
Figure 27. Horizontal Profiles of Equivalent Creep Strain at Heater Mid-Plane 50
Figure 28. Horizontal Profiles of Creep Strain Rate at Heater Mid-Plane 51
Figure 29. Horizontal Profiles at Heater Mid-Plane of Principal Stress at 0 days (In Geomechanics Notation) 52
Figure 30. Horizontal Profiles at Heater Mid-Plane of Principal Stress at 1 days (In Geomechanics Notation) 53
Figure 31. Horizontal Profiles at Heater Mid-Plane of Principal Stress at 2 days (In Geomechanics Notation) 54

Figure 32. Horizontal Profiles at Heater Mid-Plane of Principal Stress at 4 days (In Geomechanics Notation) 55
Figure 33. Horizontal Profiles at Heater Mid-Plane of Principal Stress at 8 days (In Geomechanics Notation) 56
Figure 34. Horizontal Profiles at Heater Mid-Plane of Principal Stress at 15 days (In Geomechanics Notation) 57
Figure 35. Horizontal Profiles at Heater Mid-Plane of Principal Stress at 19 days (In Geomechanics Notation) 58
Figure 36. Horizontal Profiles at Heater Mid-Plane of Principal Stress at 22 days (In Geomechanics Notation) 59
Figure 37. Vertical Profiles at Borehole Wall of Radial Displacement 60
Figure 38. Vertical Profiles at Borehole Wall of EQCS 61
Figure 39. Vertical Profiles at Borehole Wall of Creep Strain Rate 62
Figure 40. Vertical Profiles at Borehole Wall of Principal Stress at 0 days (In Geomechanics Notation) 63
Figure 41. Vertical Profiles at Borehole Wall of Principal Stress at 1 days (In Geomechanics Notation) 64
Figure 42. Vertical Profiles at Borehole Wall of Principal Stress at 2 days (In Geomechanics Notation) 65
Figure 43. Vertical Profiles at Borehole Wall of Principal Stress at 4 days (In Geomechanics Notation) 66
Figure 44. Vertical Profiles at Borehole Wall of Principal Stress at 8 days (In Geomechanics Notation) 67
Figure 45. Vertical Profiles at Borehole Wall of Principal Stress at 15 days (In Geomechanics Notation) 68
Figure 46. Vertical Profiles at Borehole Wall of Principal Stress at 19 days (In Geomechanics Notation) 69
Figure 47. Vertical Profiles at Borehole Wall of Principal Stress at 22 days (In Geomechanics Notation) 70
Figure 48. Comparison of COSA II Displacement Profile with Calculated Displacements 71

TABLES

Table 1. Finite Element Mesh Gradation Used in Quarter-Borehole Model 23
Table 2. Asse “Speisesalz” Salt Properties Estimated from Laboratory Test Data for MD Creep Constitutive Model..... 24
Table 3. Specified Temperature at Borehole Wall for HFCP Benchmark Calculation 35
Table 4. Thermal Properties Used for Salt..... 38

1. INTRODUCTION

The Geomechanical modeling efforts and results for two benchmark calculations performed by Sandia National Laboratories (Sandia) under the third phase of an overall joint project investigating the behavior of advanced geomechanical constitutive models for rock salt are described and discussed in this report. Sandia recently joined the third phase of the project and is a contributing partner to this U.S./German joint effort entitled "Comparison of current constitutive models and simulation procedures on the basis of model calculations of the thermo-mechanical behavior and healing of rock salt". The bulk of the information below is a summary of the information contained and provided in the "Outline of the Joint Project" (Hampel 2010a).

1.1. Project Objectives

The first goal of the joint project is to check the ability of numerical modeling tools to correctly describe the relevant deformation phenomena in rock salt under various influences. Achieving this goal will lead to increased confidence in the results of numerical simulations regarding the secure storage of radioactive wastes in rock salt, thereby enhancing the acceptance of the results. These results may ultimately be used to make various assertions regarding both, the stability analysis of an underground repository in salt during the operating phase, and the long-term integrity of the geological barrier against the release of harmful substances into the biosphere in the post-operating phase. Among the numerical tools are constitutive models which are used in computer simulations for the description of the thermal, mechanical, and hydraulic behavior of the host rock under various influences and for the long-term prediction of this behavior into the future. A second goal of the project is to investigate and demonstrate the possibilities for further potential development and improvement of these constitutive models.

1.2. Previous Work (Phases I & II)

There have been two previous phases to the joint project in which the work involved only the efforts of various German partners without participation by the U.S. The first phase "Modeling of the mechanical behavior of rock salt: Comparison of current constitutive models and simulation procedures" was performed between 04-01-2004 and 11-30-2006 by five German project partners (Dr. Andreas Hampel, Consultant; the Institute for Geomechanics GmbH (IfG); Karlsruhe Institute of Technology; Leibniz University Hannover; Technical University Clausthal) and the BGR Hannover, Germany. In this first phase of the joint project, the different constitutive models of the partners were checked and compared in detail against both, semi-analytical back-calculations of various laboratory deformation tests and two-dimensional (2-D) simulations of simple, but typical, underground structures in rock salt.

In a subsequent second phase to the joint project "Comparison of current constitutive models and simulation procedures on the basis of 3-D model calculations of the mechanical long-term behavior of real underground structures in rock salt," the five German project partners (detailed above) performed the work between 08-01-2007 and 07-31-2010. Using their different constitutive models, in this phase of the project, the partners performed three-dimensional (3-D) benchmark calculations of an actual, heavily stressed, underground structure in the Angersdorf salt mine in Germany. Associated with the calculation of damage, the increase of permeability in

the excavation damaged zone (EDZ) was taken into account. For comparisons with the simulation results, in-situ fracture and permeability measurements were performed in the mine in order to characterize the actual states of stress and the porosity (dilatancy). In the simulations, the behavior of the underground structure was predicted up to 100 years after the excavation of the mine.

Both phases I & II of the joint project were focused on the disposal of non-heat-generating chemical-toxic wastes in rock salt. Therefore, only the mechanical behavior of the host rock at *ambient temperatures* was considered. However, the disposal of high-level radioactive waste in a rock salt repository is likely to heat the surrounding host rock to *high temperatures* (e.g., German disposal concept: up to 200° C). Thus the strong temperature dependence on the mechanical behavior of rock salt must be described reliably with constitutive models used in computer simulations of high-level radioactive waste repositories.

1.3. Description & Goals of Phase III Effort

The current and third phase of the joint project focuses on the disposal of heat-generating radioactive wastes in rock salt. In the past, extensive investigations of the thermo-mechanical behavior of rock salt have been performed and used for the development of constitutive models. However, a comparison of the different models and their theoretical physical bases remains incomplete and is thus the ultimate goal of this phase of the joint project. Therefore, in the third phase, coupled thermo-mechanical 3-D benchmark simulations will be performed in order to calculate and compare the evolution of stresses, strains, dilatancy (i.e., volumetric strain), damage, and permeability in rock salt under the influence of high evolving temperatures.

An important question that arises in the analysis and assessment of the disposal of radioactive wastes is the secure encapsulation of the harmful substances for very long times. To address this, the long-term reliability/effectiveness of the geological barrier (rock salt) has to be assured. Therefore, the healing of damaged salt in the EDZ, generated during excavation of the underground openings, and the associated decreased permeability (by several orders of magnitude) have to also be described reliably with the constitutive models in question. The modeling of healing and the associated permeability decrease have not been subjected to comparison among the constitutive models in the previous two phases of the joint project.

As a basis and for the comparisons with the simulation results, existing experimental data from laboratory tests and in-situ measurements will be used. For the thermo-mechanical behavior of rock salt, numerous laboratory results are available. However, the previous phases of the joint project have shown that for a detailed and in-depth inspection of the constitutive models, additional specific laboratory tests are required. In addition, the project participants agreed that the existing data base for healing is insufficient for such a comprehensive assessment of the constitutive models. Therefore, additional laboratory testing will be required in order to complete the comparison of the modeling of healing in rock salt.

In addition to the comparisons of the simulation results of the partners with each other and with data from laboratory tests, 3-D computer simulations of specific actual underground structures will be performed as a crucial check and comparison of: (1) the capabilities of the constitutive

models; (2) their applicability to the underground structures; and (3) their numerical behavior in computer simulations. Each partner will perform the jointly selected and defined simulation tasks with his respective constitutive model and computer program. For the evolution and extension of the EDZ and the healing of damage, the situation around a former bulkhead in the Asse Mine will be simulated. The simulation results of the partners will be compared with each other and with existing in-situ data from convergence and permeability measurements at the respective locations in the Asse Mine. However, prior to addressing damage and healing, the first two simulation tasks defined for this phase of the joint project deal with the thermo-mechanical behavior of rock salt. To address this, the previous in-situ isothermal and heater experiments of the Netherlands Energy Research Foundation, ECN, will be simulated. These experiments were fielded in a 300 m deep dry-drilled borehole in the Asse Mine (Germany). It is these two benchmark simulations, herein called the Isothermal Free Convergence (IFC) and Heated Free Convergence Probe (HFCP), of the borehole experiments in the Asse Mine that are the subject of this report.

2. DESCRIPTION OF THE EXPERIMENTS FOR THE IFC & HFCP BENCHMARKS

Two Netherlands Energy Research Foundation reports document and describe in detail the IFC (Doeven et al. 1983) and HFCP (Prij et al. 1986) benchmark experiments. In addition, a report on an earlier series of benchmark calculations, known as COSA II, provides clarifications relevant to these two experiments (Lowe & Knowles 1989). In this section we summarize the information available in these three documents for the experiments and provide only a brief description of the important features that are relevant to the numerical simulation of each.

2.1. General Description

As mentioned previously, the benchmarks reported in this document were based on experiments conducted in the late-70 to early-80's timeframe in the 300 m deep "Dutch borehole" in the Asse Mine in Germany. The Asse Mine is situated in a salt dome near Wolfenbüttel in Lower Saxony. A former potash and salt mine, it is has also been used for research and development work on the disposal of radioactive wastes in salt formations. Among the experiments performed in the mine was a series of borehole tests conducted by the Netherlands Energy Research Foundation ECN. These experiments were all performed in a single approximately 300 mm diameter borehole drilled from an open chamber at a level 750 m below the ground surface in the mine to a total depth of 1050 m below the ground surface. It is noted that the borehole was below the depth of the majority of the extensive mine workings.

The borehole was drilled at the end of 1979 and allowed to deform freely, as a consequence of salt creep-induced closure, without restraint or heating (i.e., so-called "isothermal free convergence") until June 1982. From June 1982 until mid-1985 several heated experiments were also performed at different depths in the borehole. Essentially two types of heated experiments were performed, the so-called heated pressure probe (HPP) and heated free convergence probe (HFCP) experiments. The two benchmarks described in this report are associated with the free convergence period (IFC) and one of the heated experiments (HFCP). A schematic illustration of the locations of these experiments is shown in Figure 1.

2.2. Isothermal Free Convergence (IFC)

After the drilling of the borehole and during the period of isothermal free convergence, according to Doeven et al. (1983), measurements were made in the borehole using a video camera and an inspection probe that were suspended inside the hole. The video camera was positioned such that it could view the set of instruments on the inspection probe. These included six displacement dial gages, a compass, two temperature gages, and two clocks. The dial gages were positioned circumferentially at 60 degree intervals around the center of the hole such that three measurements of the borehole diameter, at the same depth, could be made simultaneously. The measurements were made automatically, controlled by a timer, and stored on video tape.

The majority of the measurements were taken 8 m above the bottom of the borehole, at a depth of 292 m below the chamber floor. The measurements were taken every two or three days over a period of 834 days, starting shortly after the drilling of the borehole. Drilling of the borehole to

its final depth was completed on 12/18/1979, with convergence measurements apparently commencing on 12/21/1979 and ending in March 1982 when corrosion of the inspection system was deemed to have limited the reliability of the measurements. The convergence measurements at the 292 m depth are given in the benchmark specifications of Appendix A.

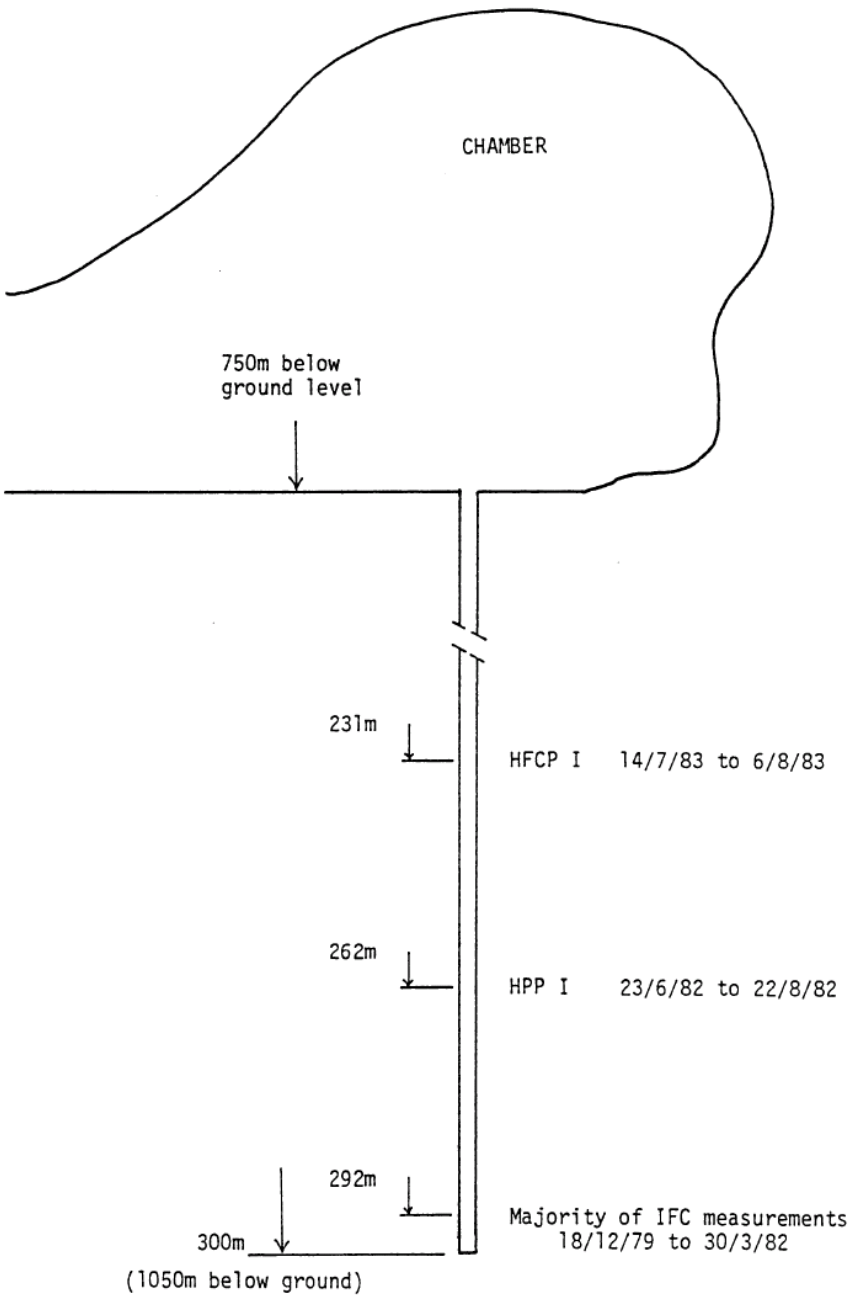

Figure 1. Schematic Showing Locations of Experiments (Lowe & Knowles 1989)

2.3. Heated Free Convergence Probe (HFCP)

According to Lowe & Knowles (1989), the probe for the heated free convergence probe (HFCP) experiment consisted of a straight tube of about 180 mm in diameter. The tube was divided into five sections, with the three middle sections being a total of 3 m in length and heated. The two end sections, of 1.5 m each, were included to avoid deformation of the salt over the ends of the heated sections. The heating was imparted by a wire wound in a spiral groove around the outside of the tube. Insulating shields were fitted above and below the heated sections in order to minimize the flow of heat in the axial direction. Of the five HFCP experiments conducted, the one chosen for the benchmark was the one conducted at the 231 m level during July and August of 1983. The HFCP arrangement is illustrated in Figure 2.

Instrumentation on the probe consisted of 30 swinging arm systems to measure the borehole convergence, along with about 50 thermocouples for temperature measurements. The swinging arm systems were distributed along the length and around the circumference of the probe, and the thermocouples were positioned to measure temperatures on the body of the probe and on the ends of the swinging arms where that contacted the salt.

The power output by the heater was 6000 Watts for 19 days, at which time the salt first contacted the probe. The heater was then switched-off to avoid trapping the probe in the hole, but measurements were continued for an additional 3 days.

The temperature measurements, however, were not as useful as originally envisioned because heat conduction in the swinging arms meant that the readings on the borehole wall were not representative of those in the salt. Furthermore, the temperature readings on the probe itself were lost due to a failure of the measuring system, and only estimates based on the other HFCP experiments are available. Nonetheless, reasonable estimated values of the temperature at the borehole wall are available (Lowe & Knowles 1989) and have been given in the benchmark specifications of Appendix A. It should be noted that the specifications of both the IFC and the HFCP benchmarks have been carefully detailed in Appendix A to provide the information necessary for the conduct of the numerical simulations.

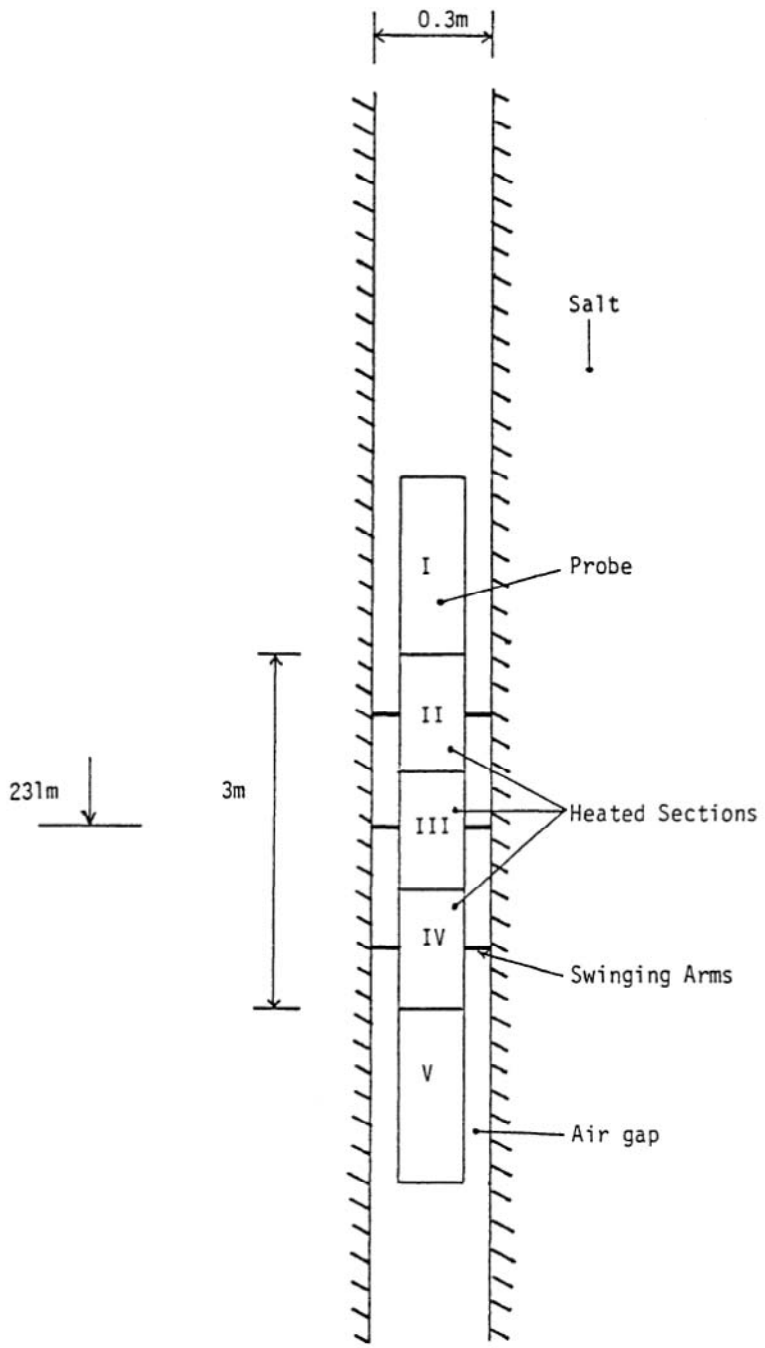

Figure 2. Schematic of Heated Free Convergence Probe (HFCP) Make-Up (Lowe & Knowles 1989)

3. IFC BENCHMARK CALCULATION

In this section, the development of the IFC Benchmark calculation is described. The idealized configuration used, the computer simulation tool that was exercised, the constitutive model for the salt that was used, the computational grid, the adjustment of parameters, and the final results from the numerical model are described and discussed.

3.1. Idealized Configuration

The numerical model representing the borehole closure of the Isothermal Free Convergence (IFC) benchmark problem was relatively straight forward. The majority of the isothermal measurements were taken in the borehole at a depth of 292 m from the open chamber floor (see Figure 1), so the convergence of the borehole at this elevation could be modeled with the equivalent of an "axisymmetric" borehole model. This is shown schematically in Figure 3, where the thickness of the model, t, can be arbitrary as long as it is relatively small. Per the specifications, the initial borehole diameter was 315 mm for an initial radius of 15.75 cm, and the far-field radial boundary was set to 20 m. The configuration was all-salt with an initial stress of 24 MPa (corresponding to the 292 m depth from the chamber floor), and the upper and lower boundaries of the slice were fixed against vertical displacement (as indicated by the rollers in the figure). The far-field radial boundary condition was set to an applied traction (i.e., a pressure, P) of 24 MPa.

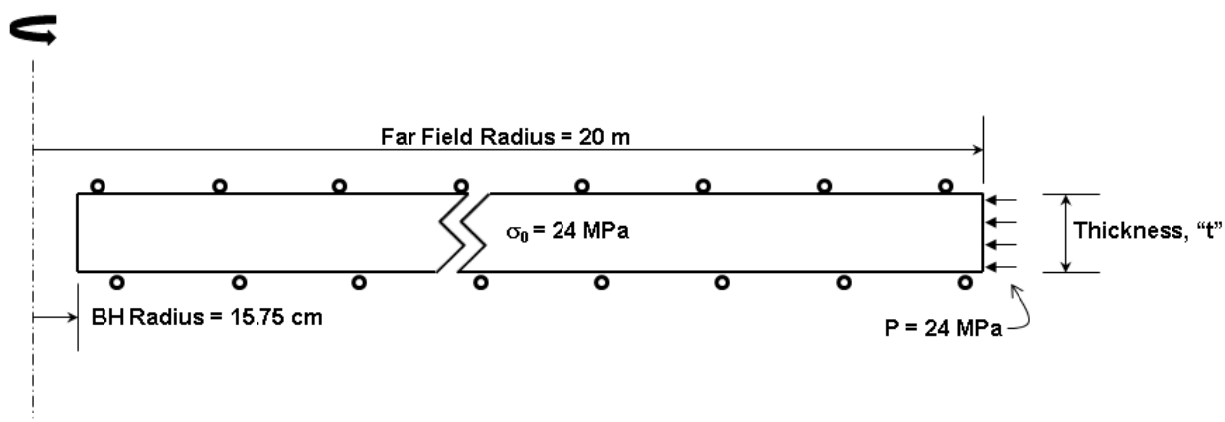

Figure 3. Idealized Configuration for IFC Benchmark Problem

Two major tools were needed for the numerical simulation of the problem defined in the idealized configuration, a numerical simulation tool that can be used to solve a numerical discretization of the physics encompassed by the idealized configuration and a constitutive model that accurately describes the behavior of the material comprising the idealized configuration. The next two subsections describe each of these tools, SIERRA Mechanics and the Multi-mechanism Deformation (MD) Creep Model for salt.

3.2. SIERRA Mechanics

The SIERRA Mechanics suite of codes has been developed by Sandia National Laboratories (Edwards & Stewart 2001) and has been exercised and undergone a preliminary evaluation for applicability to this class of problems (Stone et al. 2010, Argüello & Rath 2012). The development of the SIERRA Mechanics code suite has been funded by the USA Department of Energy (DOE) Advanced Simulation and Computing (ASC) program for more than ten years. The goal is the development of massively parallel multi-physics capabilities to support the Sandia engineering sciences mission. SIERRA Mechanics was designed and developed from its inception to run on the latest and most sophisticated, massively parallel computing hardware. It has the capability to span the hardware range from a single workstation to computer systems with thousands of processors. The foundation of SIERRA Mechanics is the SIERRA toolkit, which provides finite element application-code services such as: mesh and field data management, both parallel and distributed; transfer operators for mapping field variables from one mechanics application to another; a solution controller for code coupling; and included third party libraries (e.g., solver libraries, communications package, etc.). The SIERRA Mechanics code suite is comprised of application codes that address specific physics regimes. The two SIERRA Mechanics physics code modules that are used as the launching point for an eventual fully integrated Thermal-Hydrological-Mechanical-Chemical (THMC) coupling in a repository setting, with adaptive solution control, are Aria (Notz et al. 2007) and Adagio (SIERRA Solid Mechanics Team 2010).

3.2.1. Aria

The physics currently supported by Aria include: the incompressible Navier-Stokes equations, energy transport equation, and species transport equations, as well as generalized scalar, vector, and tensor transport equations. A multi-phase porous flow capability has been recently added to Aria. Aria also has basic geochemistry functionality available through embedded chemistry packages.

3.2.2. Adagio

The mechanics portion of the THMC coupling is handled by Adagio. It solves for the quasi-static, large deformation, large strain behavior of nonlinear solids in three dimensions. Adagio has some discriminating Sandia-developed technology for solving solid mechanics problems that involves matrix-free iterative solution algorithms for efficient solution of extremely large and highly nonlinear problems. This technology is well-suited for scalable implementation on massively parallel computers.

The THMC coupling is done through a solution controller within SIERRA Mechanics called Arpeggio. For the IFC benchmark problem, only the solid mechanics module Adagio was needed for the simulation. In addition, the MD creep constitutive model that is incorporated into the Library of Advanced Materials for Engineering [LAME] (Scherzinger et al. 2007), a third-party library of material models, was also used for modeling the rock salt mechanical behavior. It is accessible by SIERRA Mechanics.

3.3. Multi-mechanism Deformation (MD) Creep Constitutive Model

The Multi-mechanism Deformation (MD) creep model originally developed by Munson & Dawson (1979, 1982, & 1984) and later extended by Munson et al. (1989) was used in these analyses. The MD model mathematically represents the primary and secondary creep behavior of salt due to dislocations under relatively low temperatures (compared to the melting temperature) and low to moderate stresses which are typical of mining and storage cavern operations. Three micromechanical mechanisms, determined from deformation mechanism maps (Munson 1979), are represented in the model: a dislocation climb mechanism active at high temperatures and low stresses; an empirically observed mechanism active at low temperatures and low stresses; and a dislocation slip mechanism active at high stresses. These creep mechanisms are assumed to act such that the total steady state creep rate can be written as the sum of the individual mechanism strain rates.

$$\dot{\varepsilon}_s = \sum_{i=1}^{3} \dot{\varepsilon}_{s_i} \tag{1}$$

The influence of temperature on the creep strain rate is included through an Arrhenius term. The steady state creep strain rates for the first and second mechanisms are identical in form and are implemented using a power law model while the third mechanism (dislocation slip) is represented using an Eyring type model.

$$\dot{\varepsilon}_{s_1} = A_1 \left(\frac{\sigma_{eq}}{G} \right)^{n_1} e^{\frac{-Q_1}{RT}} \tag{2}$$

$$\dot{\varepsilon}_{s_2} = A_2 \left(\frac{\sigma_{eq}}{G} \right)^{n_2} e^{\frac{-Q_2}{RT}} \tag{3}$$

$$\dot{\varepsilon}_{s_3} = \left(B_1 e^{-Q_1/RT} + B_2 e^{-Q_2/RT} \right) \sinh\left[q \left(\frac{\sigma_{eq} - \sigma_0}{G} \right) \right] \times H\left(\sigma_{eq} - \sigma_0 \right) \tag{4}$$

where σ_{eq} is the equivalent stress; T is the temperature (absolute); G is the shear modulus; A_1, A_2, B_1, & B_2 are structure factors; Q_1 & Q_2 are activation energies; R is the universal gas constant; q is the activation volume, σ_0 is the stress limit; and H is the Heaviside function with argument ($\sigma_{eq} - \sigma_0$).

From the definition of the Heaviside function, the third mechanism is only active when the equivalent stress exceeds the specified value of the stress limit σ_0. The equivalent stress appearing in these equations is taken to be the Tresca stress (Munson, et al. 1989). The Tresca stress can be written in terms of the maximum and minimum principal stresses σ_1 and σ_3 respectively ($\sigma_1 \geq \sigma_2 \geq \sigma_3$). Alternatively, the Tresca stress may be written as a function of the Lode angle, ψ, and the second invariant, J_2, of the deviatoric stress tensor, **s** (with components s_{ij}).

$$\sigma_{eq} = \sigma_1 - \sigma_3 = 2\cos\psi\sqrt{J_2} \tag{5}$$

The Lode angle is dependent on both the second and third invariant, J_3, of the deviatoric stress tensor, s_{ij}.

$$\psi = \frac{1}{3}\sin^{-1}\left[\frac{-3\sqrt{3}J_3}{2\left(J_2\right)^{3/2}}\right] \qquad -\frac{\pi}{6} \le \psi \le \frac{\pi}{6} \tag{6}$$

$$J_2 = \frac{1}{2}s_{ij}s_{ji} \tag{7}$$

$$J_3 = \frac{1}{3}s_{ij}s_{jk}s_{ki} \tag{8}$$

The kinetic equation used in the MD model is given by Equation 9 where F is a function which accounts for transient creep effects and $\dot{\varepsilon}_s$ is the steady state dislocation creep strain rate defined by Equation 1.

$$\dot{\varepsilon}_{eq} = F\dot{\varepsilon}_s \tag{9}$$

The function F has three branches: a work hardening branch (F > 1), an equilibrium branch (F = 1), and a recovery branch (F < 1).

$$F = \begin{cases} \exp\left[\Delta\left(1-\frac{\zeta}{\varepsilon_t^f}\right)^2\right] & \zeta < \varepsilon_t^f \text{ Transient Branch} \\ 1 & \zeta = \varepsilon_t^f \text{ Equilibrium Branch} \\ \exp\left[-\delta\left(1-\frac{\zeta}{\varepsilon_t^f}\right)^2\right] & \zeta > \varepsilon_t^f \text{ Recovery Branch} \end{cases} \tag{10}$$

The choice of the particular branch depends on the transient strain limit ε_t^f and the internal variable ζ. The transient strain limit is defined by Equation 11 where K_0, c, and m are material parameters, T is the absolute temperature, and G is the shear modulus.

$$\varepsilon_t^f = K_0 e^{cT}\left(\frac{\sigma_{eq}}{G}\right)^m \tag{11}$$

The internal variable, ζ, appearing in the calculation of the function, F, is obtained by integration of the evolution equation

$$\dot{\zeta} = \left(F-1\right)\dot{\varepsilon}_s \tag{12}$$

Δ and δ, appearing in Equation 10, are the work hardening and recovery parameters and are given by Equations 13 and 14 respectively. In these equations α, β, α_r, and β_r are material parameters. Typically the recovery parameter, δ, is taken to be constant (i.e. $\delta=\alpha_r$).

$$\Delta = \alpha + \beta\log\left(\frac{\sigma_{eq}}{G}\right) \tag{13}$$

$$\delta = \alpha_r + \beta_r \log\left(\frac{\sigma_{eq}}{G}\right) \tag{14}$$

If only the steady state creep response is of interest then the transient and recovery branches may be effectively turned off by setting $\alpha=0$, $\beta=0$, $\alpha_r=0$, $\beta_r=0$. The MD model can be further simplified to that of a power law creep model by setting the appropriate structure factors and activation energies to zero.

Including the bulk and shear moduli, which are both assumed constant, there are a total of 19 parameters used to define the MD model.

The MD model parameters for ASSE Speisesalz used in this analysis (and the subsequent HFCP benchmark problem) came from a fit to the model originally performed on a series of laboratory test data provided by Hampel (2010b), as described in Appendix B. The parameter estimation from the data for the MD creep model was performed by RESPEC Engineering (DeVries 2011) and is documented in a RESPEC memorandum, included as Appendix C. This fit to the laboratory data was subsequently adjusted, as will be described below, by changing only the secondary creep parameter to mimic the in situ IFC data. Once the secondary creep parameter was adjusted there were no other changes permitted and the set was then used for the subsequent HFCP benchmark calculation also.

3.4. IFC Computational Model

The idealized configuration of Figure 3 can be converted into a computational model in various ways depending on the computational tools that are available. Consequently, it should be noted that the SIERRA Mechanics toolset, described above, offers only a 3D capability (i.e., there is not a true 2-D "axisymmetric" capability in the Adagio code used for this portion of the study, as may be available in other tools). Consequently, for the IFC borehole calculations reported herein, the axisymmetric model is approximated by taking a circumferential slice to generate its 3D equivalent. The front and back circumferential faces of the resulting 3D model are then constrained against horizontal movement in that circumferential direction (i.e., no circumferential movement normal to the face). Two different computational models of the configuration were used in this study, a 5° circumferential slice (hereafter called the "5° Slice Model") and a 90° circumferential slice (hereafter called the "Quarter-Borehole Model"). The two models were developed independently by two different analysts who exercised them in a relatively independent manner with the aim of providing a cross-check of the overall results obtained for the IFC benchmark problem.

3.4.1. 5° Slice Model

The 5° Slice Model was primarily used for mesh refinement studies that investigated the effects on the borehole closure results with a varying thickness of the slice, the number of elements included through the thickness of the slice, and the number of elements included in the radial direction of the slice. Figure 4 shows the "baseline" computational mesh that was used as the starting point and was designed by an experienced analyst familiar with the level of refinement needed to perform creeping borehole problems. Hence it includes a high-level of refinement within approximately 1.5 borehole diameters of the centerline to be able to accurately capture the

large stress/strain gradients in this problem that are found in the immediate vicinity of the borehole. It is graded quite fine near the borehole wall and coarsens as it approaches the far-field radial boundary. A thickness of 0.05 m (i.e., the vertical direction shown in Figure 4) and a total of 160 uniform strain elements with 644 nodes were used for this baseline model. Using this same radial gradation, thicknesses of 0.05 (baseline), 0.1, 0.5, and 1.0 m (modeled with a single element through the thickness [TTT]) were used to investigate the sensitivity of the response to the thickness of the model. The different thicknesses were then subsequently divided into 2, 4, 20, and 40 elements uniformly distributed TTT, respectively, to investigate the sensitivity of the response to the refinement through the thickness. To assess the sensitivity of the results to refinement in the radial direction, in a sensible and systematic manner, the elements were distributed uniformly in the radial direction for this case. Values of 160, 320, 640, 1280, and 10240 uniformly spaced elements in the radial direction were used. This slice computational model was sufficiently small to permit quick turn-around time for each analysis and an efficient assessment by the analyst of the numerous runs associated with this refinement study. In all of the 5° Slice Model simulation variants, a single element in the circumferential direction was used.

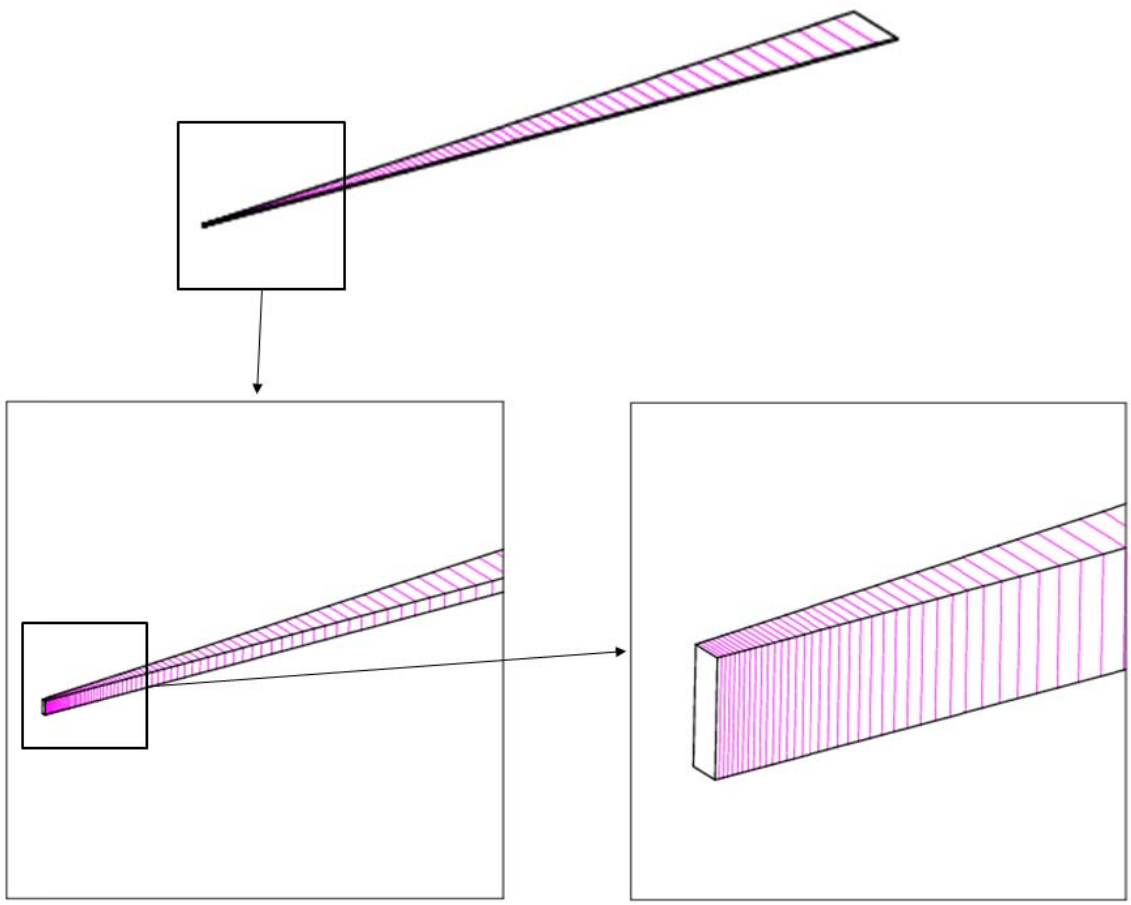

Figure 4. "Baseline" Computational Mesh Used for 5° Slice Model (Overall Mesh on Top & Progressively Zoomed-In Views on Bottom)

3.5.2. Quarter-Borehole Model

The Quarter-Borehole Model was used for calculation of the "official" benchmark results. The results from the Quarter-Borehole Model were compared against those from the 5° Slice Model to ensure consistency with that model and to further ensure the solution from the Quarter-Borehole model had numerically converged. The Quarter-Borehole Model included one element through the thickness (shown in Figure 5 as the vertical direction) and was 0.01 m thick. Figure 5 shows the computational mesh that was used in the Quarter-Borehole Model. It consisted of 3956 uniform strain elements and 8176 nodes. This mesh was also designed by an experienced analyst familiar with the level of refinement needed to perform creeping borehole problems. It, again, includes a high-level of refinement within approximately 2 borehole diameters of the centerline to be able to accurately capture the large stress/strain gradients in this problem that are found in the immediate vicinity of the borehole. It is graded quite fine near the borehole wall to yield approximately cube-shaped elements near the borehole wall and coarsens as it approaches the far-field radial boundary. As can be seen in Figure 5, the mesh density is relatively uniformly distributed close to the borehole in the radial and circumferential directions to a distance of approximately 2 borehole diameters from the centerline but coarsens from that distance out to the far field radial boundary using a so-called "paving" algorithm in Sandia's finite element mesh generation program, CUBIT (CUBIT, 2012). The element sizes, as a function of distance from the borehole wall, are list in Table 1.

Table 1. Finite Element Mesh Gradation Used in Quarter-Borehole Model

Distance Range (meters)	Element Size (meters)
0.0 – 0.25	0.01
0.25 – 1.0	0.05
1.0 – 2.0	0.10
2.0 – 5.0	0.30
5.0 - 10.0	0.60
10.0 – 15.0	1.0
>15.0	1.2

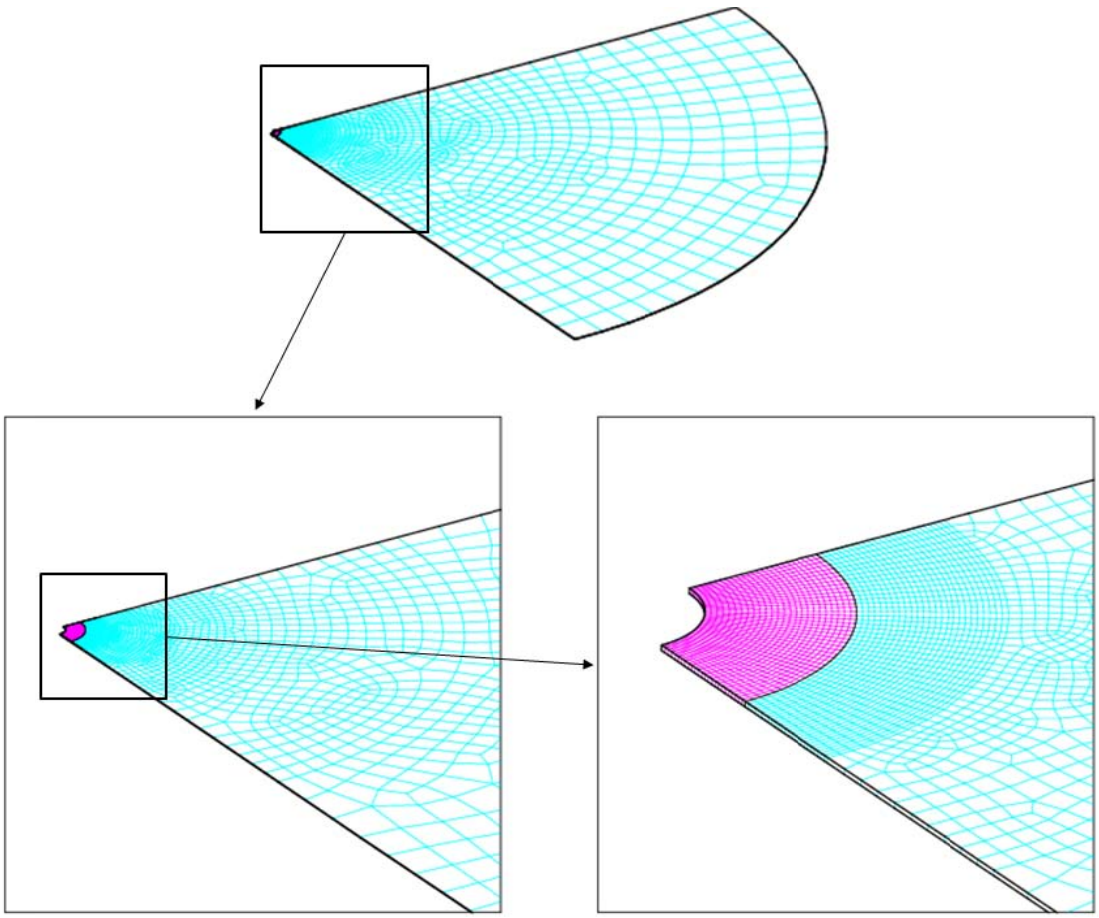

Figure 5. Computational Mesh Used for Quarter-Borehole Model (Overall Mesh on Top & Progressively Zoomed-In Views on Bottom)

3.5. Secondary Creep Parameter (A_2) Fitting

As previously discussed, the salt behavior is modeled using the MD Creep constitutive model. The various parameters for the MD model, as originally estimated by RESPEC (Appendix C) but in the Sandia implementation notation, are listed in Table 2 below. The latter six parameters (i.e., algorithmic parameters) in this table are specific to the Sandia National Laboratories' numerical implementation of the model (mainly related to the numerical integration) within SIERRA Mechanics.

Table 2. Asse "Speisesalz" Salt Properties Estimated from Laboratory Test Data for MD Creep Constitutive Model

Parameter	Value	Units
Shear Modulus	9.850e+9	Pa
Poisson's Ratio	0.27	---

A1	5.741e+17	sec^{-1}
Q1/R	12,589	Kelvin
N1	5.5	---
B1	1.180e+05	sec^{-1}
A2	2.353e+11 (11.765e+11)	sec^{-1}
Q2/R	5035.5	Kelvin
N2	5.0	---
B2	5.881e-04	sec^{-1}
SIG0	20.57e+06	Pa
QLC	4,450	---
M	3.0	---
K0	925.0	---
C	2.706e-02	$Kelvin^{-1}$
ALPHA	-12.293	---
BETA	-8.518	---
DELTAC	0.58	---
AMULT	0.85	---
ANGLE	0.1	---
EPSTOL	0.005	---
GRWFAC	1.05	---
SHKFAC	1.0	---
ITYPE	0.0	---

As expected, using the laboratory-test estimated parameters under-predicted the field-scale measured convergence data from the IFC test, and it was necessary to further adjust the secondary creep parameter, A2, to obtain a reasonable agreement with the test data. This was allowed by the specifications of Appendix A, as long as no further changes were made to the parameters when performing simulations of the HFCP test that will be described in the next section.

The fitting of the A2 parameter required both a temporal, as well as, a scalar fitting to match the measured borehole radial displacement values. Figure 6 shows the radial displacements computed with ADAGIO using the MD Creep material model for different values of the secondary creep parameter, A2, and initial time step size choices. Figure 7 shows the same data,

but at earlier times. In all the calculations the "elastic" (along with some of the very early transient) response of the salt due to excavation is subtracted from the subsequent displacement values. In the MD model, significant efforts are undertaken to estimate virgin material parameters (Munson et al. 1989). Although not completely clear from the test report of Doeven et al. (1983), it appears that the first measurement in the borehole was not taken until a day or two after the excavation was completed. Hence there is some amount of "excavation strain" that is unaccounted-for in the measurements. For this reason, we chose to subtract the first 24 hours of computed displacement from the subsequent displacement values in the fitting process.

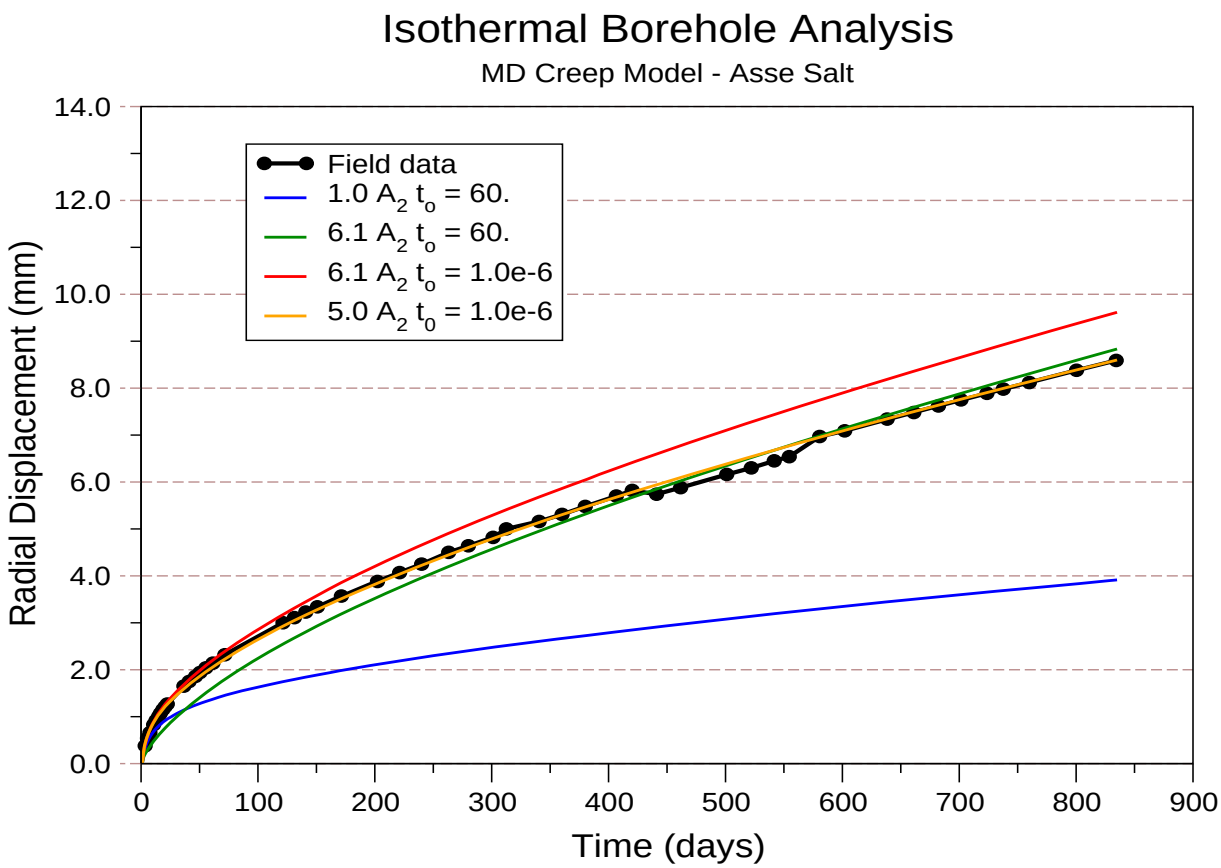

Figure 6. A2 Fitting of Radial Displacements - Isothermal Model

As seen in the Figures 6-7, increasing model parameter A2 by a factor of 6.1 matched radial displacements at late times reasonably well, but poorly at early times. Decreasing the initial time step at which the calculation was started from 60 seconds to 1.0e-6 seconds improved the fit at early times, but the predictions diverged at later times. Decreasing the scaling factor to 5.0 provided the best fit over the entire time period with an initial time step of 1.0e-6 seconds. Consequently, the value of the secondary creep parameter, A2, that was used for all calculations hereafter is five times the value shown in Table 2, or 5*(2.353e+11 sec^{-1}) = 11.765e+11 sec^{-1} (identified in parentheses and in Red colored typeset in Table 2).

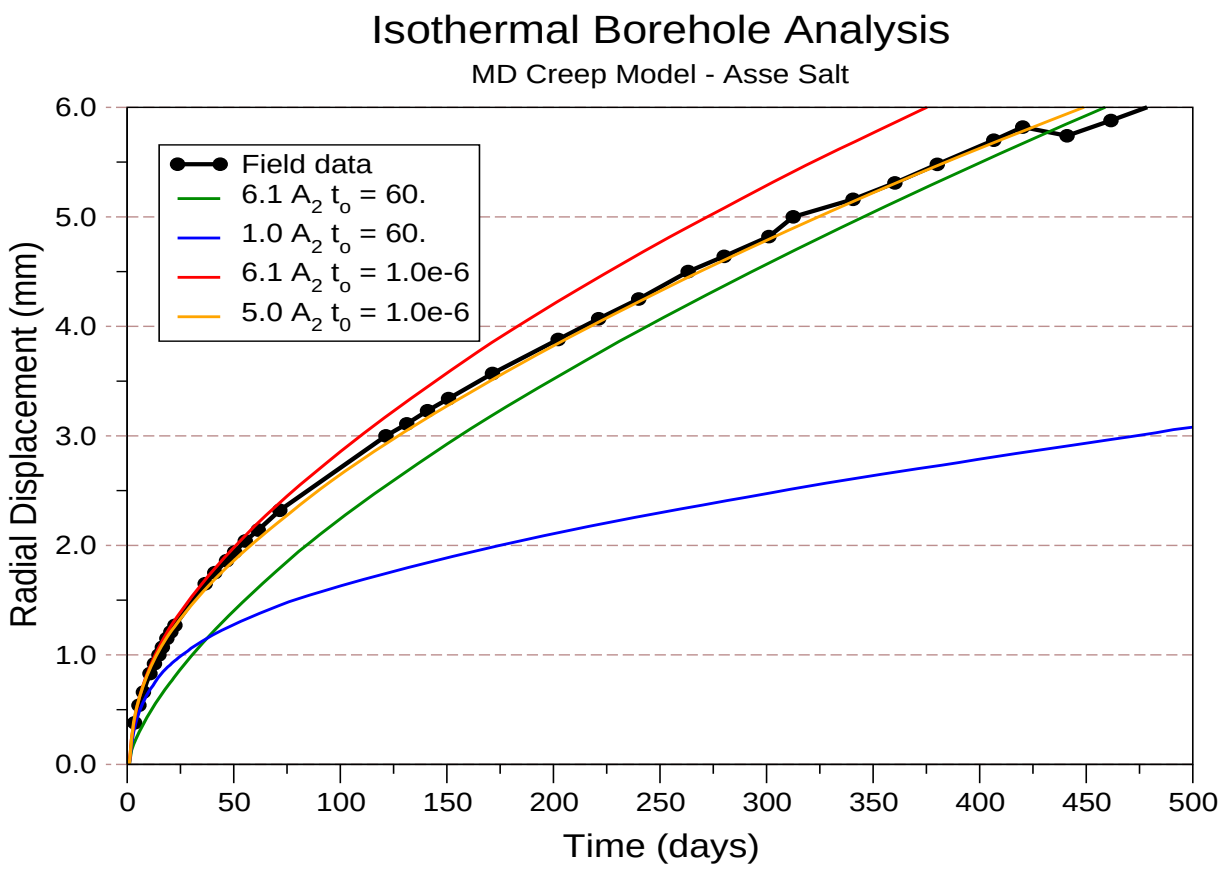

Figure 7. A2 Fitting Early Times - Isothermal Model

3.6. Results

Results of the two models used in the IFC benchmark calculations are provided herein. Results from the 5° Slice Model are presented first and describe the sensitivities of the results to the various parameters that were varied for the mesh refinement studies. The Quarter-Borehole Model results are then presented as the final results of the IFC benchmark calculation and their consistency with the numerically converged 5° Slice Model is demonstrated.

3.6.1. 5° Slice Model

Figure 8 shows the numerical model results of radial displacement history and the model's sensitivity to grid thickness (i.e., the vertical dimension). As mentioned previously, thicknesses of 0.05, 0.1, 0.5, and 1.0 m were evaluated. In each of these models, a single element TTT was used. This figure shows that the model is practically insensitive to the thickness dimension.

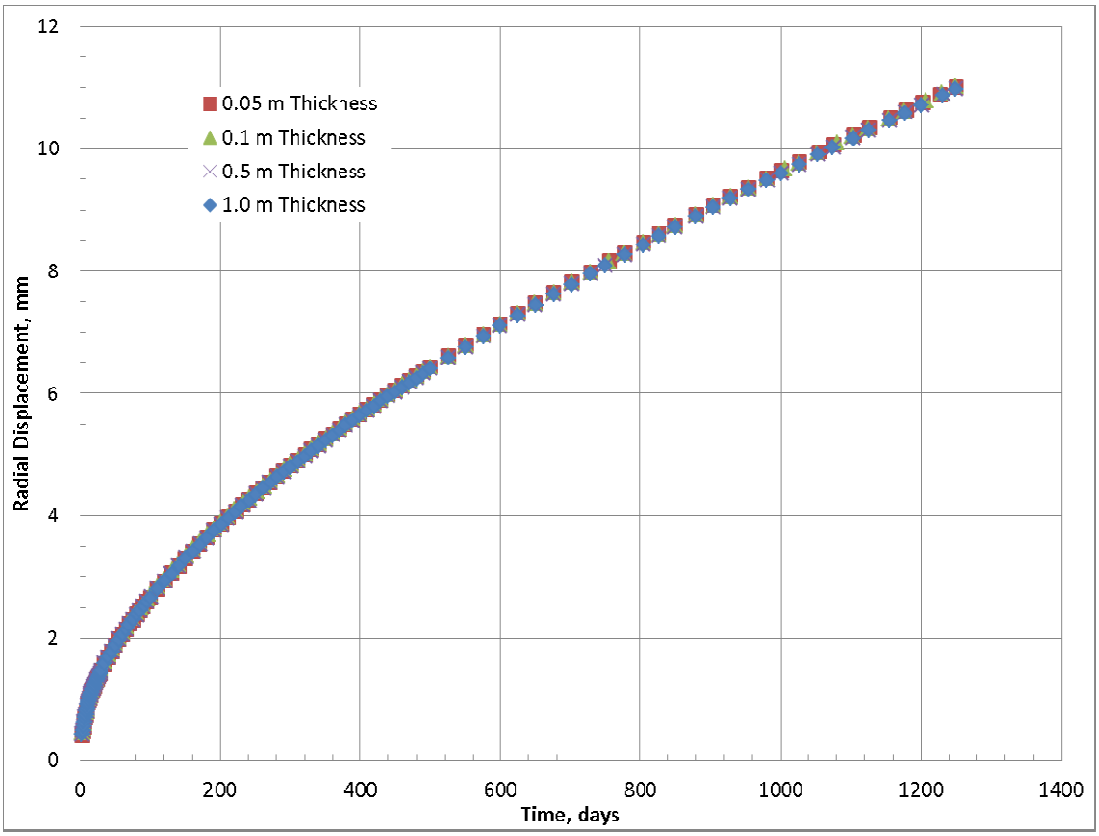

Figure 8. Comparison of Radial Displacement with Varying Model Thickness for the 5° Slice Model

Shown in Figure 9 are the numerical results depicting the sensitivity to mesh refinement through the thickness of the model. For this assessment, each of the modeled thicknesses of Figure 8 was sub-divided into 2, 4, 20, and 40 uniformly distributed elements through the thickness (TTT), respectively. This figure shows that there is, for all practical purposes, an almost imperceptible sensitivity of the radial displacement to an increased level of refinement in the thickness direction.

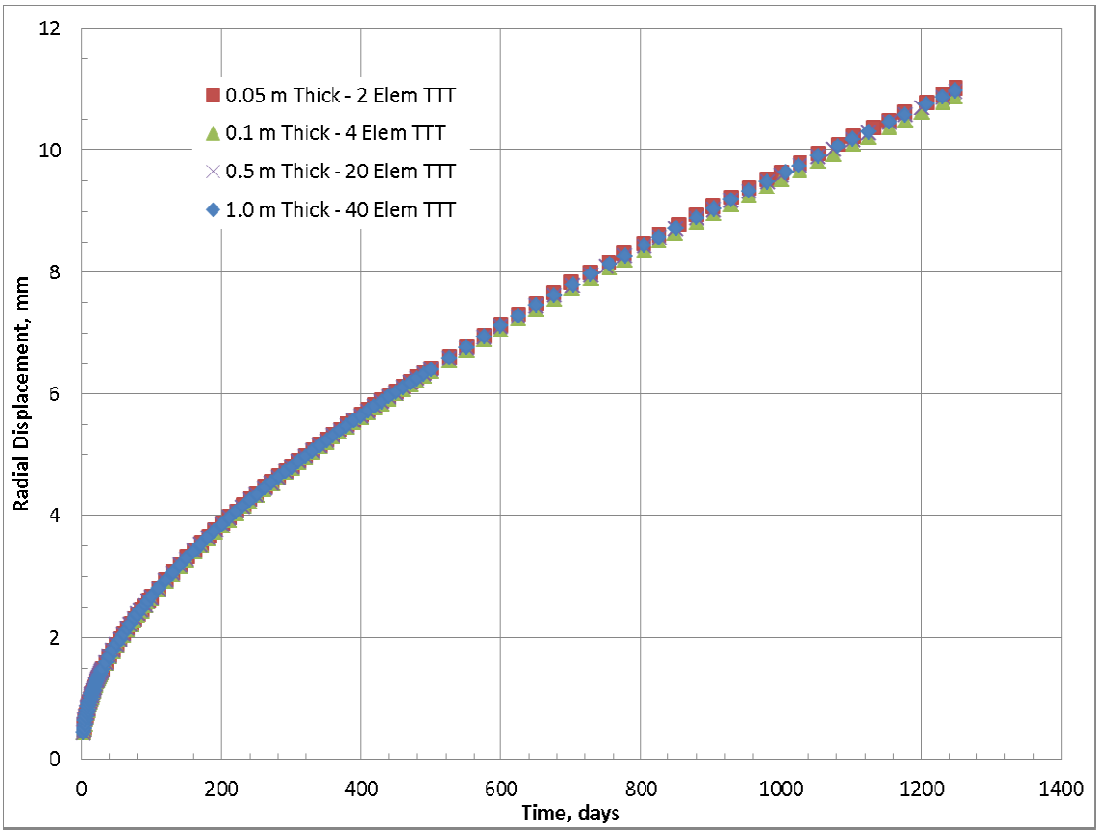

Figure 9. Comparison of Radial Displacement with Varying Number of Elements Through-the-Thickness (TTT) for the 5° Slice Model

Figure 10 shows the numerical results demonstrating the sensitivity of the model to mesh refinement in the radial direction. For this assessment the elements in the radial direction were distributed uniformly in the radial direction in order to methodically refine the mesh in a manner that made sense. Because the baseline model used 160 elements (with refinement skewed toward the borehole), this portion of the mesh refinement study started with the same 160 elements but now uniformly distributed in the radial direction. This number of elements was then doubled multiple times to 320, 640, and 1280 elements uniformly distributed in the radial direction. The figure shows that for each doubling of the elements, up to 1280, the radial displacement of the borehole increased, but incrementally less with each doubling, indicating that a numerically convergent solution was being approached. A final value of 10240 elements uniformly distributed in the radial direction (which was eight times the 1280 value) was then used to obtain the radial displacement. The figure shows that the 10240-element curve (in red) essentially overlays the 1280-element curve (in orange), indicating that indeed a numerically converged solution had been reached. The radial displacement response from the baseline model is also plotted in this figure to show that it also corresponds to the numerically converged solution. From this, there is a high degree of confidence that the baseline 5° Slice Model is providing accurate numerically converged results.

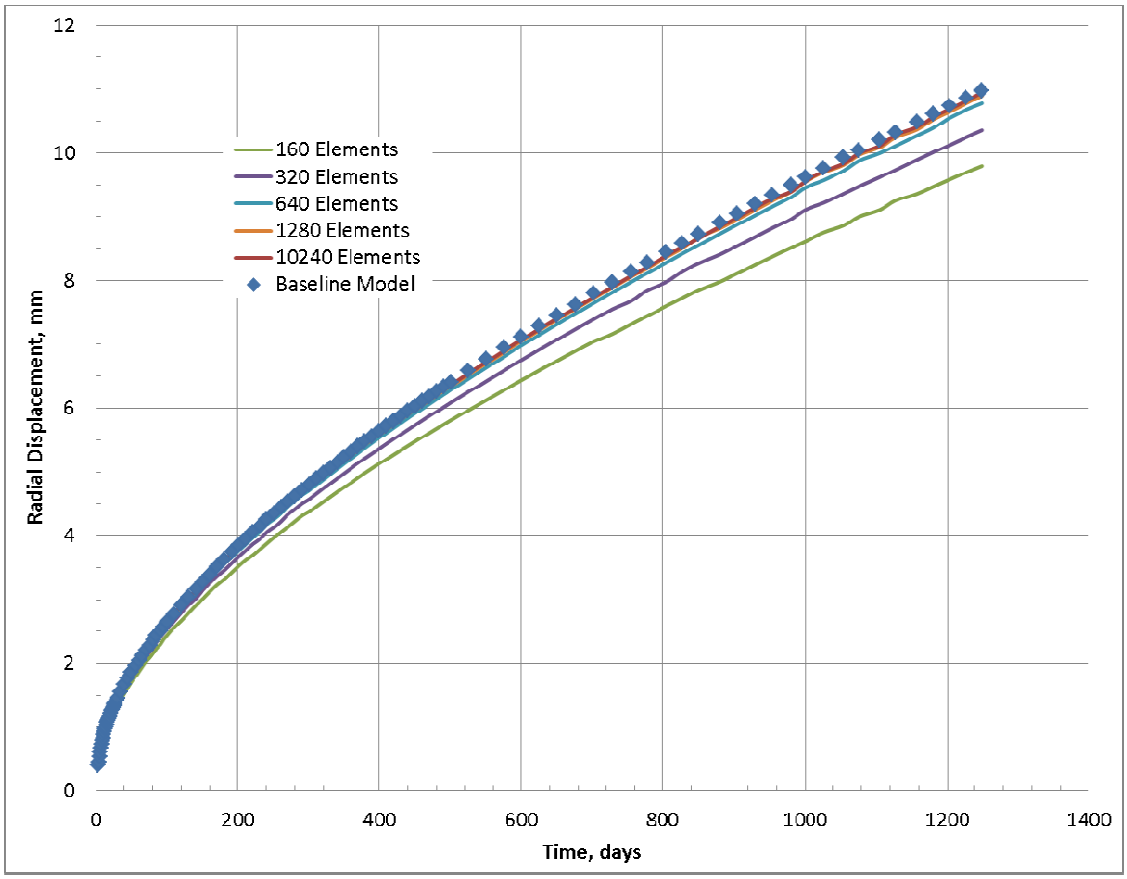

Figure 10. Comparison of Radial Displacement with Varying Number of Elements in the Radial Direction for the 5° Slice Model

3.6.2. Quarter-Borehole Model

Figure 11 shows a comparison of the Quarter-Borehole Model and the baseline 5° Slice Model computed results. The figure clearly shows that the Quarter-Borehole Model is producing a solution equivalent to that from the baseline 5° Slice Model. Consequently, there is also a high degree of confidence in the ability of the Quarter-Borehole Model to produce accurate numerically converged results.

Figure 12 shows the results from the Quarter-Borehole Model compared to the IFC borehole convergence data and the results from the baseline 5° Slice Model out to 900 days of simulation (Figure 11 with the data now overlaid on it). This figure shows that excellent agreement with the IFC convergence data is achieved, thereby providing high-confidence in the computed results with the models.

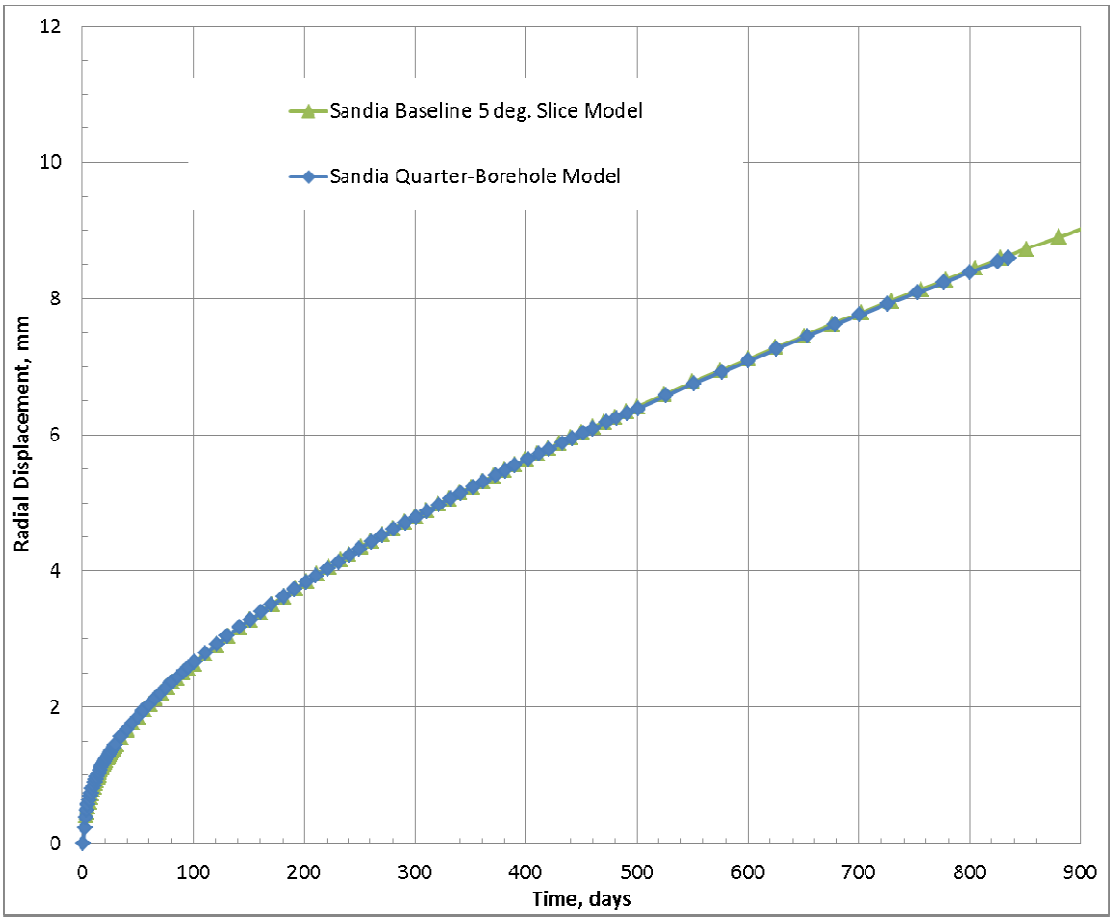

Figure 11. Comparison of Radial Displacement Results from Baseline 5° Slice Model to those from Quarter-Borehole Model

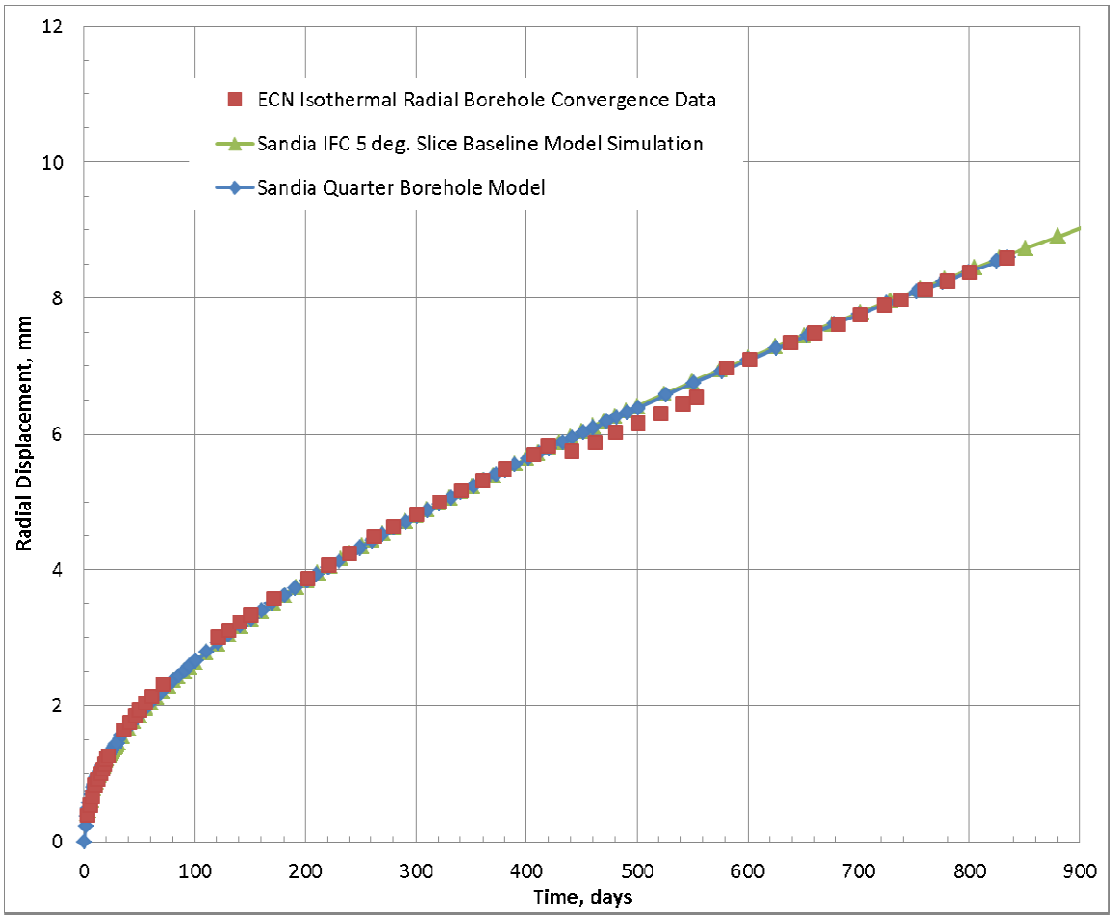

Figure 12. Comparison of Quarter-Borehole Model Results with Measured Convergence Data and Results from the Baseline 5° Slice Model

4. HFCP BENCHMARK CALCULATION

This section describes the development of the HFCP Benchmark calculation. The idealized configuration that was used, the computer simulation tools that were exercised, the constitutive model's temperature-dependence, the computational grid, and the final results from the numerical model are described and discussed.

4.1. Idealized Configuration

The numerical model used to simulate the Heated Free Convergence Probe (HFCP) benchmark borehole closure problem, with an idealized configuration shown in Figure 13, was also straight forward.

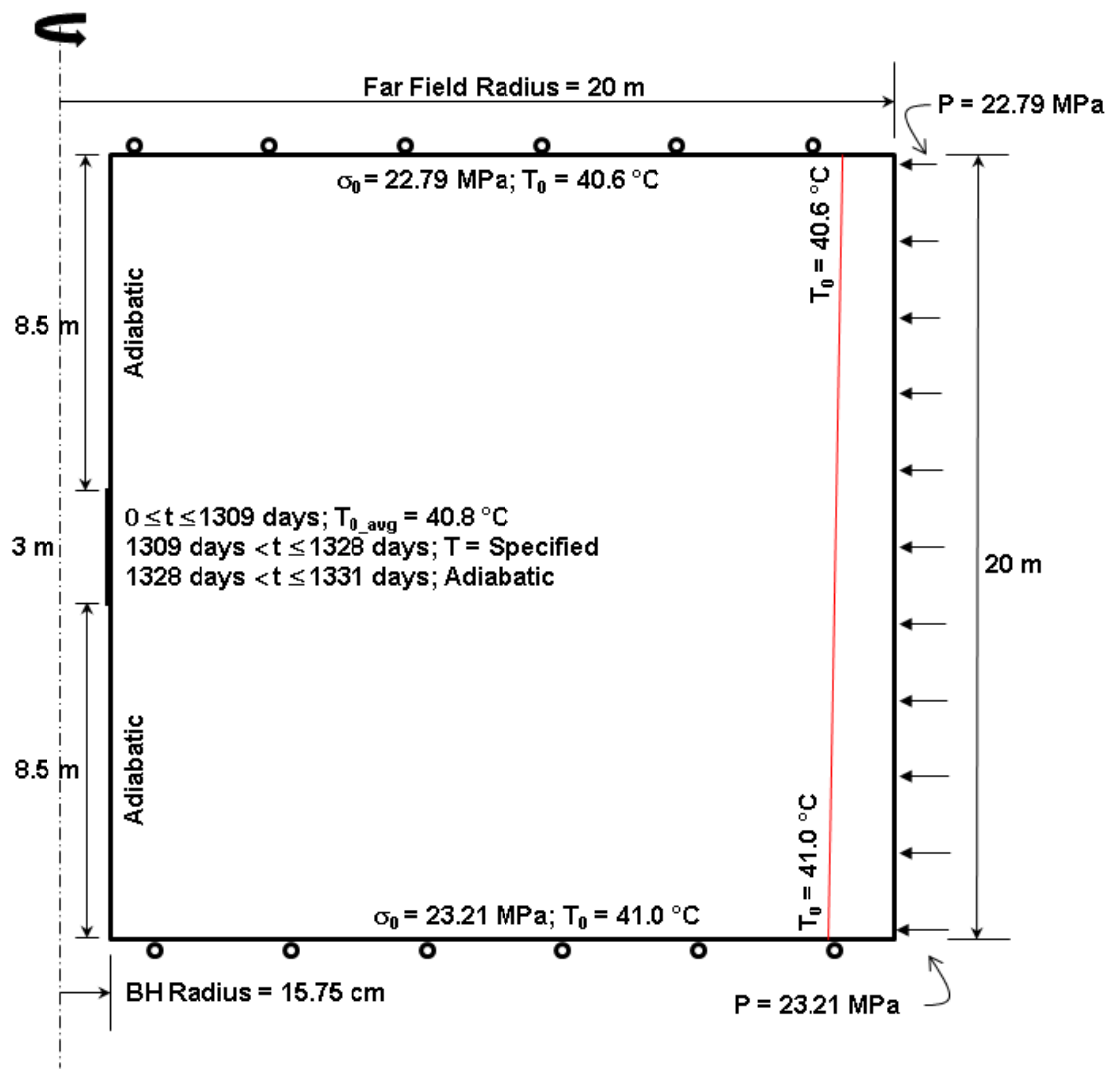

Figure 13. Idealized Configuration for HFCP Benchmark Problem

For this test, as previously mentioned, a heated 3 m central section of the probe provided the heat load that was applied to the borehole. The various temperature and borehole convergence measurements taken during the test were taken in the borehole near the center of this heated zone. The center of the zone is located at a depth of 231 m from the open chamber floor (see Figure 1) at a depth of 981m below the surface. The heating and convergence of the borehole at this elevation could therefore be modeled with a relatively local model, again using an "axisymmetric" borehole model description. This is shown schematically in Figure 13, where the thickness of the model is now 20 m, per the benchmark specifications of Appendix A. As before, the initial borehole diameter was 315 mm, for an initial radius of 15.75 cm, and the far-field radial boundary was set to 20 m.

4.1.1 Mechanical Initial/Boundary Conditions

The configuration was all-salt and had prescribed in it an initial stress state that varied linearly with the 20 m depth of the configuration, starting at 22.79 MPa at the top and increasing to 23.21 MPa at the bottom. This leads to an initial stress of 23 MPa (corresponding to the 231 m depth from the chamber floor) at the center of the 3 m long heated zone that is located mid-depth of the configuration. This heated zone is denoted by the thick black line in Figure 13. The upper and lower boundaries of the configuration were fixed against vertical displacement (as indicated by the rollers in the figure). The far-field radial boundary condition at the right was set to an applied traction (i.e., a pressure P) that varied linearly from a value of 22.79 MPa at the top of the configuration to a value of 23.21 MPa at the bottom of the configuration.

4.1.2 Thermal Initial/Boundary Conditions

The initial temperature of the configuration also varied linearly with depth, starting at a value of 40.6 °C at the top and increasing to a value of 41.0 °C at the bottom, for a gradient of 0.02 °C/m. This corresponds to an initial temperature at the center of the heated zone of 40.8 °C. The upper and lower boundaries of the configuration were assumed to be sufficiently removed away from the heated zone that the temperatures at those boundaries would not change with time. Consequently the top boundary of the configuration was set to a temperature value of 40.6 °C and the bottom boundary was set to a temperature value of 41.0 °C, both of which remained constant with time. Likewise, the far-field radial boundary at the right was also assumed to be sufficiently removed away from the heated zone such that the temperature at that boundary would not change with time. The temperature at that boundary was set to a constant in time temperature value that varied linearly with depth. It started at 40.6 °C at the top and increased to 41.0 °C at the bottom, as indicated schematically by the red line in Figure 13.

The boundary of the borehole, ranging from a distance 7.5 m above to 7.5m below the 3 m heated zone was defined as an adiabatic boundary. The 3 m mid-depth "heated zone" started off isothermally with an average temperature of 40.8 °C (linearly varying from 40.77 °C at the top of this 3 m to 40.83 °C at the bottom). After 1309 days, the heater in the experiment was turned-on and the temperature began to increase. The temperature at the borehole wall along the 3 m zone was then applied as a uniform temperature according to the benchmark specification of Appendix A and as shown in Table 3. Nineteen days thereafter, the heater in the experiment was

turned-off, and the boundary condition along the 3 m section reverted to an adiabatic condition for the remainder of the simulation.

Table 3. Specified Temperature at Borehole Wall for HFCP Benchmark Calculation

Δt days	t(abs) days	T °C
0	1309	40.8
0.1	1309.1	94
0.5	1309.5	153
1	1310	173
2	1311	185
3	1312	191
5	1314	199
10	1319	213
15	1324	223
19	1328	229

4.2 Simulation Tools

For the HFCP benchmark problem, three modules of the SIERRA Mechanics toolset, described briefly in Section 3.2, were exercised. The Aria fluid/thermal physics module computed the thermal response due to the applied heat load and the Adagio solid mechanics physics module handled the quasi-static large deformation mechanical response of the salt using the MD Creep model described earlier. The coupling of the two physics regimes was handled by a third SIERRA Mechanics toolset module, known as the Arpeggio coupled solution controller module.

Arpeggio handles the coupling in the following general manner. Aria is coupled to Adagio through nodal temperatures, transferring its computed temperature field to Adagio. Adagio accepts the temperature field from Aria and updates its temperature field on its nodes. Adagio is coupled back to Aria through nodal displacements, transferring its computed displacement field to Aria. Aria accepts the displacement field and updates its corresponding nodal coordinates. This transfer operation between the two physics modules occurs at discrete time points, and thus accomplishes a “loosely-coupled” union of Aria and Adagio. The Aria and Adagio finite element meshes can be discretized differently to account for different refinement locations. However, for this problem a different discretization for the thermal and mechanical meshes was not necessary.

4.3 Temperature-Dependence in MD Model

For this HFCP coupled thermo-mechanical simulation problem, the mechanical response of the salt will be influenced significantly by the rise in temperature in the vicinity of the heated zone. It is important to note that the temperature-dependence in the MD Creep Constitutive Model, described in subsection 3.3, is exponential in the various mechanisms of the secondary creep strain contribution (Eqs. 2-4). It is also exponential in the transient strain limit contribution (Eq. 11). This exponential dependence of the creep strain permits significantly accelerated radial

convergence of the borehole compared to the isothermal response of the IFC benchmark problem.

4.4 HFCP Computational Model

Once again, the idealized configuration of Figure 13 can be converted into a computational model in various ways depending on the computational tools that are available. As was the case with the IFC benchmark problem of section 3, only a 3D capability is available in SIERRA Mechanics (i.e., a true 2-D "axisymmetric" capability is not available in the toolset, as may be available in other tools). Consequently, for the HFCP borehole calculations reported herein, the axisymmetric model is approximated by taking a circumferential slice to generate its 3D equivalent. Although SIERRA Mechanics has the capability to handle different computational meshes for different physics applications, this capability was not needed for this problem and the same computational mesh is used for both the mechanical and thermal responses. In terms of the mechanical response, the front and back circumferential faces of the resulting 3D model are constrained against horizontal movement in that circumferential direction (i.e., no circumferential movement normal to the face). Likewise, in terms of thermal response, the front and back circumferential faces of the resulting 3D model are designated as being adiabatic. In this HFCP study, a 15° circumferential slice model was used. Furthermore, on the basis of the IFC study, the mesh refinement of the HFCP computational model was comparable to that used in the earlier IFC benchmark Quarter-Borehole Model.

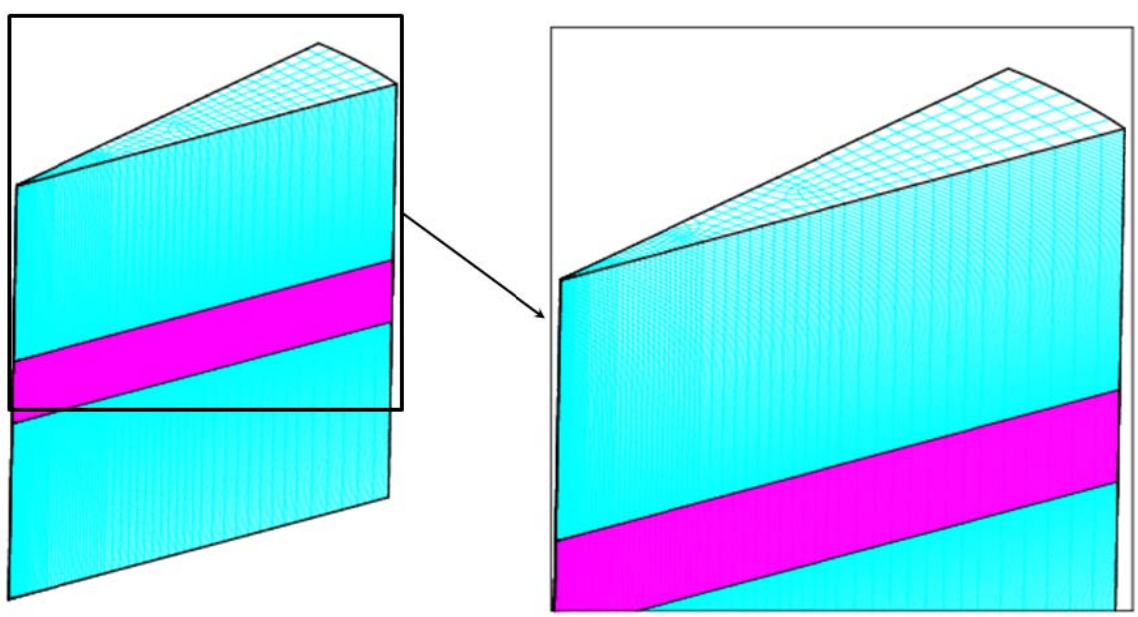

Figure 14. Computational Mesh Used for HFCP Model (Overall Mesh on Left & Zoomed-In View on Right)

The HFCP computational mesh is shown in Figures 14-15. On the left side of Figure 14 the overall computational mesh is shown. It contains 334829 elements nodes and 281868 uniform

strain elements. The vertically central portion, shown in the color magenta, is the 3 m zone where the heating occurs in the vicinity of the borehole. The turquoise-colored portions, above and below the magenta, represent the rest of the idealized configuration. Shown on the right side of Figure 14 is an enlarged portion of the mesh (zoomed-in) to demonstrate that there is some coarsening vertically in the mesh away from the central zone (although difficult to see because of the mesh density). Figure 15 shows the overall central portion of the mesh and a series of zoomed-in images (clockwise from the top left) of the same central portion now isolated from the rest of the mesh. With each enlargement, more detail of the mesh is evident, with the final image showing that the mesh is indeed of roughly the same density as that for the Quarter-Borehole model used in the earlier IFC benchmark problem. As seen in Figure 15, for approximately 2 borehole diameters in the radial direction from the centerline, the mesh is quite fine and the elements are uniformly distributed in all directions and then coarsen-out (in a "paved" fashion) in the radial and circumferential directions, but remain uniformly distributed in the vertical direction.

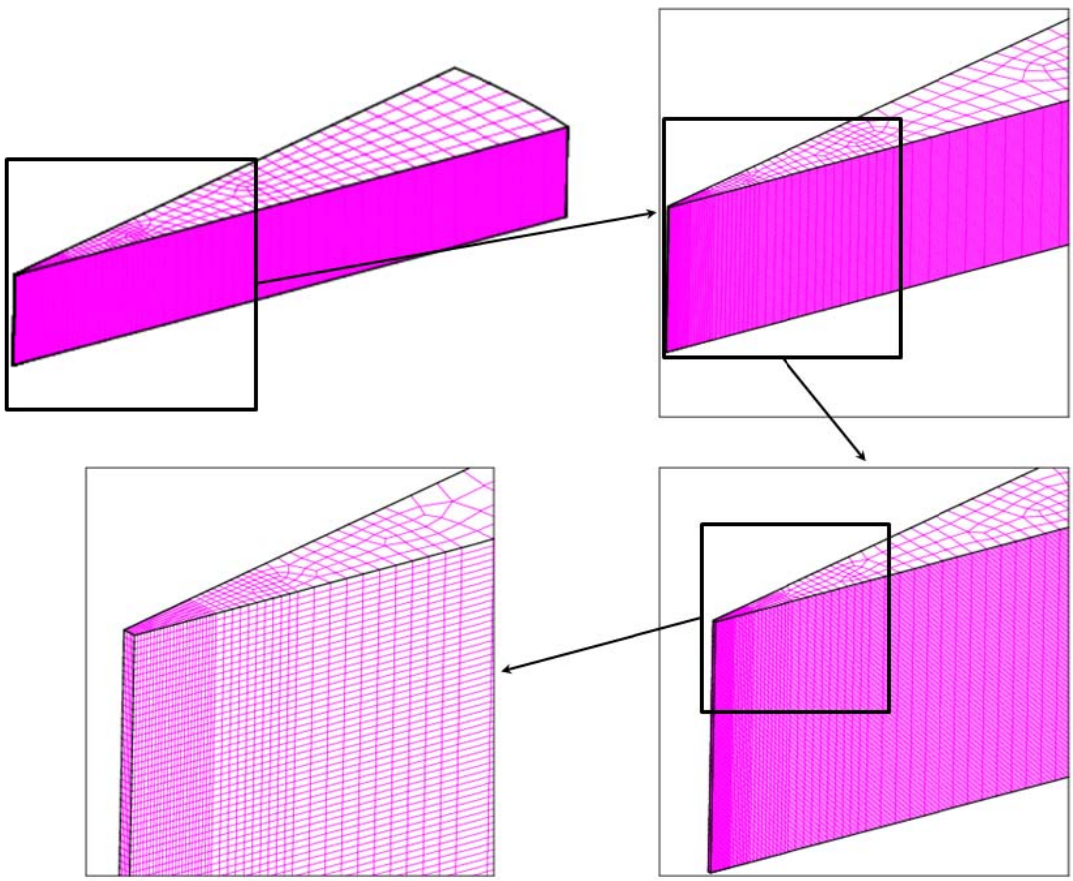

Figure 15. Central Portion of Computational Mesh Used for HFCP Model (Overall Mesh on Top & Progressively Zoomed-In Views Clockwise from There)

4.5 Results

Results of the HFCP benchmark calculation are provided herein. The first subsection details the thermal results. The second one details the mechanical results, showing the accelerated borehole convergence due to the heating of the borehole.

4.5.1 Thermal

Temperature histories are shown first in the following sequence of figures for the selected points shown in Figure 16 below (taken from the COSA II report). These temperature histories are plotted with time adjusted to start with the beginning of the heating phase. Vertical and horizontal temperature profiles are also plotted for selected times during the heating and cooling down phase. The horizontal profile elevation is at the center of the heater and extends from the borehole wall to the exterior of the model. The vertical profile extends from the base of the model to the top along the borehole wall.

The thermal properties used in the analysis are listed in Table 4 below. Thermal properties such as conductivity and specific heat are functions of temperature.

Table 4. Thermal Properties Used for Salt

Parameter	Value	Units
Thermal Conductivity $\lambda = a_0 + a_1 T + a_2 T^2 + a_3 T^3$	$a_0 = 5.734$	$(W/(m - C^o))$
	$a_1 = -1.838\text{E} - 02$	
	$a_2 = 2.86\text{E} - 05$	
	$a_3 = -1.51\text{E} - 08$	
	T in units of C^o*	
Specific Heat Capacity (at constant pressure) $C_p = b_0 + b_1 T$	$b_0 = 1.8705\text{E} + 06$	$(J/(m^3 - C^o))$
	$b_1 = 3.8772\text{E} + 02$	
	T in units of C^o*	
Coefficient of Thermal Expansion	4.2E-05	$(m/(m - C^o))$
Density	2,187	(kg/m^3)
* The temperatures used in the Aria simulations were converted from centigrade to Kelvin. In the following figures the temperatures are converted from back to centigrade using the following formula: $0K^o = -273.15\ C^0$.		

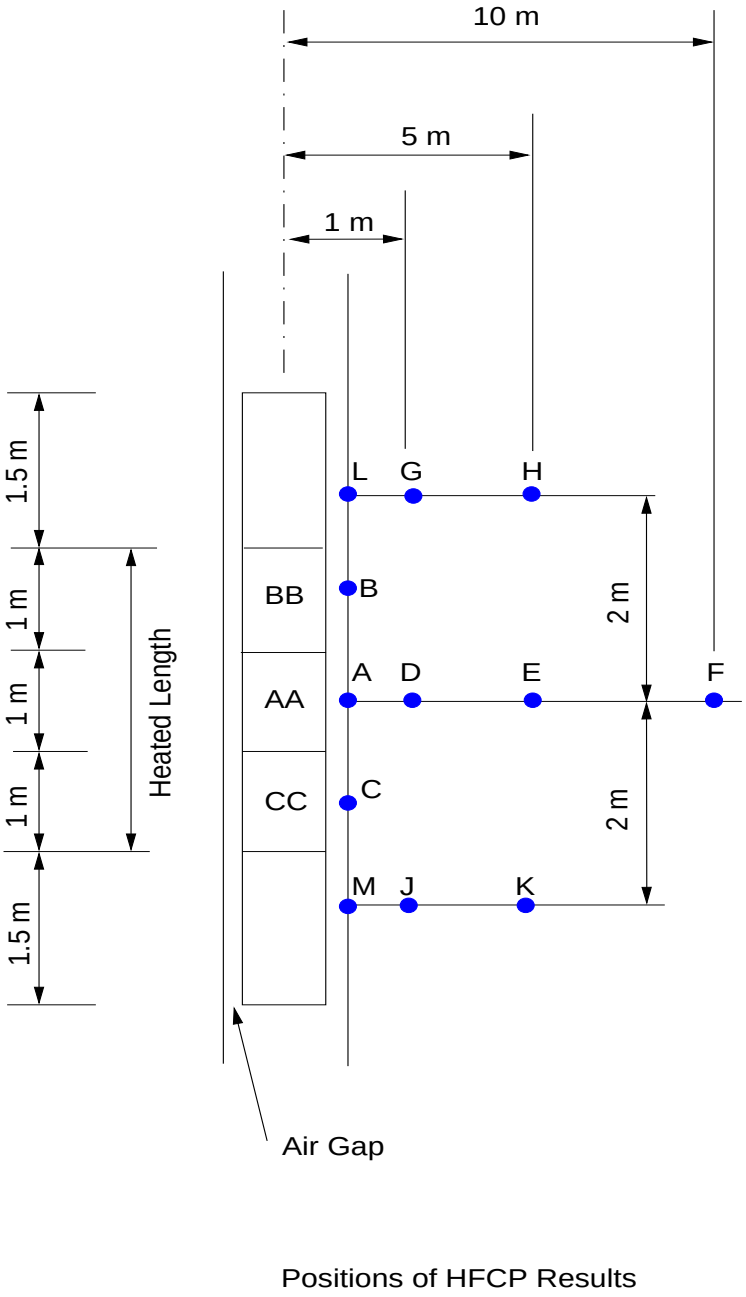

Figure 16. Time History Locations

For clarity the temperature histories are separated into three plots with different scales. Figure 17 shows the temperature histories for Points A, B, C, L, & M (identified in Figure 16). These points constitute a view of the temperature evolution as a function of depth of the model. The

figure shows that for the points in the central 3 m heated zone, there is a rapid increase in temperature immediately after the heater is turned-on for approximately the first day, followed by a slowly declining increase over the next 18 days when it reaches a peak of about 230 °C immediately before the heater is turned-off. The next three days of cool-down bring the temperature down to approximately 62.5 °C at 22 days, for points B and C. The central point A remains a bit warmer, at about 72.5 °C, on day 22. Points L and M are half a meter above and below the central heated zone, respectively, and show a much lower temperature increase, peaking at approximately 75 °C immediately before the heater is turned-off, dropping to about 60 °C after 3 days of cool-down.

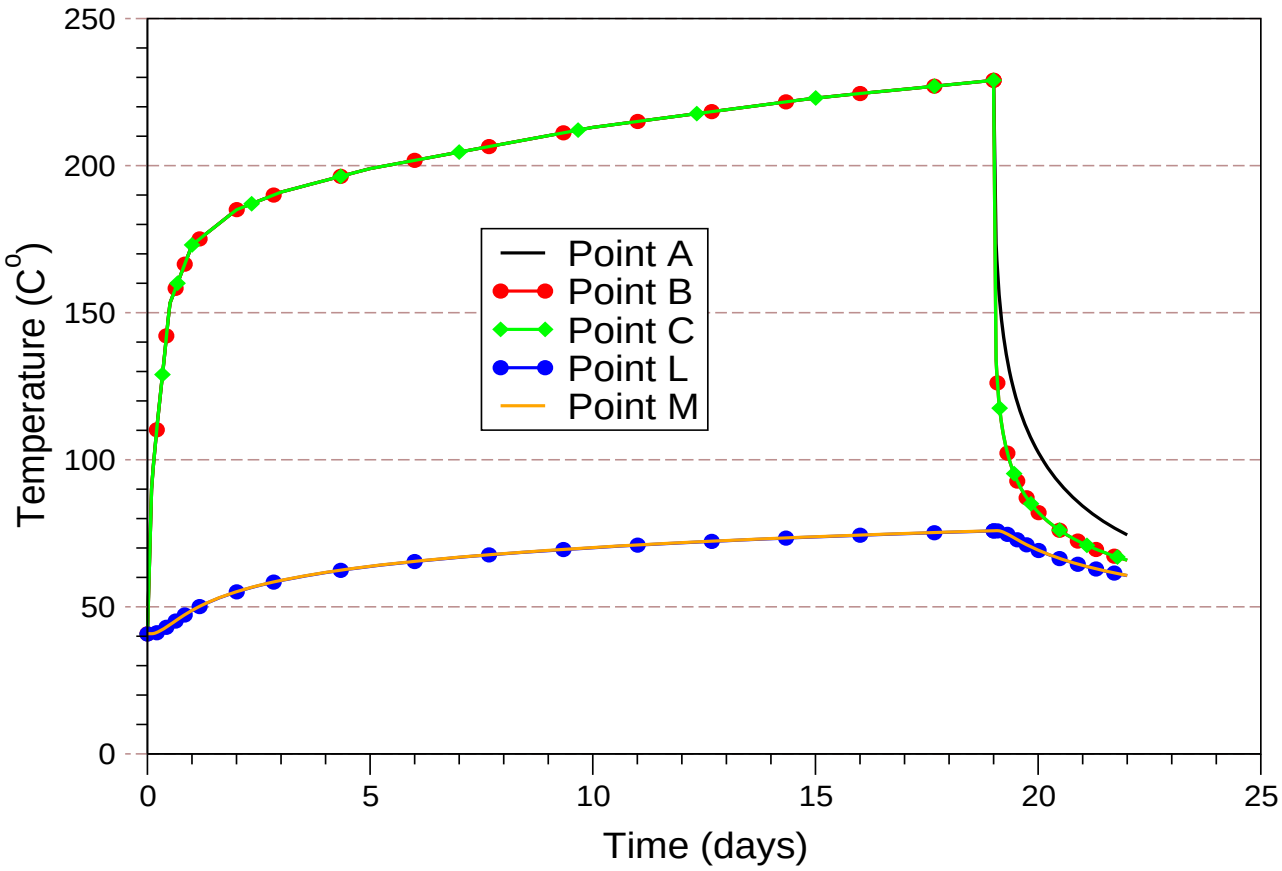

Figure 17. Temperature Histories for Points A, B, C, L, and M

Figure 18 shows the temperature histories for Points A, D, E, & F (identified in Figure 16). These points constitute a view of the temperature evolution as a function of radial distance away from the borehole in the model (note that Point A is repeated in the figure for completeness). The figure shows that radially, the point nearest the borehole wall (Point A) is the one that is heated most quickly and develops the highest temperature of the group (as expected). Point D, which is radially about 0.84 m further away, shows a more moderate increase in temperature, rising less

rapidly and peaking at approximately 85 °C, immediately before the heater is turned-off. After three days of cool-down, it drops to approximately 66 °C. Points E and F, which are 4.84 m and 9.84 m away from Point A, respectively, see essentially an insignificant increase in temperature from the initial value.

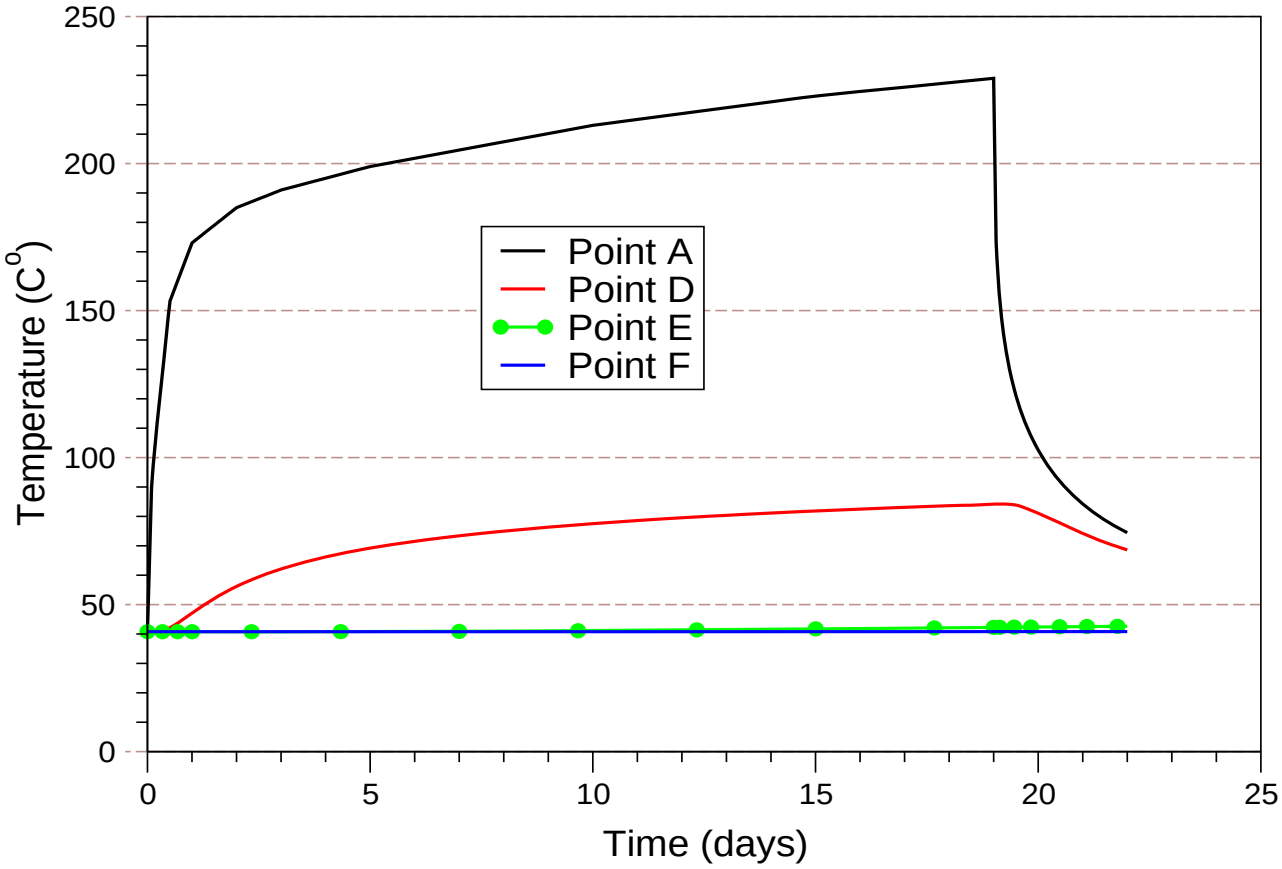

Figure 18. Temperature Histories for Points A, D, E, and F

Figure 19, shows the temperature histories for Points G, H, J, & K (identified in Figure 16). These are the two pairs of points above and below the 3 m central heated section that are further out into the configuration away from the heat source, with G & J closer-in radially than H & K. The figure shows that the temperatures in Points G & J develop similarly to each other and both reach a maximum temperature of about 62.5 °C, immediately before the heater is turned-off. Both also cool-down over 3 days to a temperature of approximately 58 °C. Likewise, the temperatures in Points H & K also develop similarly to each other, but in this case, the temperature increase is quite modest and reaches a maximum at the end of 22 days (~ 42 ºC).

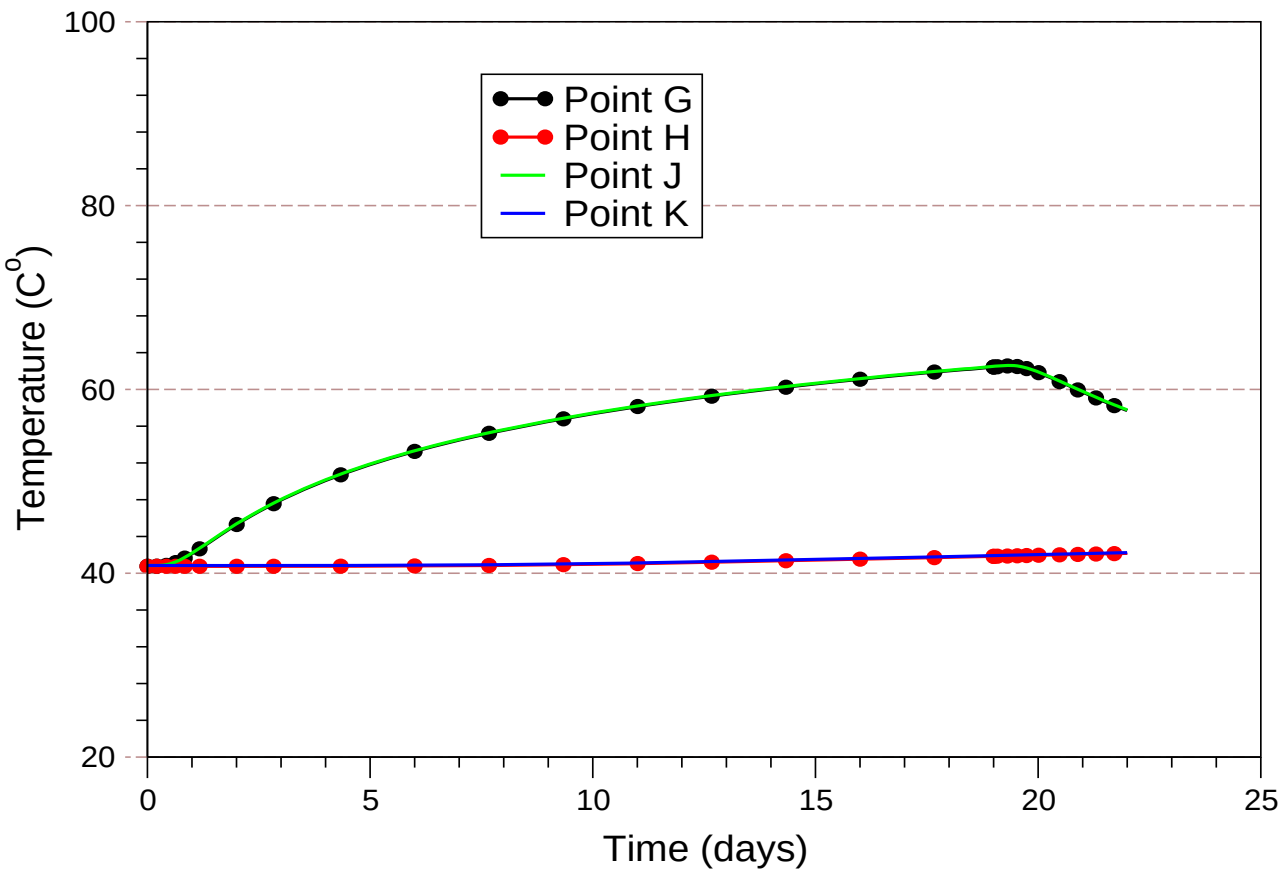

Figure 19. Temperature Histories for Points G, H, J, and K

The horizontal and vertical temperature profiles shown in Figures 20-21 are plotted for eight times, starting when the heater is turned on, to when it is turned off at 19 days, and through the cool-down phase at 22 days. The times for the profiles are, 0, 1, 2, 4, 8, 15, 19, and 22 days.

Figure 20 shows the horizontal temperature profile, vertically centered through the heated zone, extending from the borehole wall to the far-field extent of the model. Recall that the initial temperature at this location is 40.8 °C. The figure clearly shows that, once the heater is turned-on, the temperature at the borehole wall rapidly increases to approximately 172 °C at 1 day and decays slowly with distance toward the far-field to the initial temperature. This trend of temperature decay with distance continues for the remaining times shown, gradually encompassing more material that is heated above the initial temperature radially with distance. The peak temperature at the borehole wall increases with time and reaches a value of approximately 228 °C at 19 days, immediately before the heater is turned-off. By day 22, after three days of cool-down, the peak temperature at the borehole wall is approximately 72.5 °C.

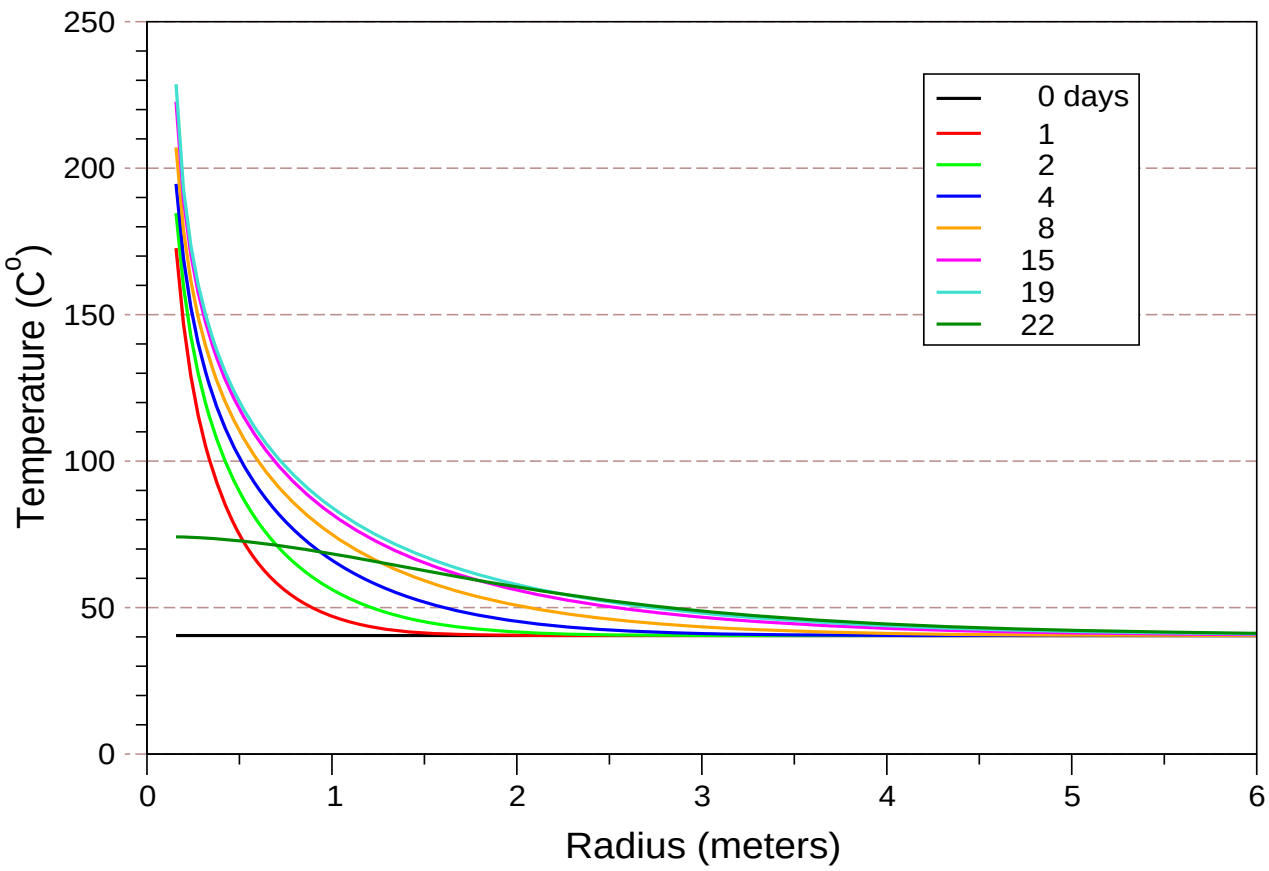

Figure 20. Horizontal Temperature Profiles

Figure 21 shows a vertical profile of temperatures at the borehole wall, from the bottom to the top of the model. The initial temperature varies from 41.0-40.6 °C from the bottom to the top. The figure shows that, as expected, the temperature along the 3 m long central heated portion of the model increases rapidly once the heater is turned-on. While the zones above and below the central zone also become hotter, the temperature increase in those is less and decrease with distance from the vertical center of the model. The temperatures increase with time to reach a maximum at 19 days, immediately before the 3 day cool-down period commences. At day 22, or after three days of cool-down, the temperature in the middle of the heated central zone has dropped to about 72.5 °C.

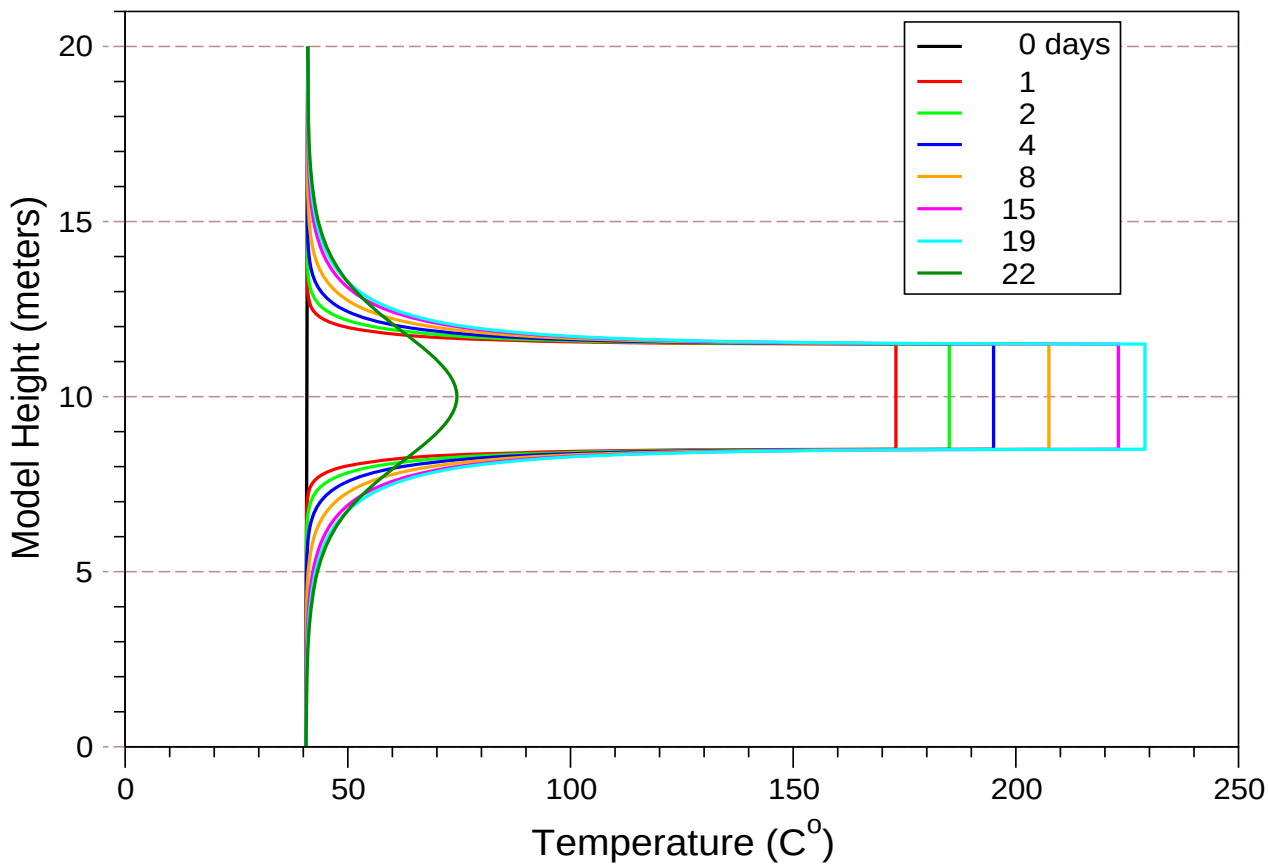

Figure 21. Vertical Temperature Profiles

4.52. Mechanical

The MD Creep model parameters used in the mechanical analysis are the fitted values derived from the isothermal calculations, as detailed in Section 3. The format of the plots that will be used for the mechanical results is similar to that of the thermal results. Namely, history variables for the radial displacements, and principal stresses are plotted for nodes and elements adjacent to the borehole at the mid-plane of the heater. Vertical and horizontal profiles of nodal and elemental quantities are plotted for the same times and locations as were the temperature profiles. The mechanical quantities plotted for the profiles include; radial displacements, principal stresses, creep strain (equivalent creep strain) and creep rate.

The radial displacement history response plots at the borehole wall have been adjusted to show relative displacement (i.e., the initial displacement from 1,309 days of creep was subtracted). The reader should note that in the vertical and horizontal profiles, the displacement from the isothermal creep is left-in the plotted results.

Figure 22 shows the predicted radial displacement history of a point at the borehole wall surface at the heater mid-plane. The radial displacement is seen to increase rapidly after initial heater

turn-on and slows gradually after about 5 days until the heater is turned-off. During the 3 day cool-down period, the increase in radial displacement increases negligibly and a maximum value of 0.053 m is reached at day 22.

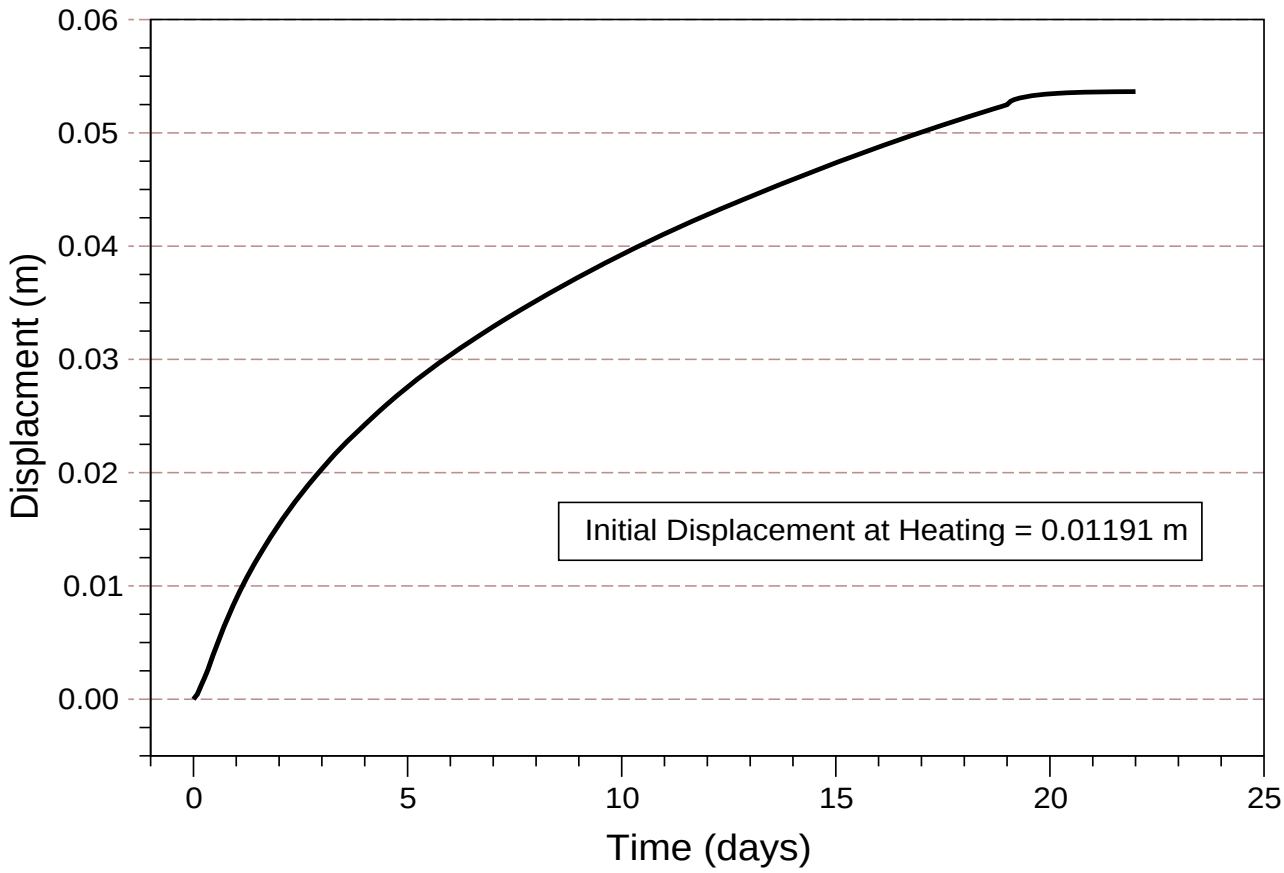

Figure 22. Radial Displacement History at Heater Mid-Plane

Figure 23 shows the principal stress histories in the element immediately adjacent to the borehole wall. Initially before the heater is turned-on, the maximum (Sigma 1) and intermediate (Sigma 2) principal stresses are equivalent (approximately 12 MPa), while the minimum principal stress (Sigma 3) is close to zero. As heating proceeds, (after an initial jump) by the end of the first day or so, both the maximum and the intermediate stresses have decreased to approximately 11 MPa. Thereafter, until the heater is turned-off at 19 days, the maximum principal stress continues to decrease slightly, but the intermediate principal stress, drops to a value slightly above that of the minimum principal stress, or about 2 MPa. During cool-down, the various principal stresses re-adjust differently: the maximum principal stress (Sigma 1, green) drops rapidly to nearly 0 MPa and then rises up to nearly 20 MPa and settles at 15.0 MPa at day 22; the minum principal stress (Sigma 2, red) falls to 0 MPa and then approaches 0.7 MPa at day 22; and the intermediate

principal stress (Sigma 3, black) rapidly drops to -15 MPa (compression) and then rises to almost 0 MPa and then falls back to -5 MPa at day 22.

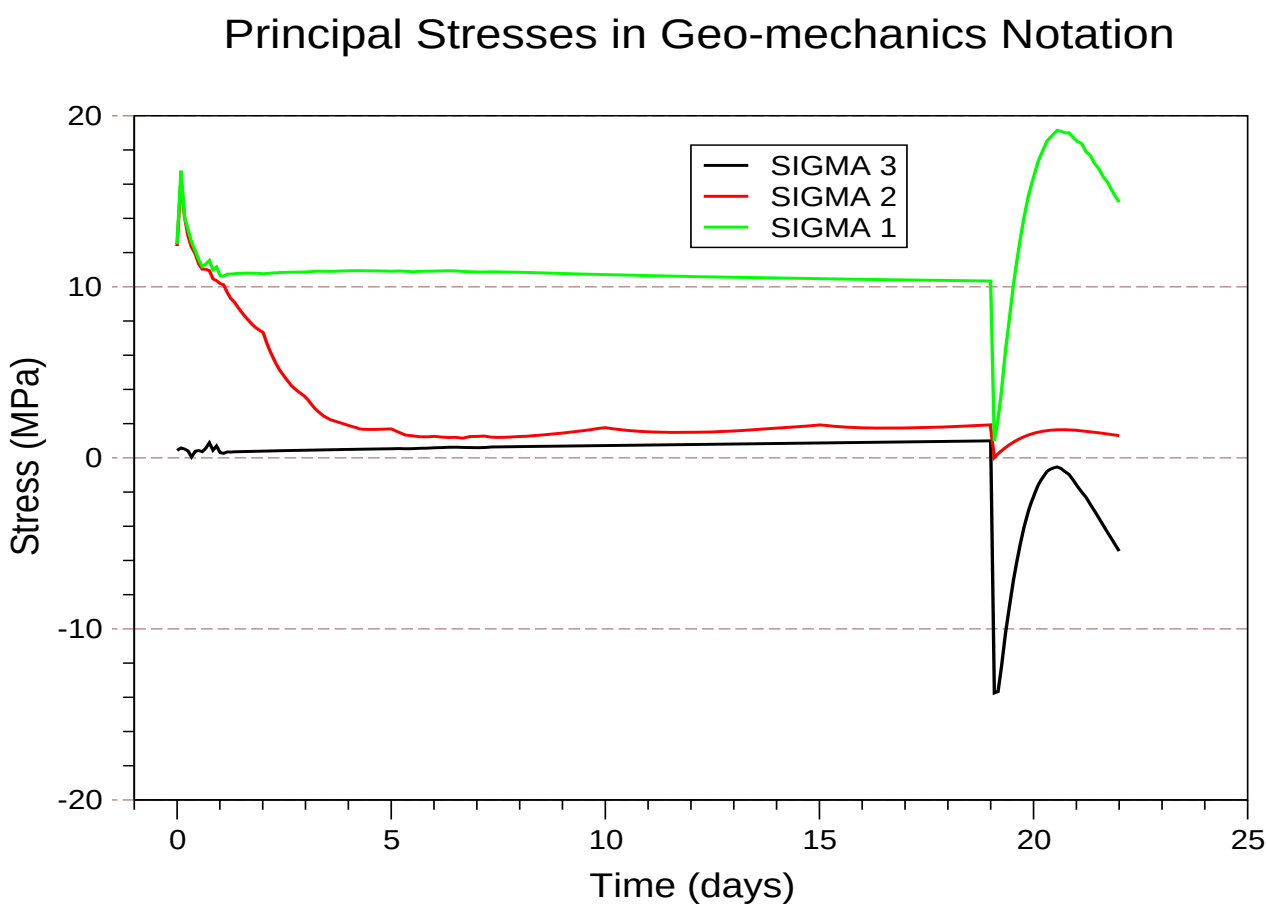

Figure 23. Principal Stress Histories at Heater Mid-Plane (In Geomechanics Notation)

Shown in Figure 24 is the equivalent creep strain ("EQCS") history in the same element at the borehole wall and at the heater mid-plane. This figure shows that the development of the equivalent creep strain closely mimics that of the borehole displacement (Figure 22). Namely, it increases somewhat rapidly from 1 to 5 days, with a slower increase thereafter until the heater is turned-off at day 19. During the 3 day cool-down period, the creep strain increases negligibly and a maximum value of approximately 0.57 m/m is reached at day 22.

Figure 25 shows the creep strain rate history at the same location. When the heater is turned-on at time zero, there is a jump in the strain rate to a value of about 1.3E-6 per second. This rate drops quickly over the first five days and then more slowly thereafter until the heater is turned-off, reaching a value of about 0.15 per second at 19 days. During the cool-down period, the rate drops-off quickly to a negligible value (on the scale of the figure) at 22 days.

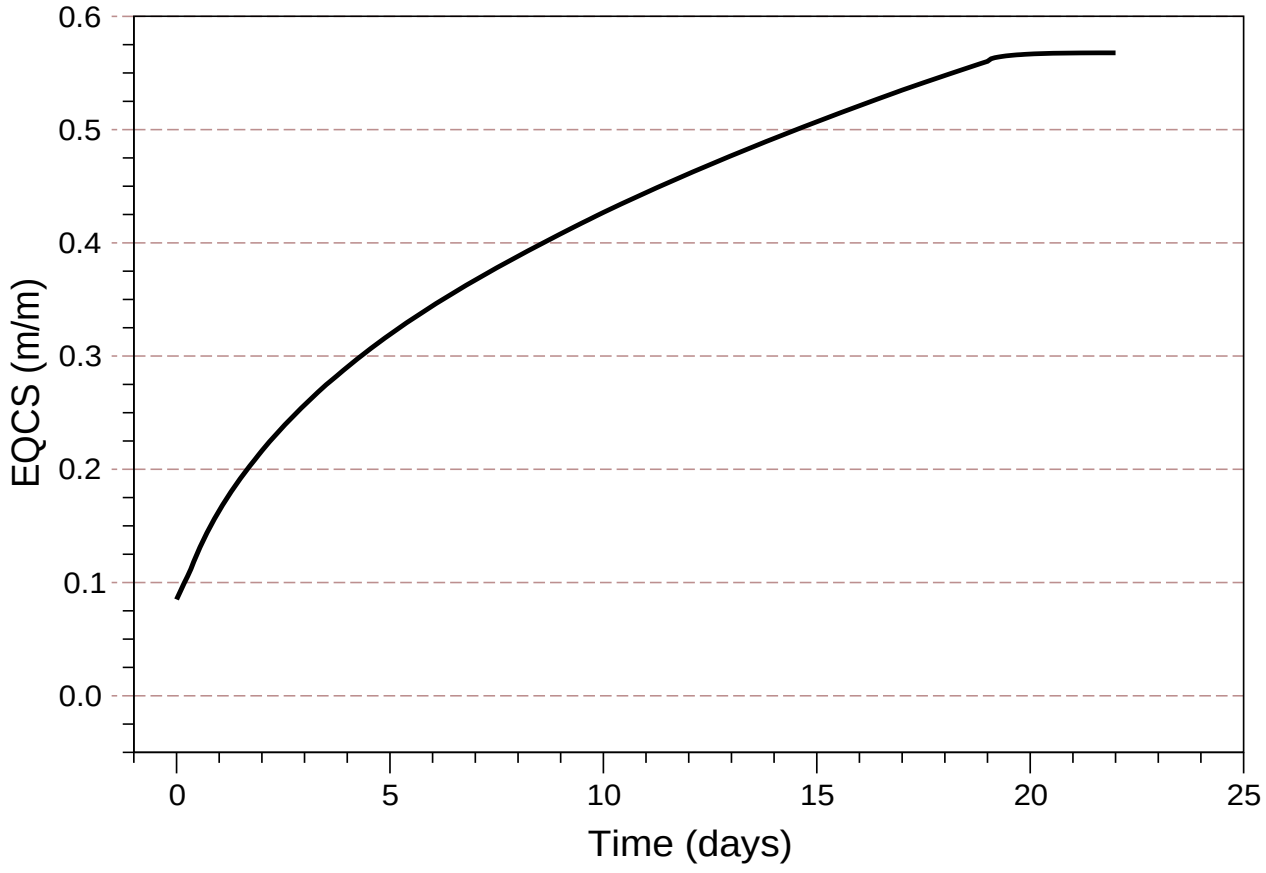

Figure 24. Equivalent Creep Strain History at Heater Mid-Plane

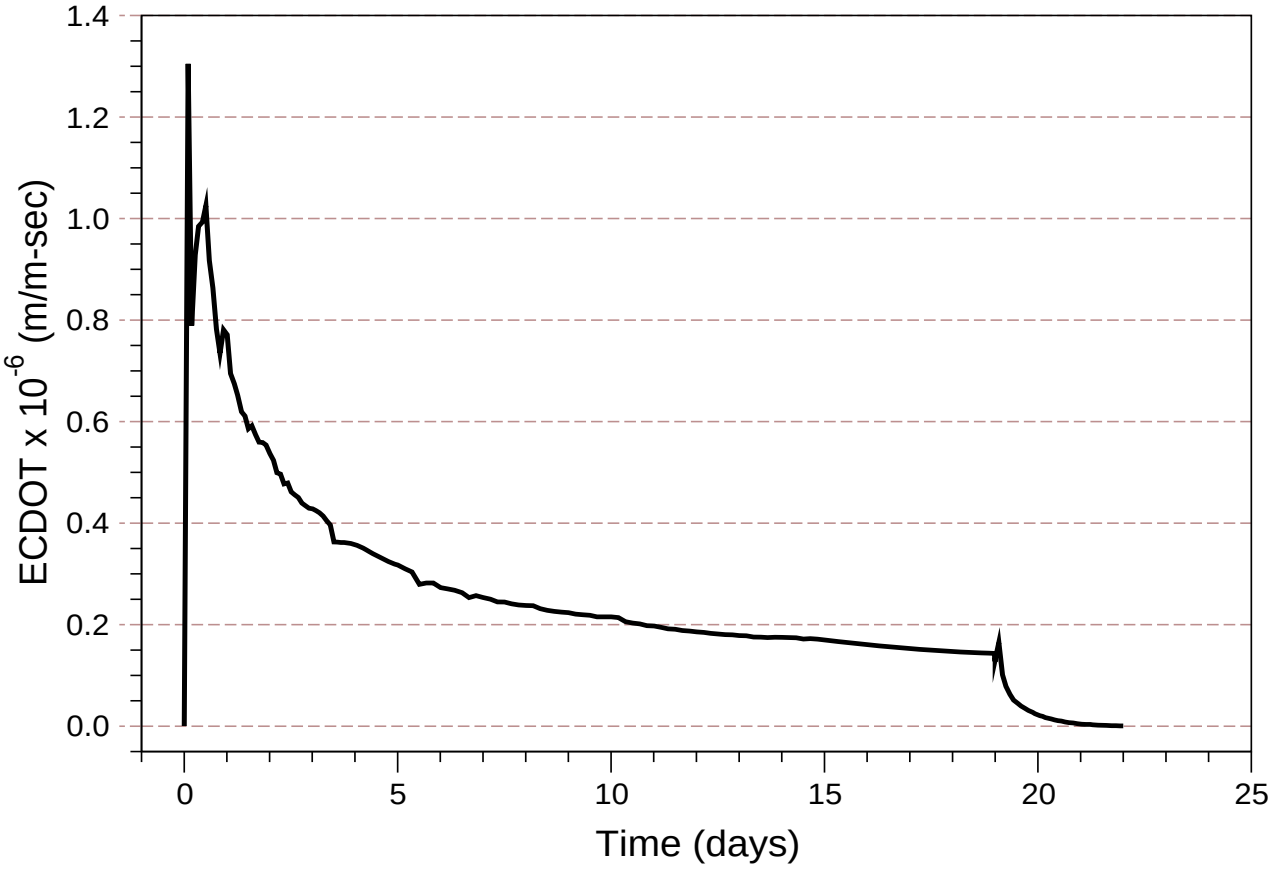

Figure 25. Creep Strain Rate History at Heater Mid-Plane

Figures 26-28 show the radial displacement, equivalent creep strain, and creep strain rate profiles, respectively, as a function of horizontal distance along the heater mid-plane from the borehole radially out to the far-field in the model. Figure 26 shows that the radial displacement of material with distance quickly diminishes within the first 2.5 m from the borehole. Figure 27 shows that the equivalent creep strain in the configuration with distance at this vertically central location also quickly diminishes within the first 1.5 m from the borehole. Similarly, Figure 28 shows that the equivalent creep strain-rate in the configuration with distance also quickly diminishes within the first 1.5 m from the borehole.

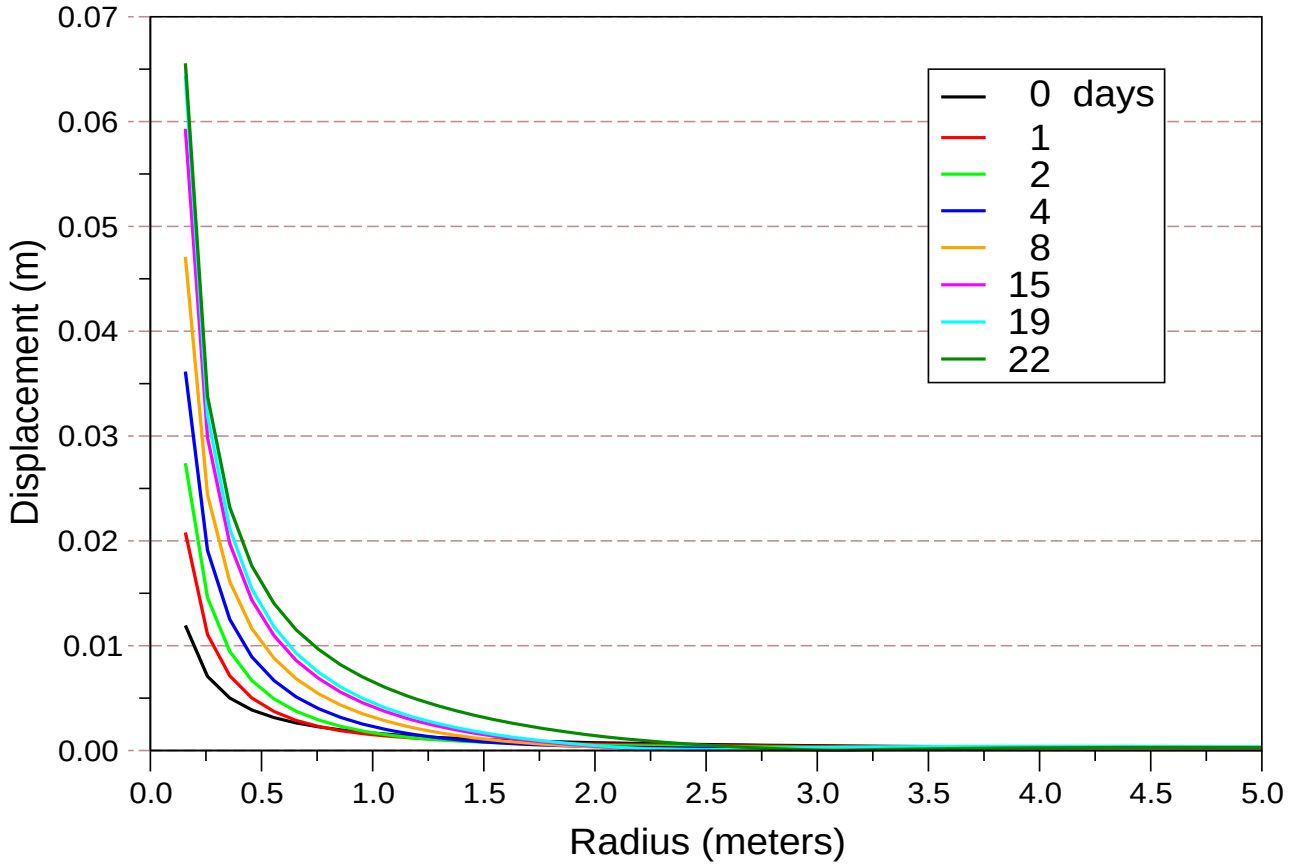

Figure 26. Horizontal Profiles of Radial Displacement at Heater Mid-Plane

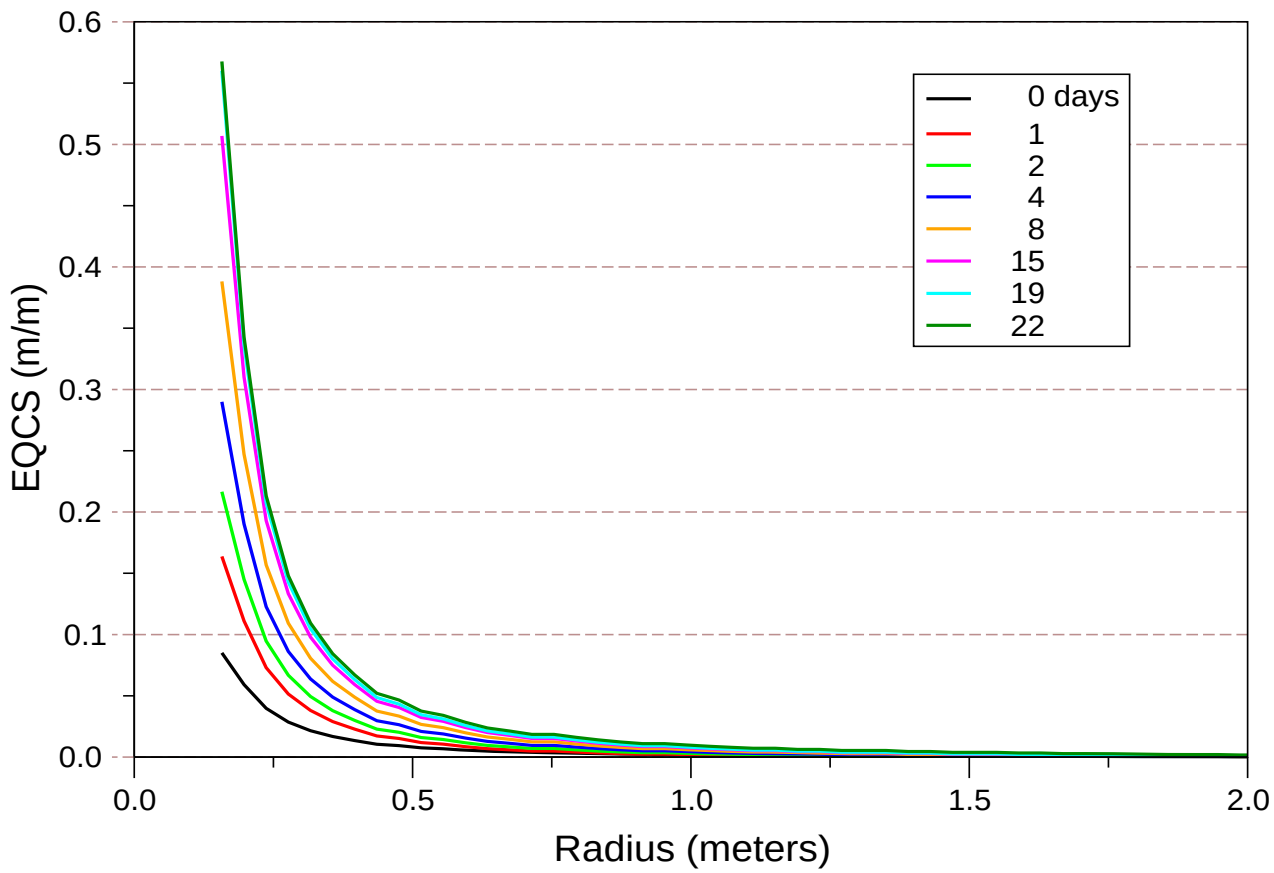

Figure 27. Horizontal Profiles of Equivalent Creep Strain at Heater Mid-Plane

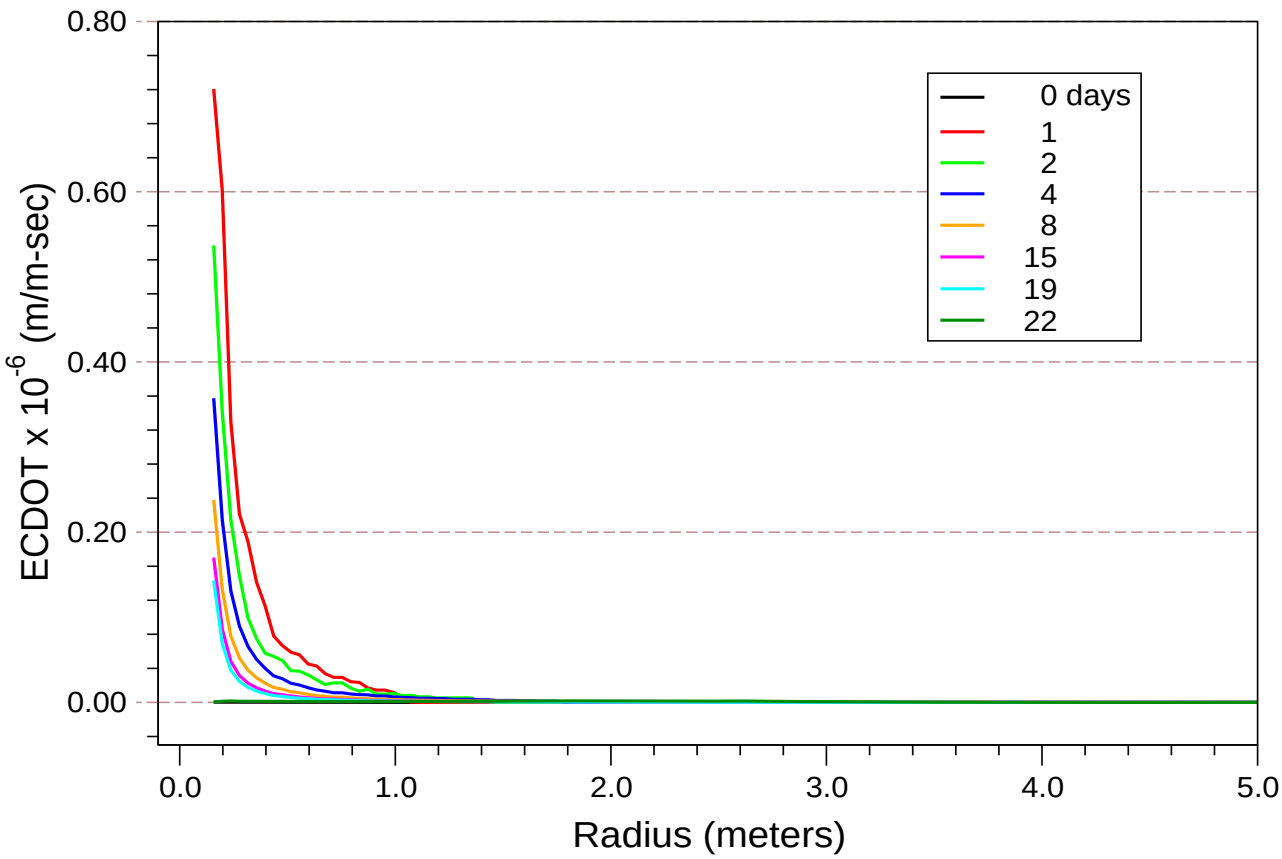

Figure 28. Horizontal Profiles of Creep Strain Rate at Heater Mid-Plane

It is difficult to show horizontal profiles for the three principal stresses varying with time on the same figure because the curves would be too crowded for clarity. Consequently, the three principal stresses at each of 0, 1, 2, 4, 8, 15, 19, & 22 days are shown in Figures 29-36, respectively. These figures show the evolution of the maximum (Sigma 1, green), intermediate (Sigma 2, red), and minimum (Sigma 3, black) principal stresses as a function of radial distance along the heater mid-plane in the model with time. The evolution of the principal stresses is relatively monotonic with little to note other than at the end of the cool-down period at 22 days, when the minimum principal stress becomes compressive (the only time during this sequence when this occurs). These figures are shown for completeness and for perusal by the interested reader.

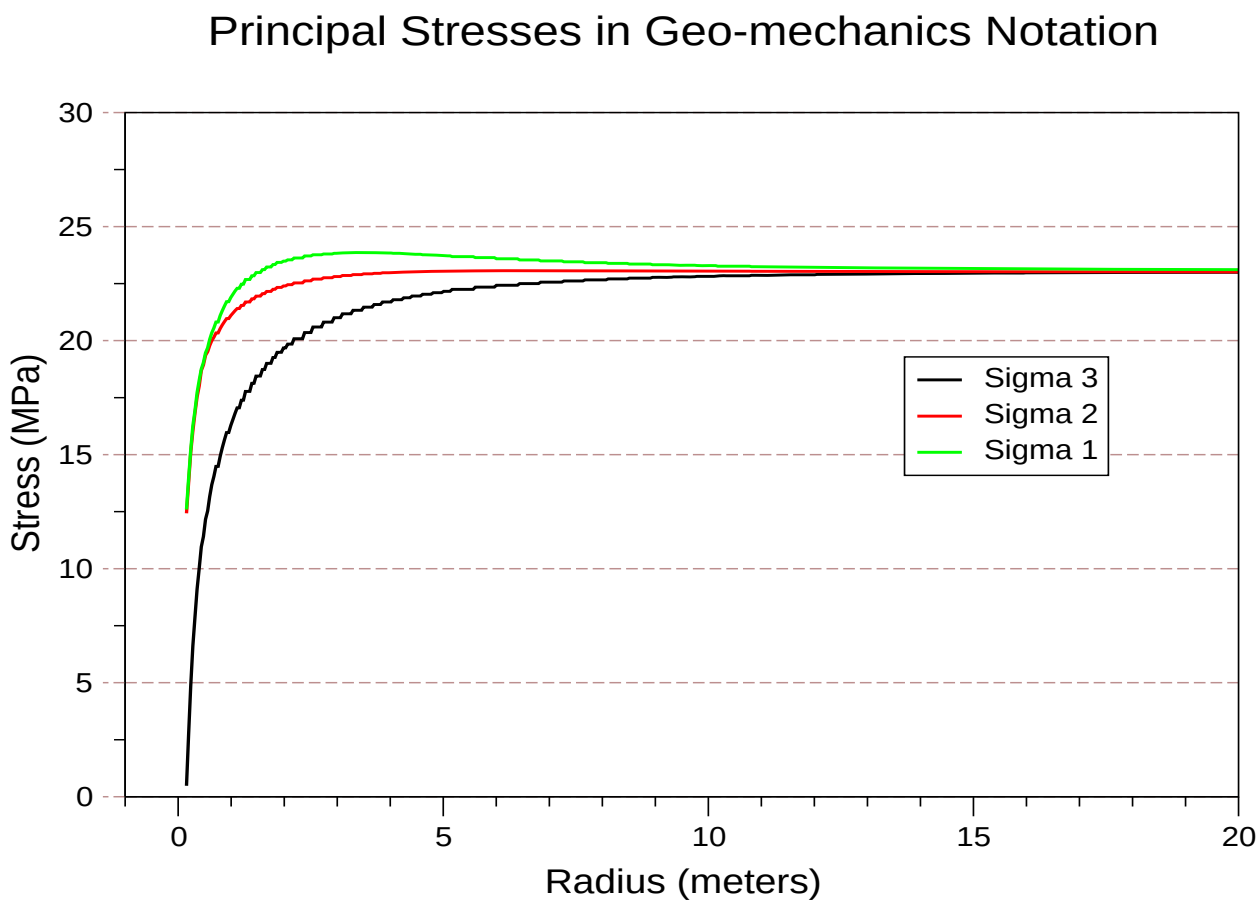

Figure 29. Horizontal Profiles at Heater Mid-Plane of Principal Stress at 0 days (In Geomechanics Notation)

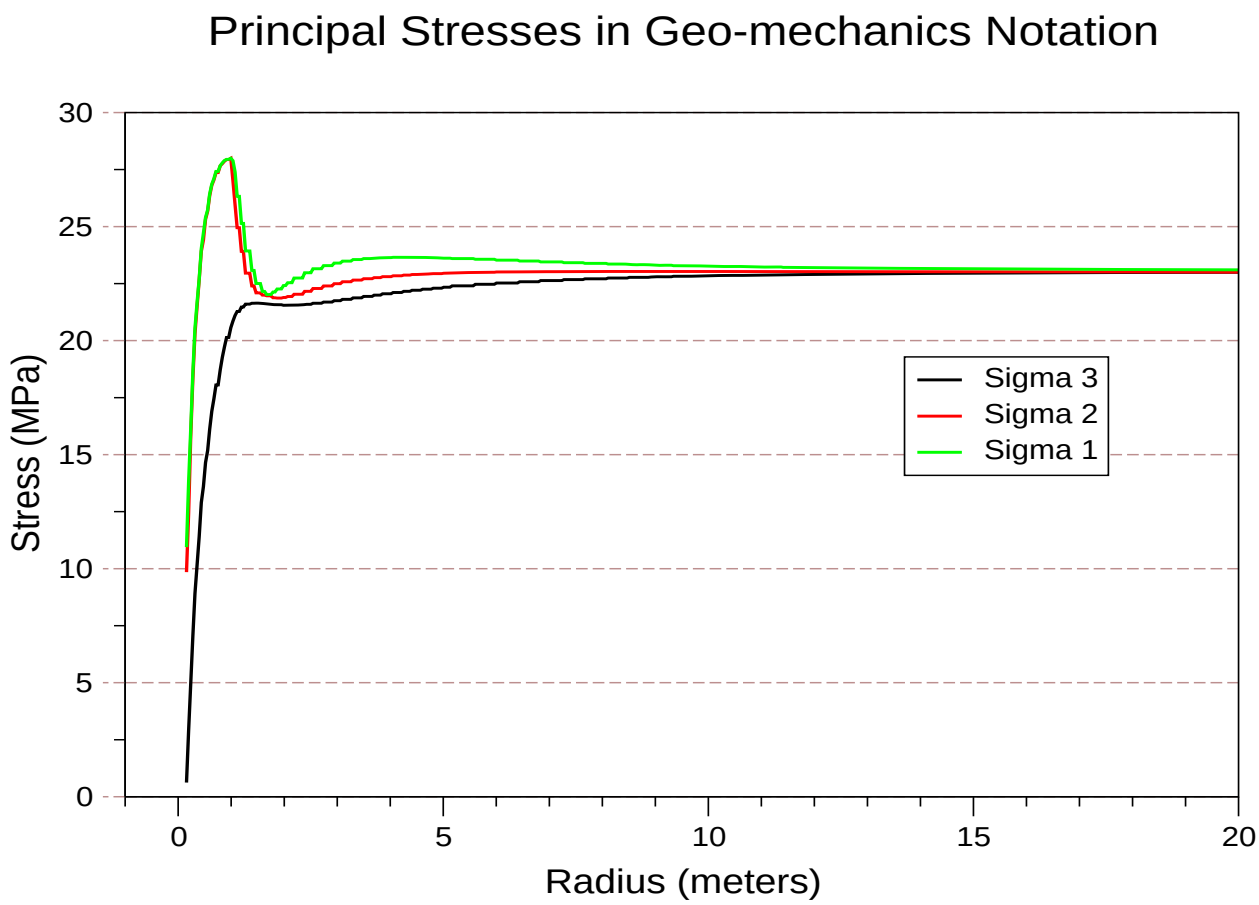

Figure 30. Horizontal Profiles at Heater Mid-Plane of Principal Stress at 1 days (In Geomechanics Notation)

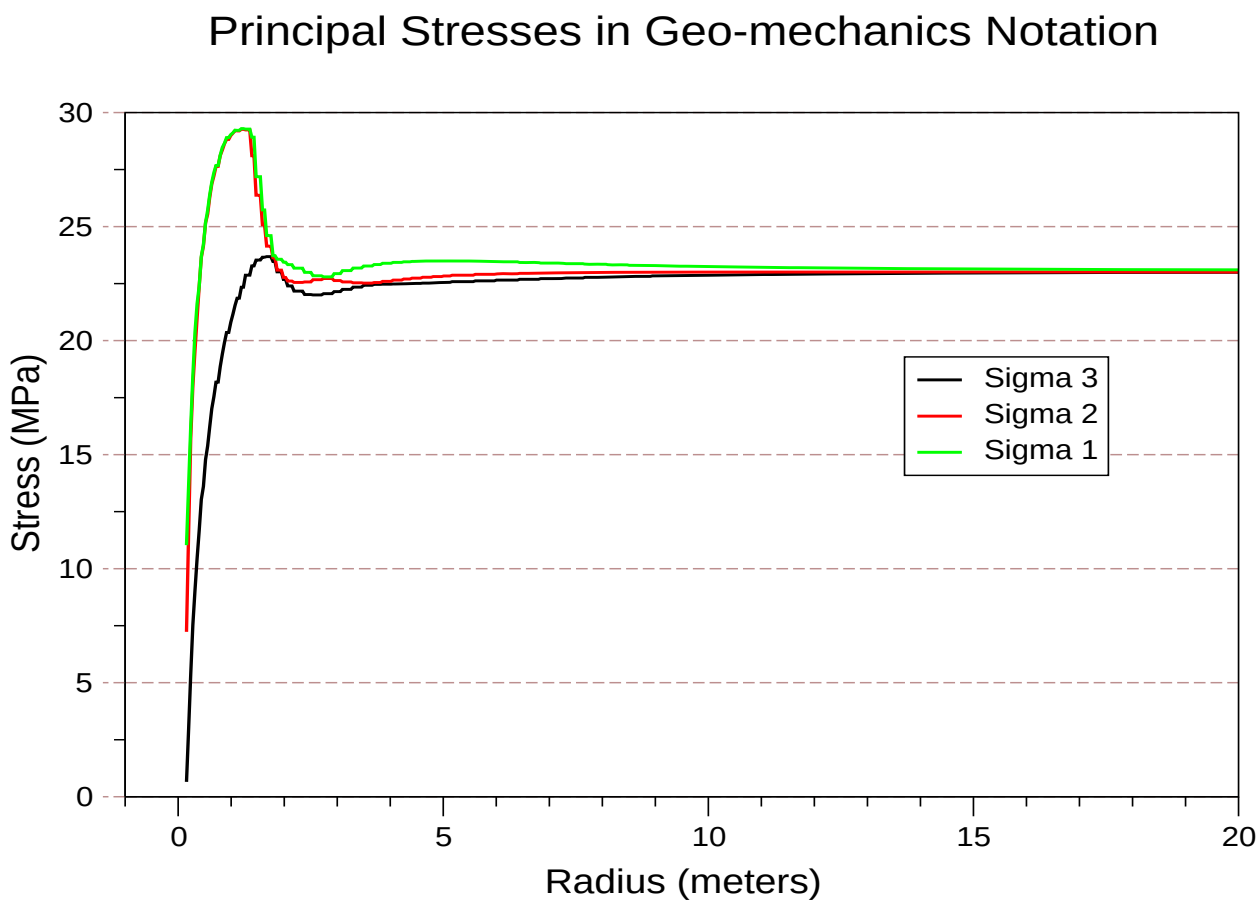

Figure 31. Horizontal Profiles at Heater Mid-Plane of Principal Stress at 2 days (In Geomechanics Notation)

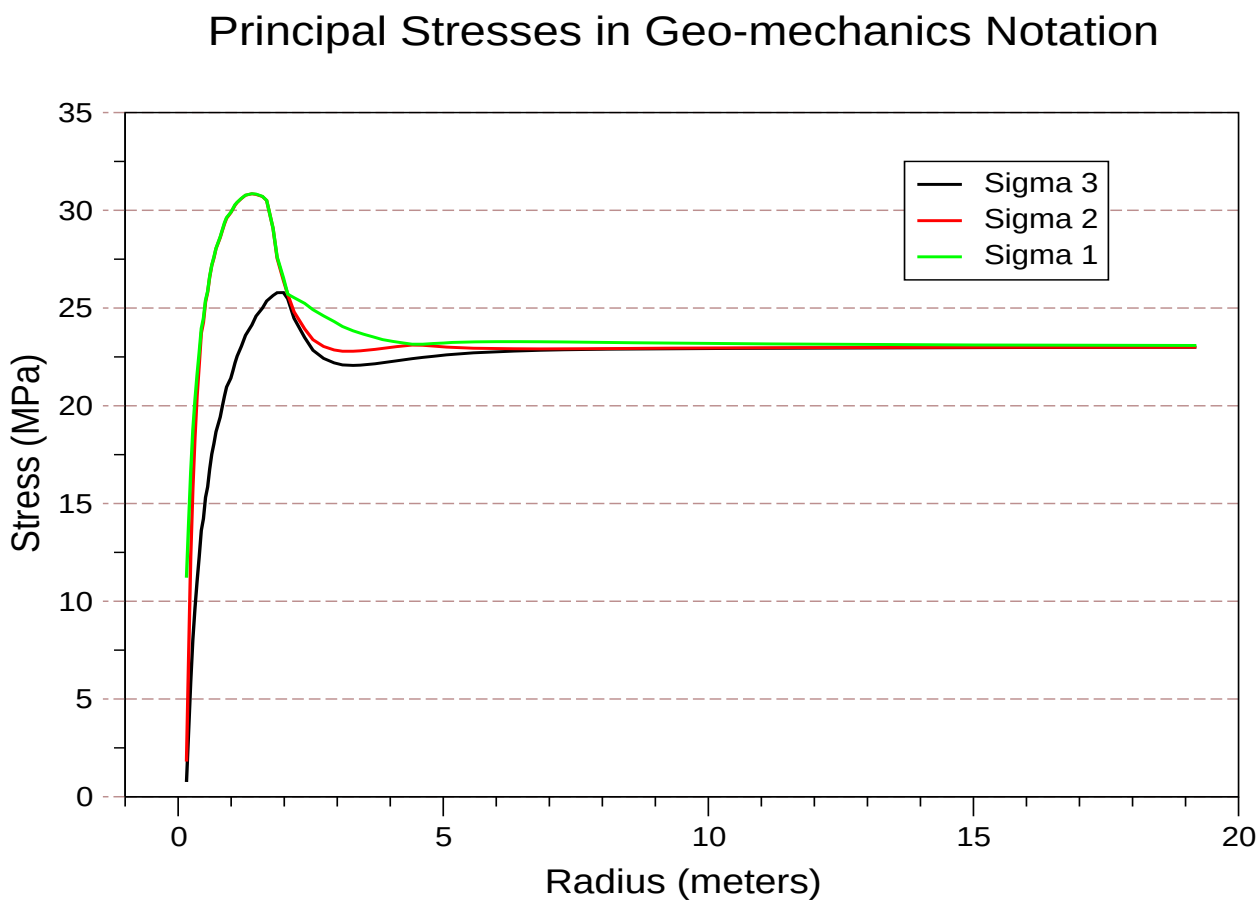

Figure 32. Horizontal Profiles at Heater Mid-Plane of Principal Stress at 4 days (In Geomechanics Notation)

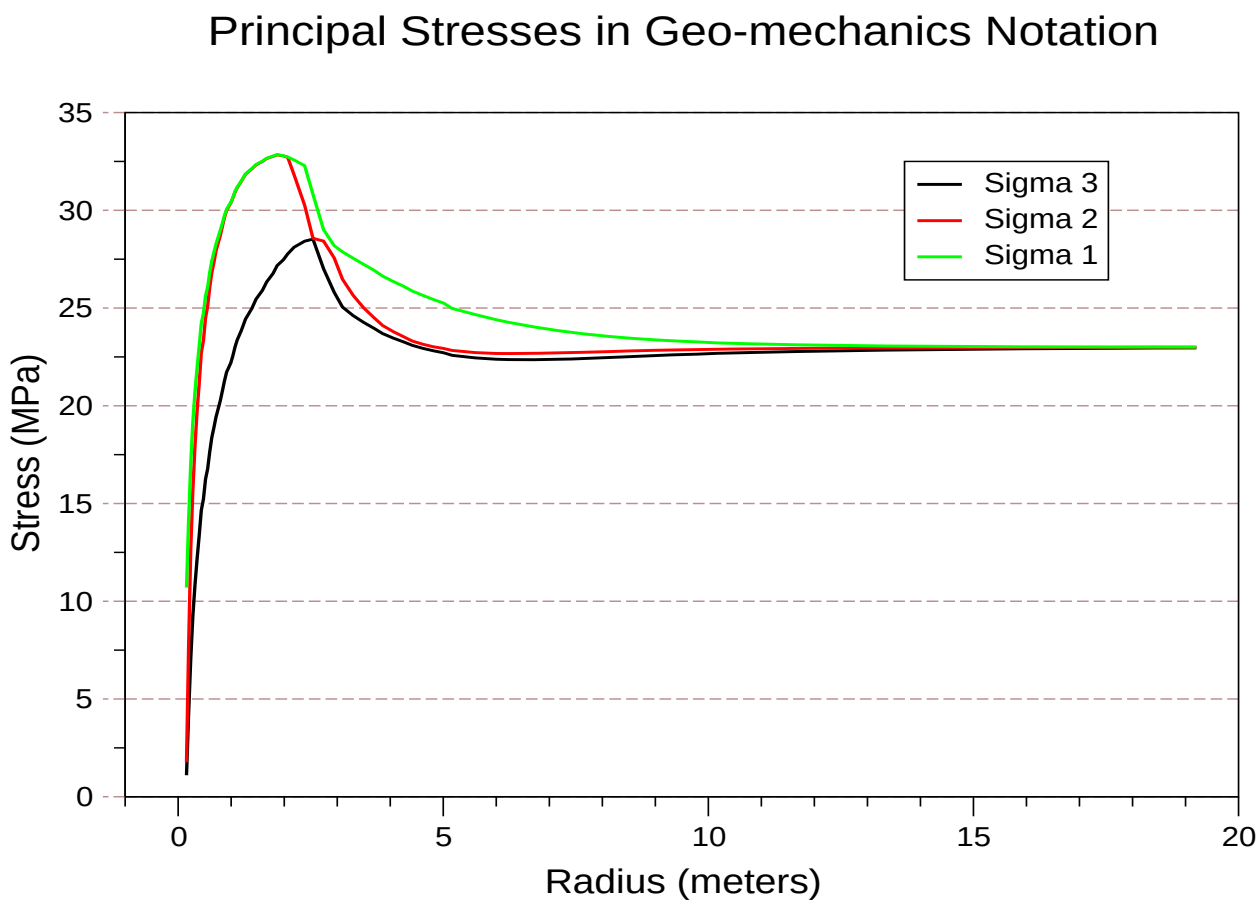

Figure 33. Horizontal Profiles at Heater Mid-Plane of Principal Stress at 8 days (In Geomechanics Notation)

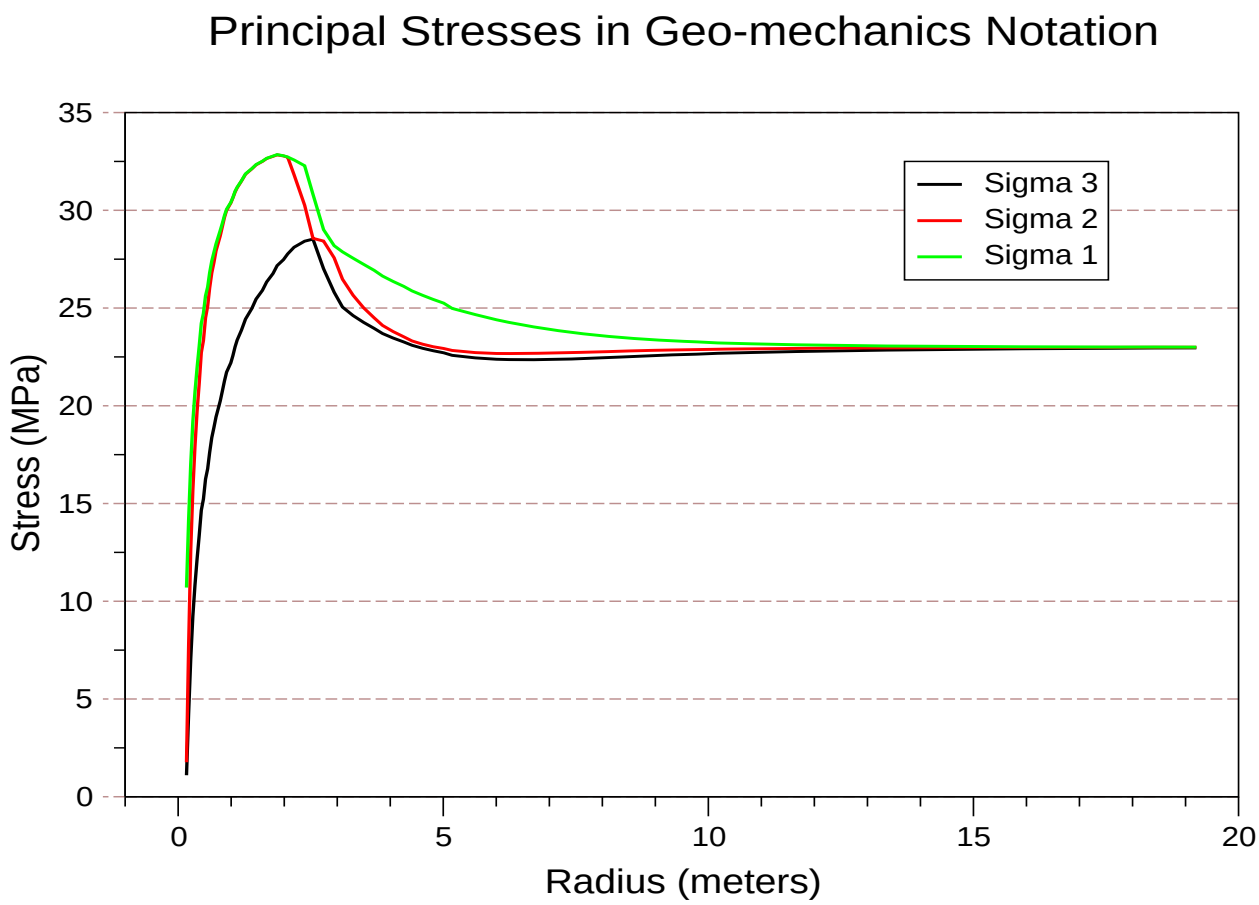

Figure 34. Horizontal Profiles at Heater Mid-Plane of Principal Stress at 15 days (In Geomechanics Notation)

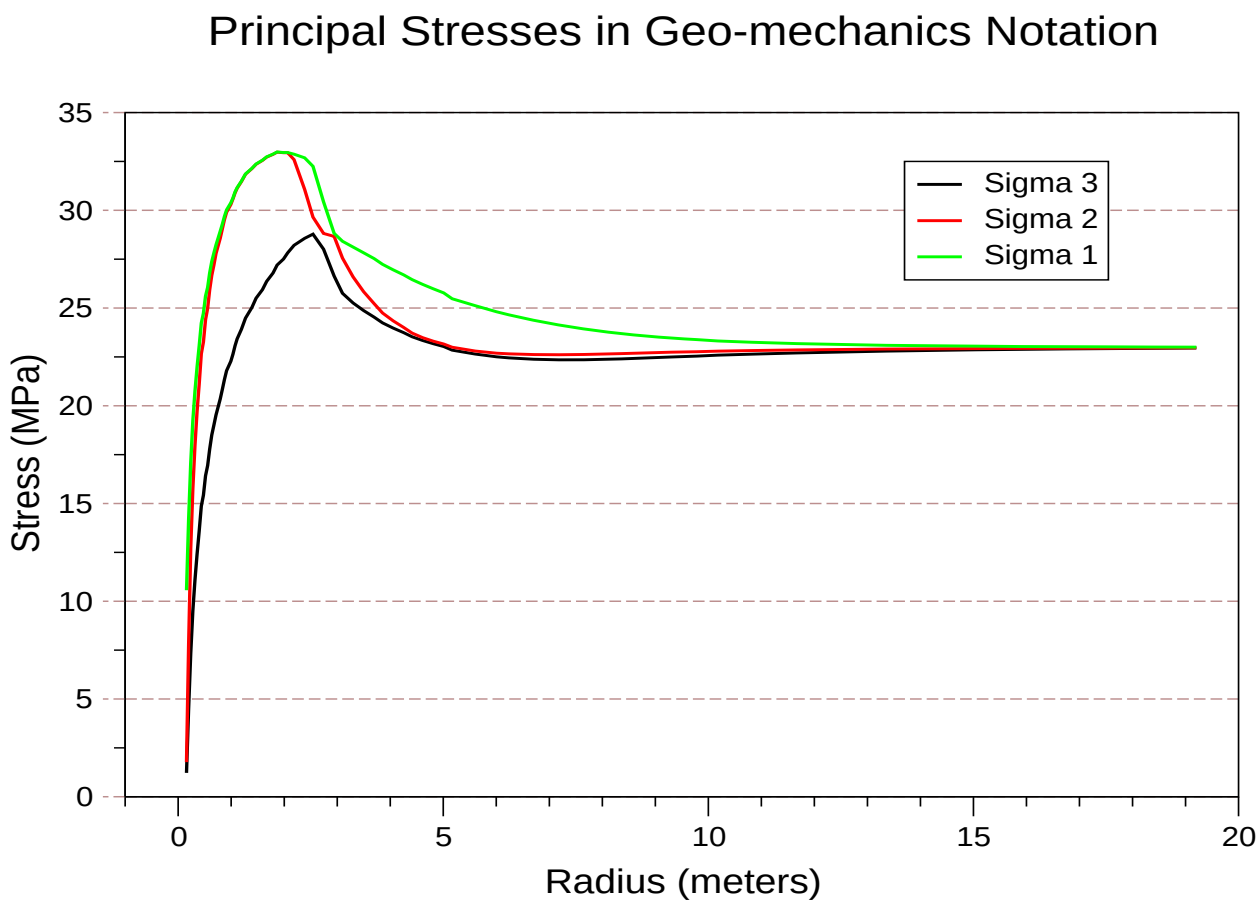

Figure 35. Horizontal Profiles at Heater Mid-Plane of Principal Stress at 19 days (In Geomechanics Notation)

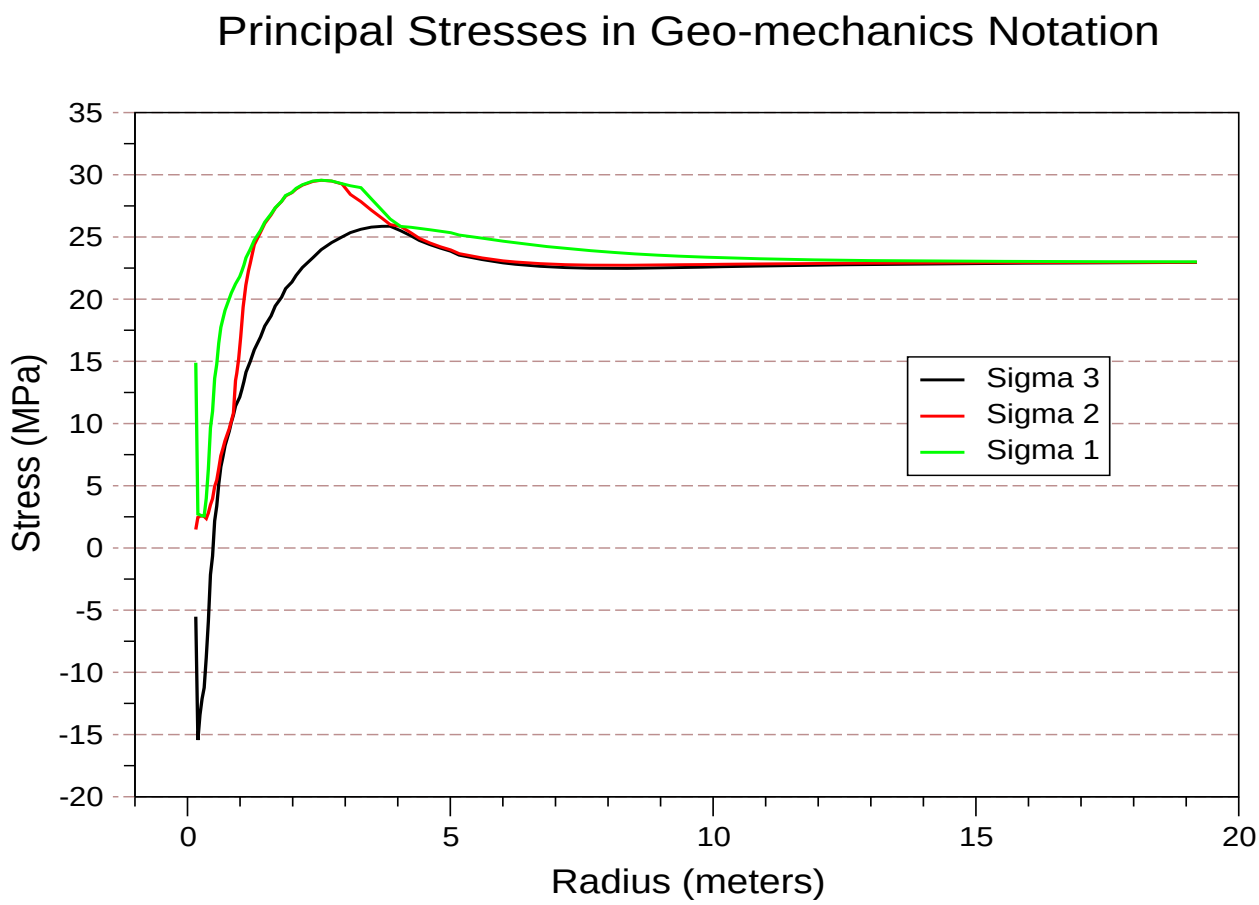

Figure 36. Horizontal Profiles at Heater Mid-Plane of Principal Stress at 22 days (In Geomechanics Notation)

Figures 37-39 show the radial displacement, equivalent creep strain, and creep strain rate profiles, respectively, as a function of vertical distance along the borehole wall from the bottom to the top of the model. Figure 37 shows that the radial displacement of material with distance quickly diminishes within the first 5 m from the heater mid-plane. Figure 38 shows that the equivalent creep strain in the configuration with vertical distance also quickly diminishes within the first 5 m from the heater mid-plane. Similarly, Figure 39 shows that the equivalent creep strain-rate in the configuration with distance also quickly diminishes within the first 5 m from the heater mid-plane.

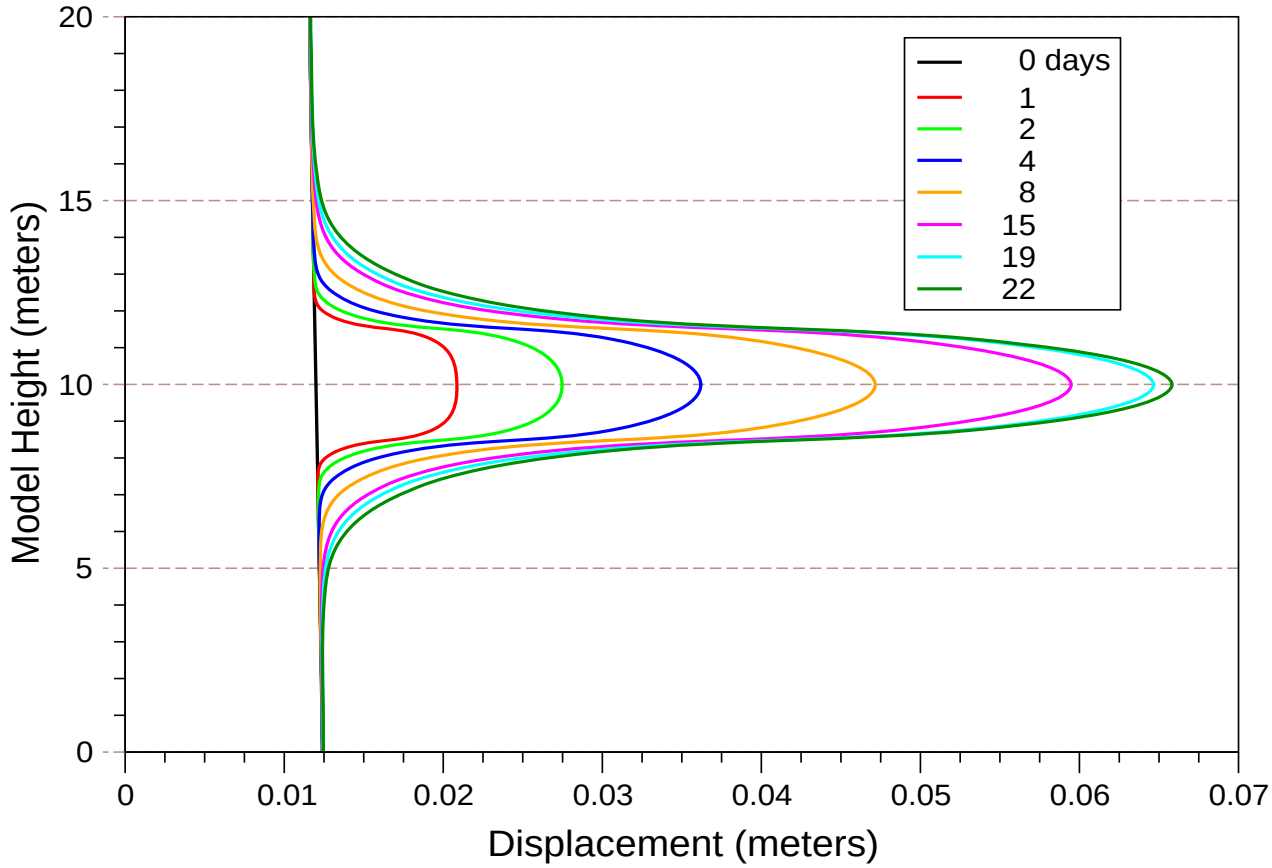

Figure 37. Vertical Profiles at Borehole Wall of Radial Displacement

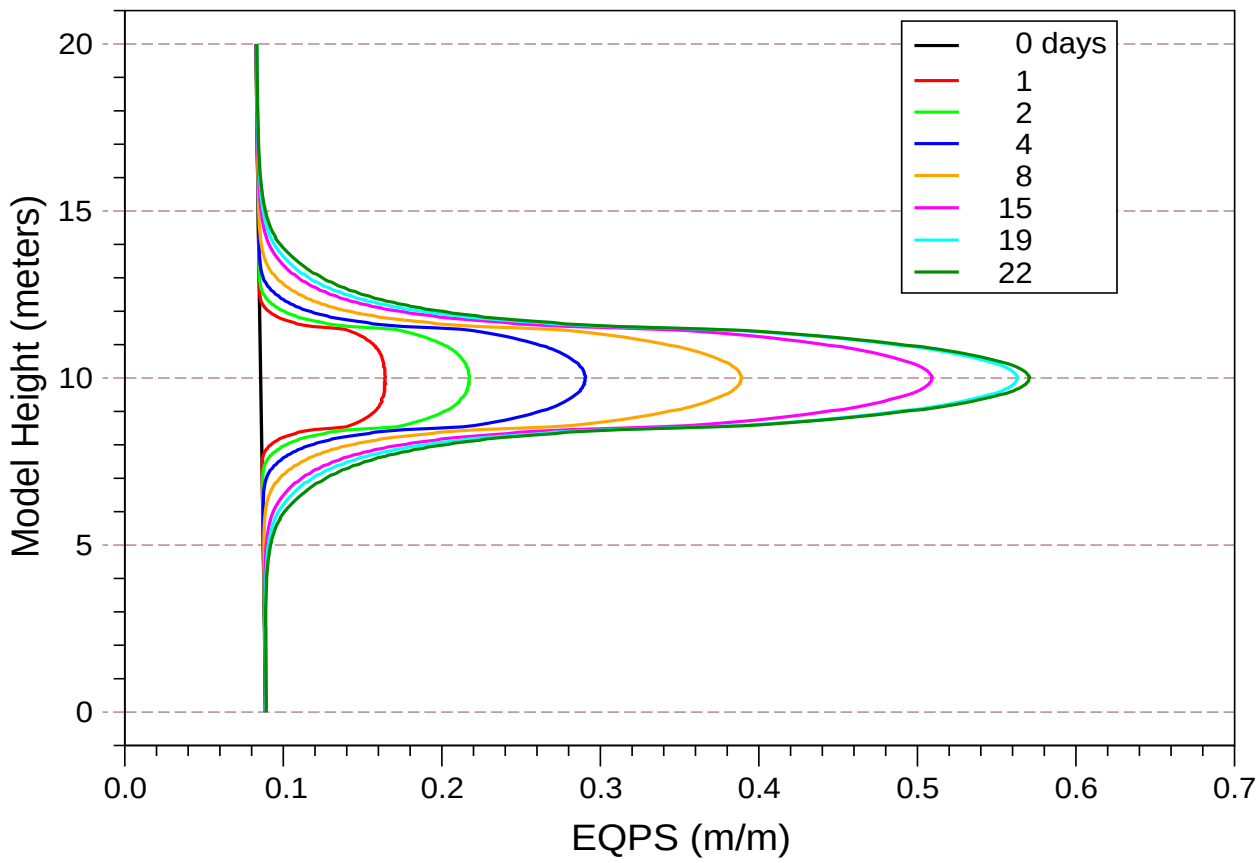

Figure 38. Vertical Profiles at Borehole Wall of EQCS

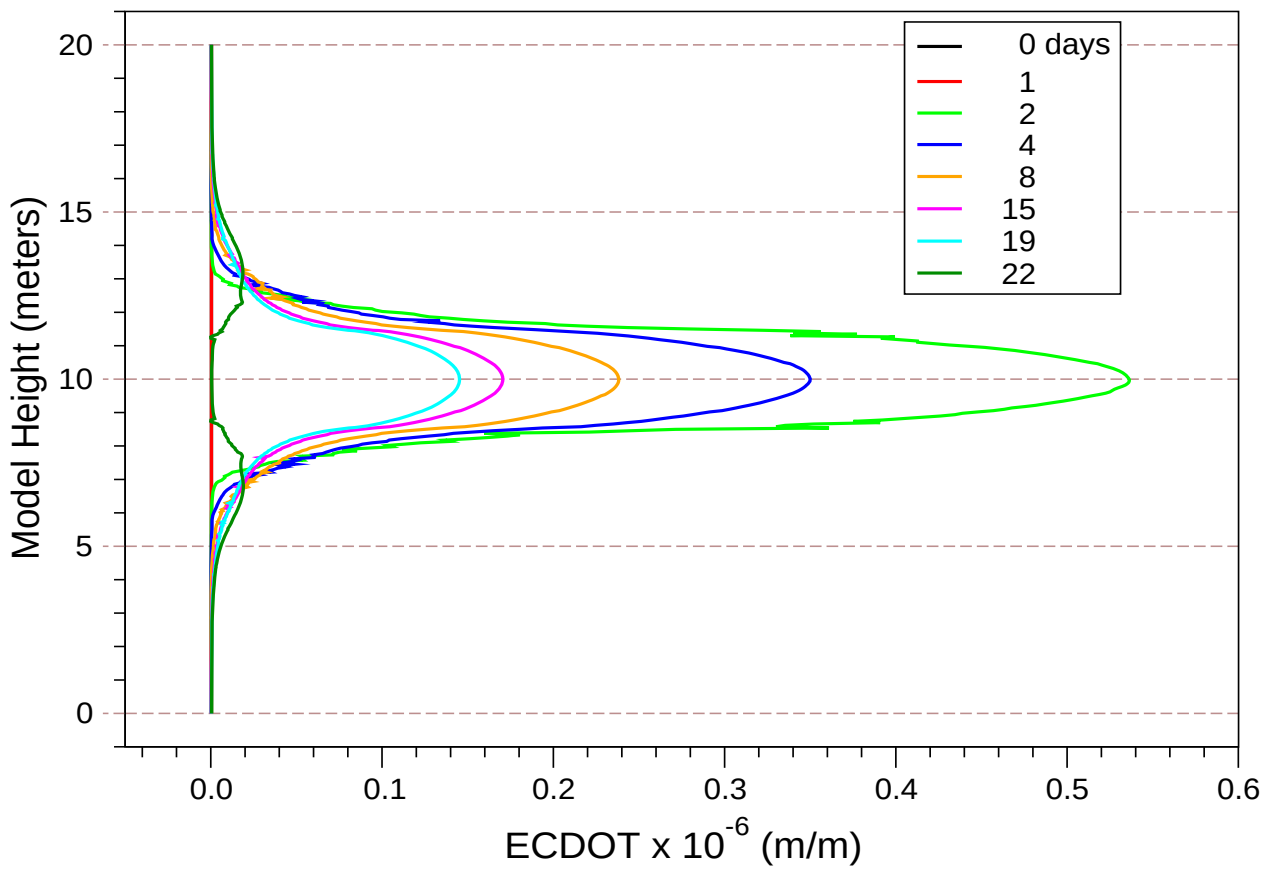

Figure 39. Vertical Profiles at Borehole Wall of Creep Strain Rate

As noted before for the horizontal profiles, it is difficult to show vertical profiles for the three principal stresses varying with time on the same figure. Consequently, the three principal stresses at each of 0, 1, 2, 4, 8, 15, 19, & 22 days are shown in Figures 40-47, respectively. These figures show the evolution of the maximum, intermediate, and minimum principal stresses as a function of vertical distance along the borehole wall from bottom to top of the model with time. The evolution of the principal stresses is relatively monotonic, after the first day, with little to note other than at the end of the cool-down period at 22 days, when the minimum principal stress becomes compressive (the only time during this sequence when this occurs). As before, these figures are shown for completeness and for perusal by the interested reader.

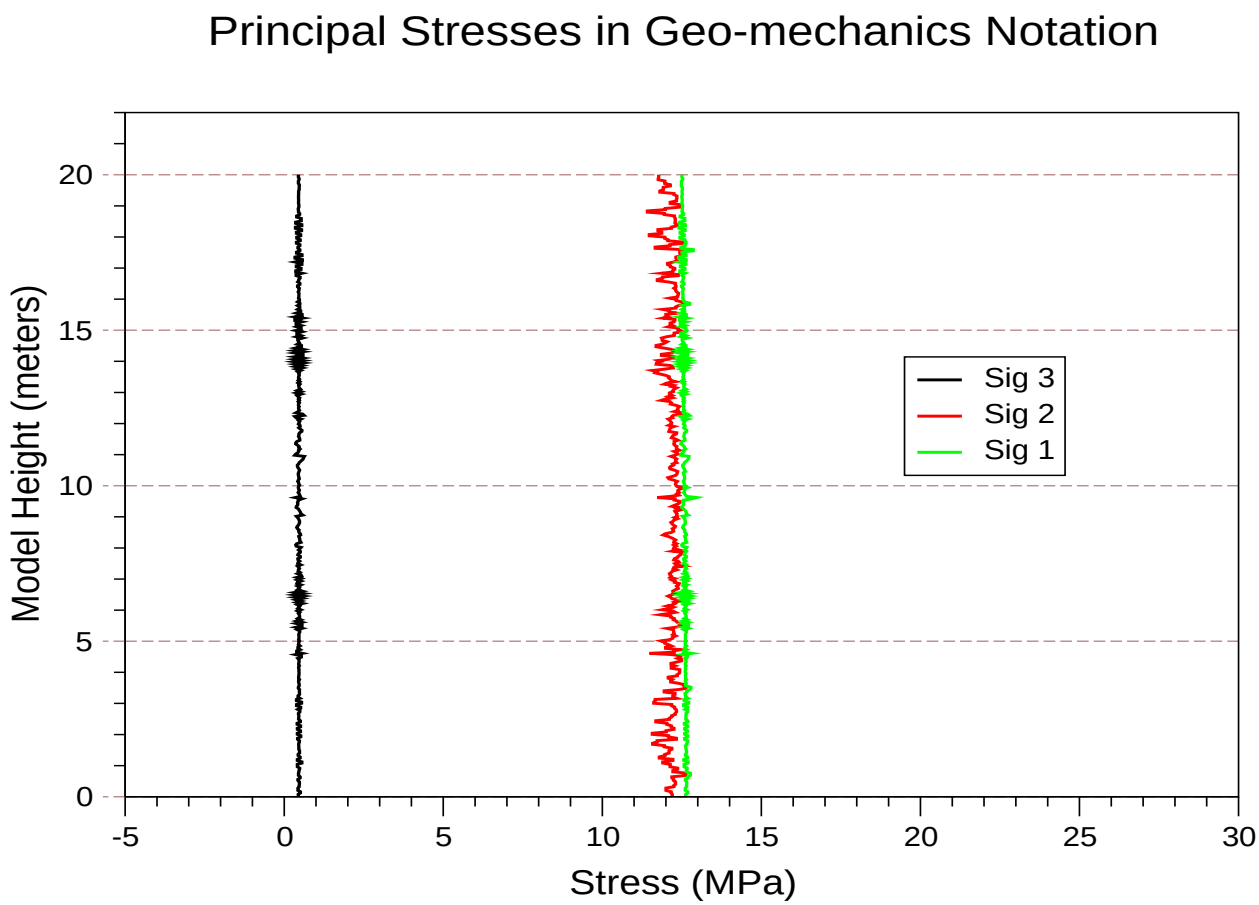

Figure 40. Vertical Profiles at Borehole Wall of Principal Stress at 0 days (In Geomechanics Notation)

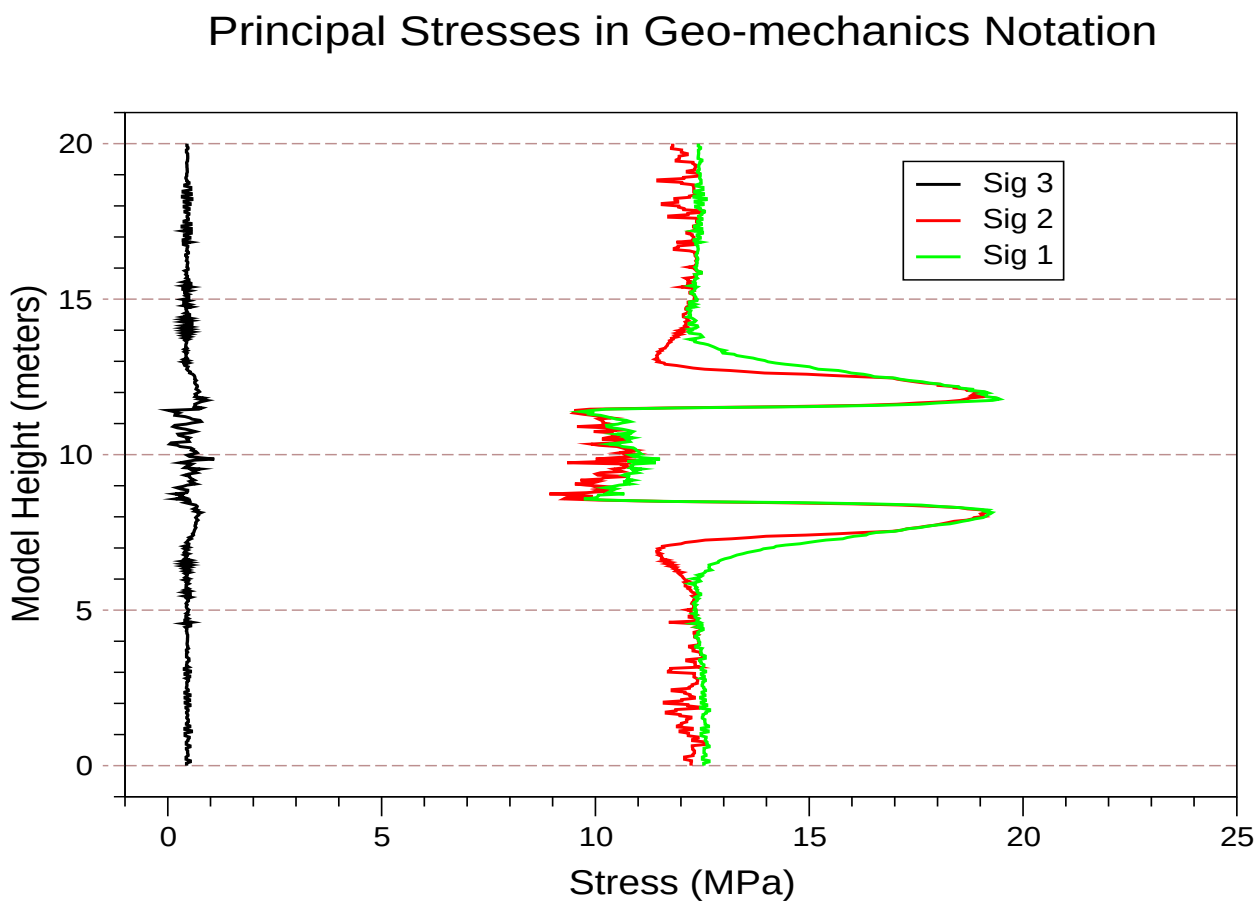

Figure 41. Vertical Profiles at Borehole Wall of Principal Stress at 1 days (In Geomechanics Notation)

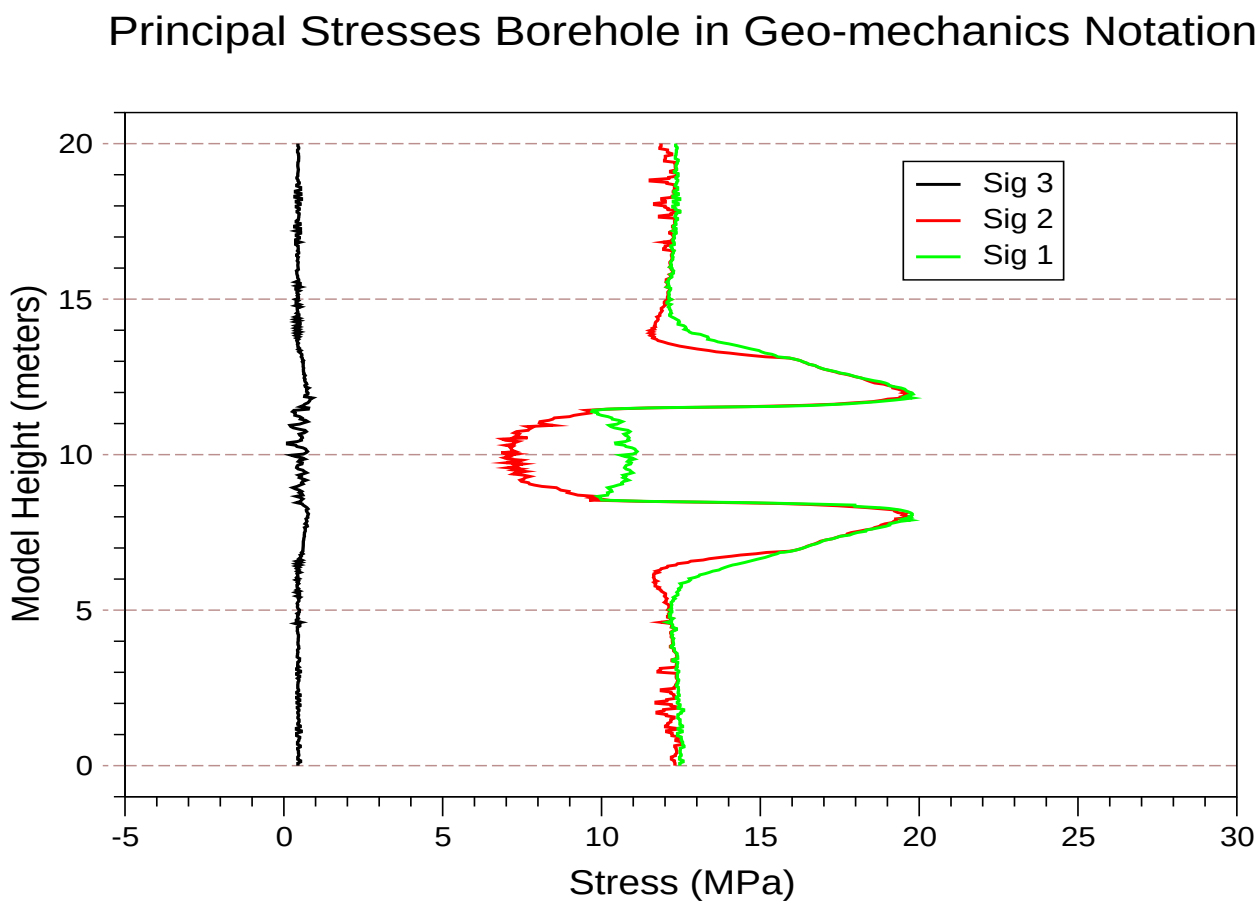

Figure 42. Vertical Profiles at Borehole Wall of Principal Stress at 2 days (In Geomechanics Notation)

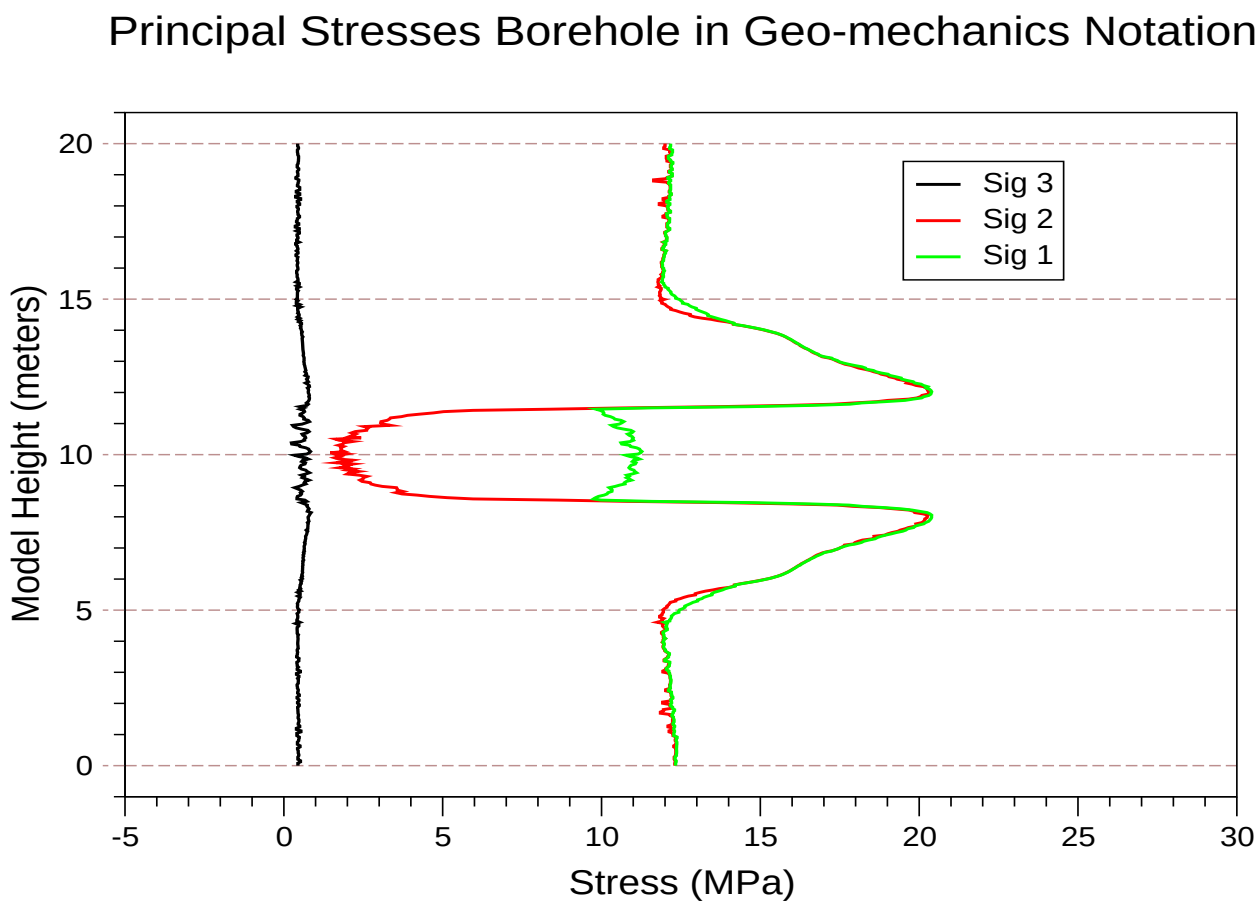

Figure 43. Vertical Profiles at Borehole Wall of Principal Stress at 4 days (In Geomechanics Notation)

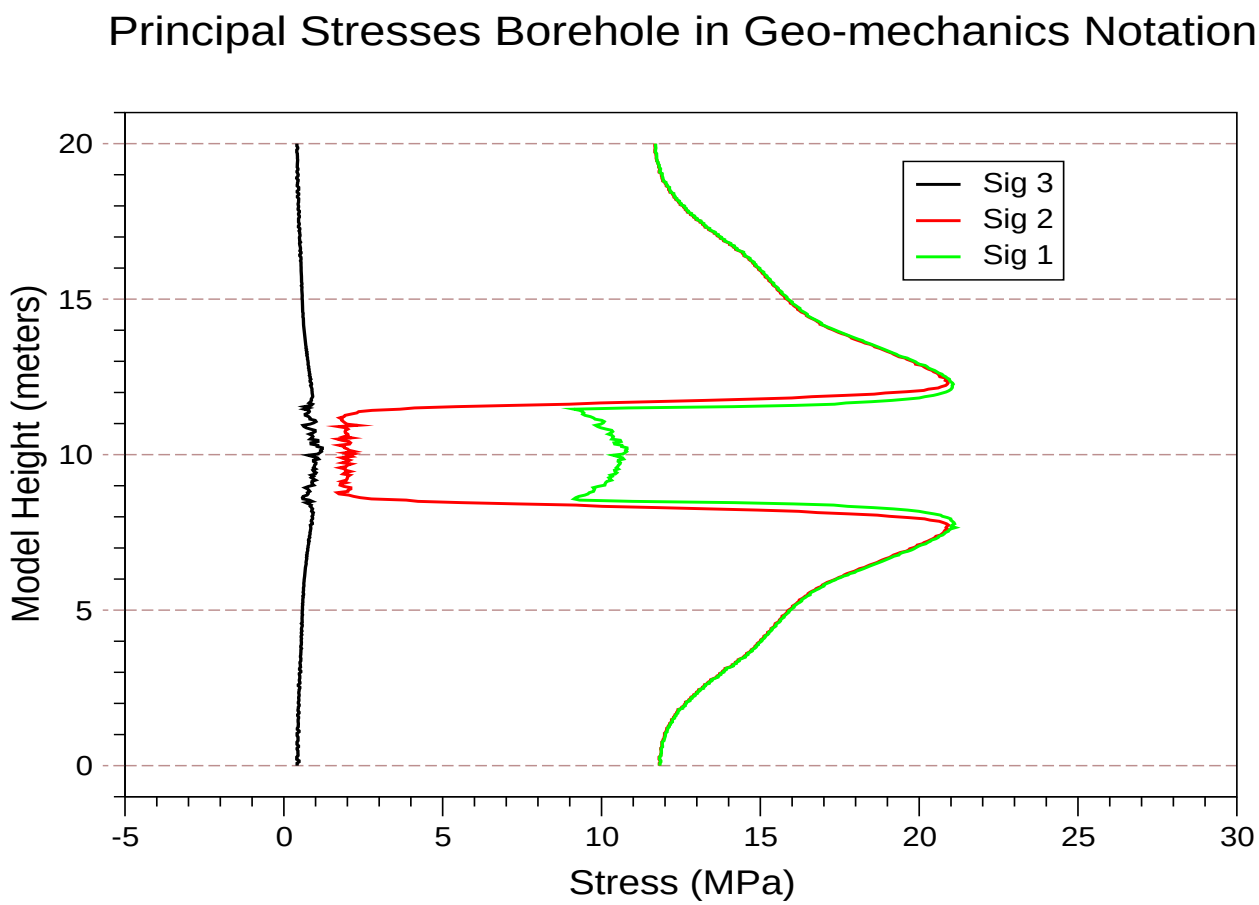

Figure 44. Vertical Profiles at Borehole Wall of Principal Stress at 8 days (In Geomechanics Notation)

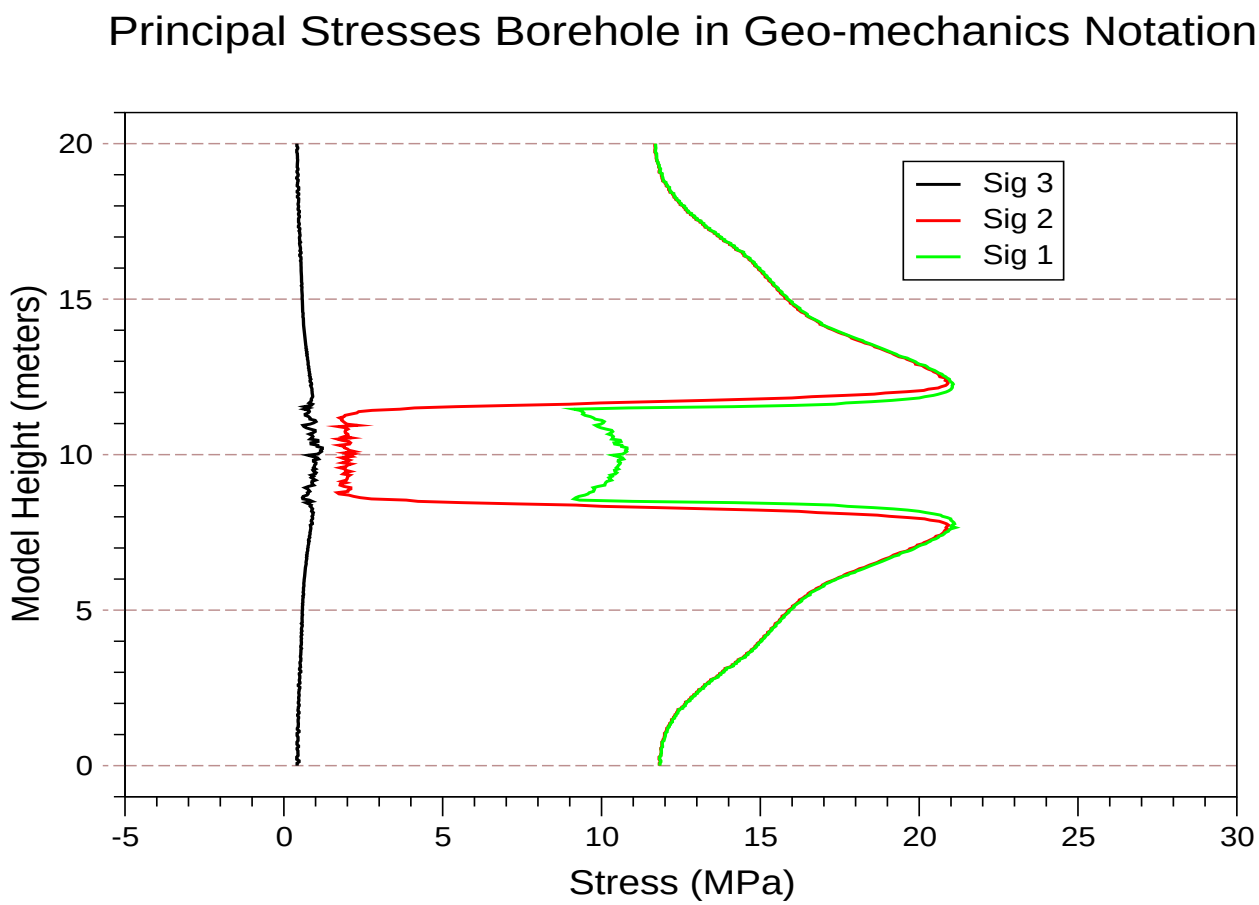

Figure 45. Vertical Profiles at Borehole Wall of Principal Stress at 15 days (In Geomechanics Notation)

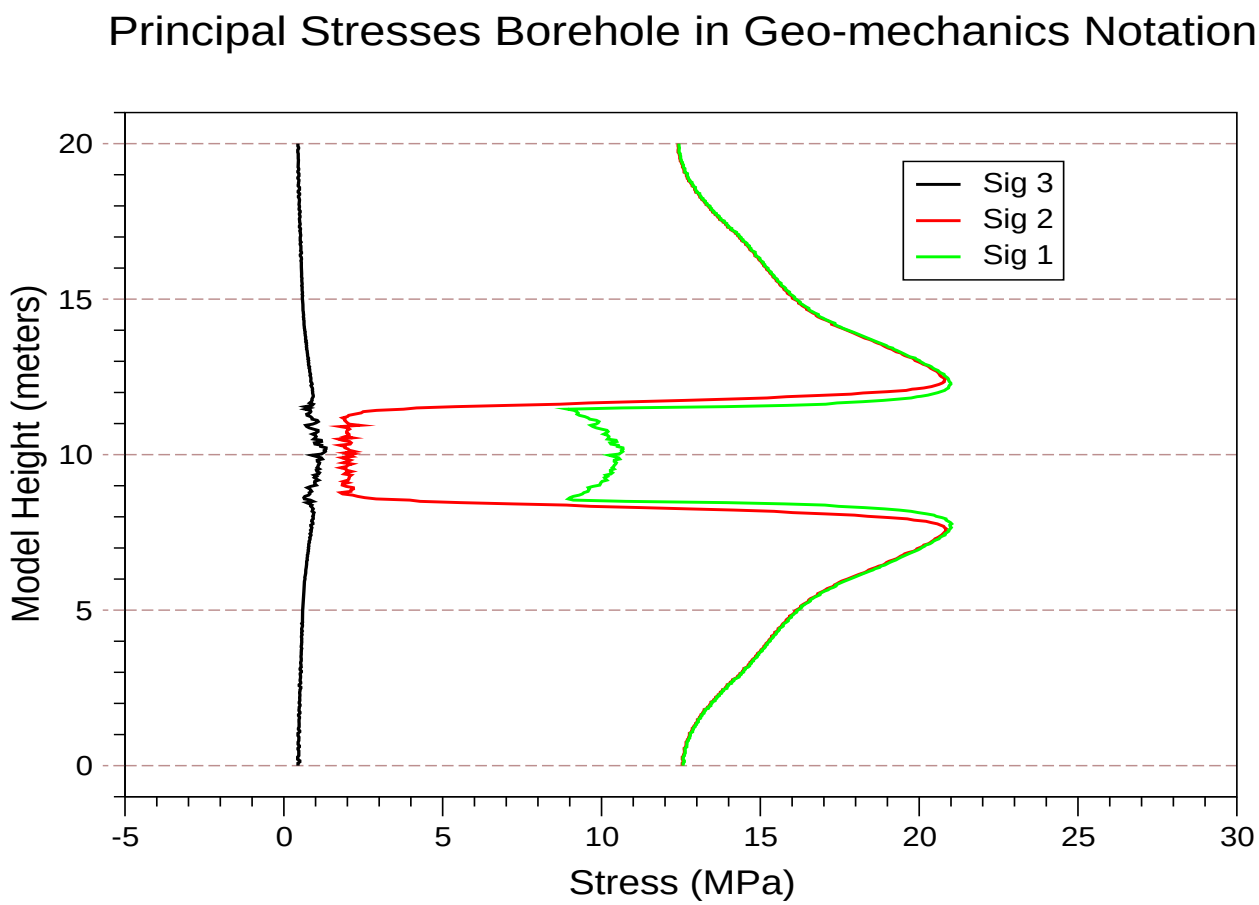

Figure 46. Vertical Profiles at Borehole Wall of Principal Stress at 19 days (In Geomechanics Notation)

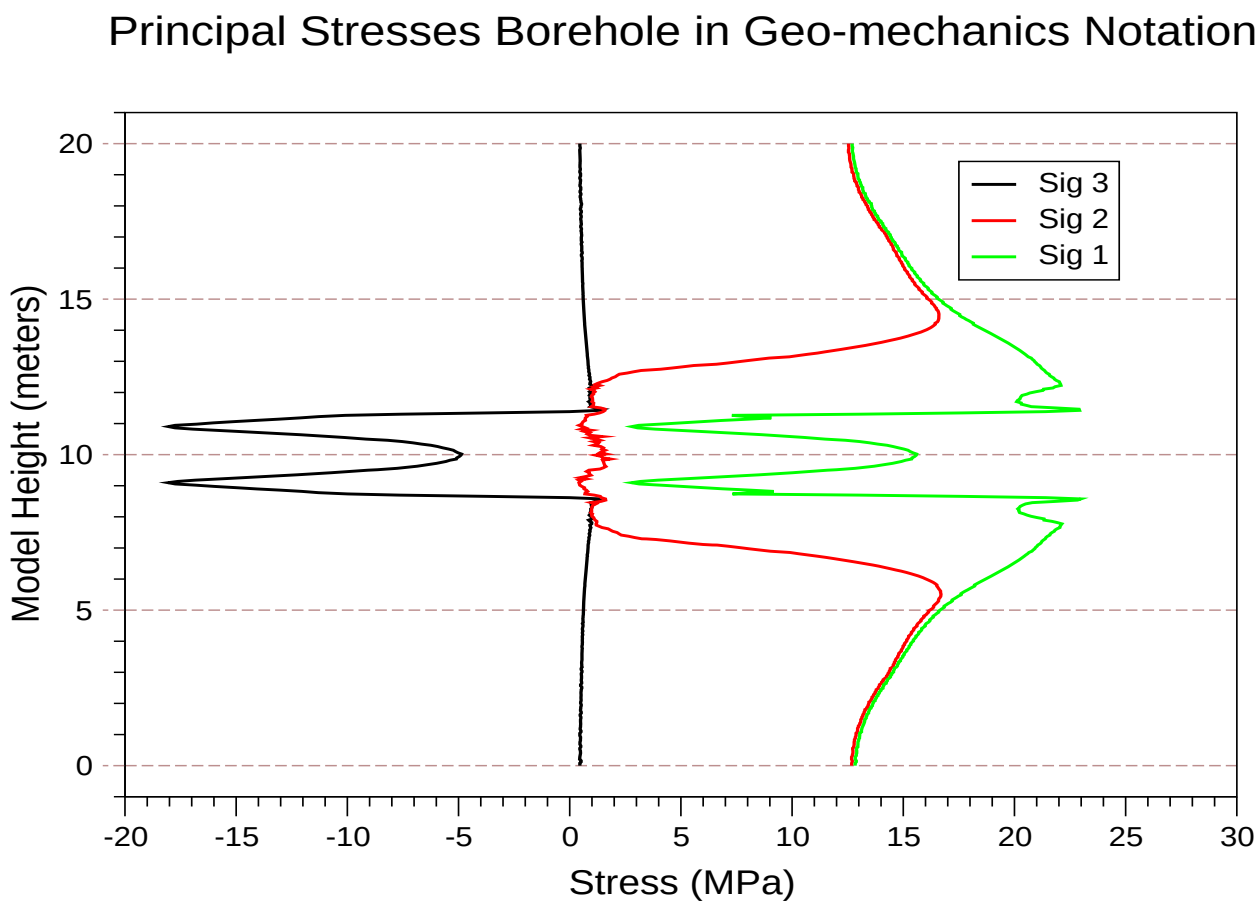

Figure 47. Vertical Profiles at Borehole Wall of Principal Stress at 22 days (In Geomechanics Notation)

After presentation of the various computed results in the previous figures, it is informative to compare the computed displacement profile of the borehole wall with the data collected from the ECN HFCP in-situ experiment. To this end, Figure 48 shows a comparison of the borehole profile with the measured data found in the COSA II report (Lowe & Knowles 1989, Fig. 6.9, p. 60). The displacements of the borehole wall profile are somewhat over-predicted, in general, by the computational model (on the order of 20-30% in the vicinity of the heater mid-plane).

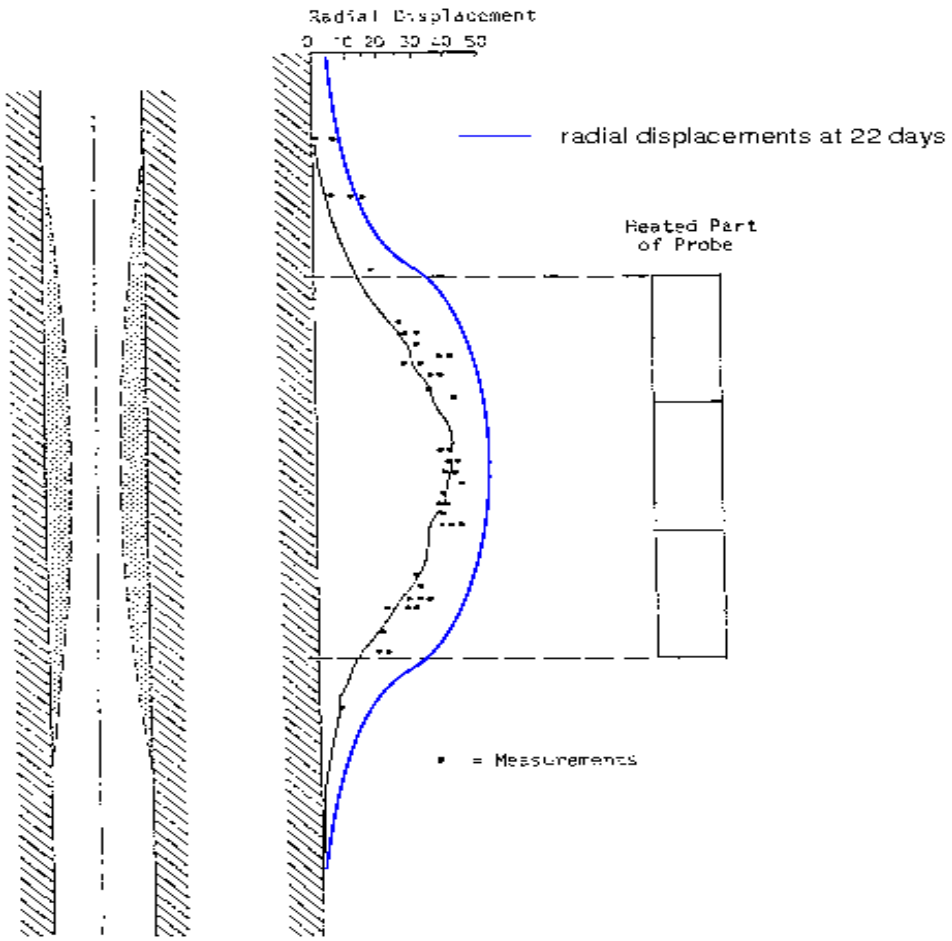

Figure 48. Comparison of COSA II Displacement Profile with Calculated Displacements

5. SUMMARY & CONCLUSIONS

The geomechanical modeling efforts and results for two benchmark calculations performed by Sandia National Laboratories (Sandia) under the third phase of an international joint project investigating the behavior of advanced geomechanical constitutive models for rock salt have been described and discussed in this report. As noted, Sandia joined the third phase of the project in FY2011 and is a contributing partner to this U.S./German joint effort entitled "Comparison of current constitutive models and simulation procedures on the basis of model calculations of the thermo-mechanical behavior and healing of rock salt".

The benchmark calculations that have been reported in this document were aimed at numerically simulating the response of two experiments conducted in the late-1970 to early-1980's timeframe in the 300 m deep "Dutch borehole" in the Asse Mine in Germany. Among the experiments performed in the mine was a series of borehole tests conducted by the Netherlands Energy Research Foundation ECN. These experiments were all performed in a single 300 mm (approximate) diameter borehole drilled from an open chamber at a level 750 m below the ground surface in the mine to a total depth of 1050 m below the ground surface.

The borehole was drilled at the end of 1979 and allowed to converge freely, as a consequence of salt creep-induced closure, without restraint or heating (the so-called isothermal free convergence, or IFC) until June 1982. From June 1982 until mid-1985 several heated experiments were then conducted at different depths in the borehole. Among the heated experiments was the so-called heated free convergence probe (HFCP) experiment. The two benchmarks that have been described in this report are associated with the free convergence period (IFC) and one of the heated experiments (HFCP).

The IFC analyses were conducted with two models. One was a computationally fast 5° Slice Model that was used in a mesh sensitivity/convergence study to provide confidence in the numerically predicted results from the second model. The second numerical model was a Quarter-Borehole Model from which the final IFC benchmark results were obtained and reported. The IFC benchmark calculation was an isothermal calculation that allowed for the adjustment of the MD Creep Model parameters, derived from laboratory-based test data, in order to match (as closely as possible) the in-situ radial displacement results from the fielded IFC experiment. By adjusting the secondary creep parameter (i.e., A2) in the MD model, the simulation results for radial displacement were extremely well-matched to the in-situ experimental results. No further adjustments to the MD model parameters were made in performing the second HFCP benchmark calculation.

The HFCP benchmark analyses used a single computational model with a comparable degree of mesh refinement to that of the IFC Quarter-Borehole Model. This model was run isothermally for 1309 days, prior to initiating the application of the heat load (simulating the heaters in the experiment). It was then run for an additional 19 days with the heat load on, followed by a three day cool-down period. Results from the HFCP computational model showed that, as expected, the central portion of salt in the configuration becomes the most heated and involved in the evolution of the deformation of the borehole. In spite of the various uncertainties in the test and

in the specification of the problem, the computed borehole displacement profile is in reasonable agreement with the in-situ data.

6. REFERENCES

Argüello, J.G. & Rath, J.S. 2012. SIERRA Mechanics for Coupled Multi-Physics Modeling of Salt Repositories, In P. Bérest, M. Ghoreychi, F. Hadj-Hassen, M. Tijani (eds), *Mechanical Behavior of Salt VII*. London: Taylor & Francis Group.

CUBIT, 2012. "A Finite Element Method Meshing Tool," Sandia National Laboratories: Albuquerque, NM. Version 13.1, Build 47471.

DeVries, K.L. 2011. Munson-Dawson Model Parameter Estimation of Sondershausen and Asse Salt. RESPEC Technical Memorandum to T. W. Pfeifle of Sandia National Laboratories, January 25, 2011.

Doeven, I., Soullié, P.P., & Vons, L.H. 1983. Convergence Measurements in the Dry-Drilled 300 m Borehole in the Asse-II Saltmine. *European Appl. Res. Rept. – Nucl. Sci. Technol.*, 5(2):267-324.

Edwards, H.C. & Stewart, J.R. 2001. SIERRA: A Software Environment for Developing Complex Multi-Physics Applications. In K.J. Bathe (ed.), *First MIT Conference on Computational Fluid and Solid Mechanics*. Amsterdam: Elsevier.

Hampel, A. 2010a. Outline of the joint project "Comparison of current constitutive models and simulation procedures on the basis of model calculations of the thermo-mechanical behavior and healing of rock salt." Personal Communication: attachment to e-mail of Thursday, April 29, 2010 to Francis D. Hansen, Sandia National Laboratories.

Hampel, A. 2010b. Comparison of Constitutive Models "Joint project I (2004-2006) Tables and Figures (translated for Sandia) taken from A. Hampel (2006): Final scientific report to joint project I, Essenheim." Personal Communication: attachment to e-mail of Wednesday, September 29, 2010 to Francis D. Hansen, Sandia National Laboratories.

Lowe, M.J.S. & Knowles, N.C. 1989. COSA II Further benchmark exercises to compare geomechanical computer codes for salt. EUR 12135, Commission of the European Communities, Nuclear Science and Technology, W.S. Atkins Engineering Sciences, Epsom, Surrey, U.K.

Munson, D.E. & Dawson, P.R. 1979. Constitutive Model for the Low Temperature Creep of Salt (With Application to WIPP). SAND79-1853, Sandia National Laboratories, Albuquerque, NM.

Munson, D.E. & Dawson, P.R. 1982. A Transient Creep Model for Salt during Stress Loading and Unloading. SAND82-0962, Sandia National Laboratories, Albuquerque, NM.

Munson, D.E. & Dawson, P.R. 1984. Salt Constitutive Modeling using Mechanism Maps. *Proc. 1st International Conference on the Mechanical Behavior of Salt*, Clausthal-Zellerfeld: Trans Tech Publications.

Munson, D.E., Fossum, A.F., & Senseny, P.E. 1989. Advances in Resolution of Discrepancies between Predicted and Measured in Situ WIPP Room Closures. SAND88-2948, Sandia National Laboratories, Albuquerque, NM.

Munson, D.E. 1979. Preliminary Deformation-Mechanism Map for Salt (with Application to WIPP). SAND70-0079, Sandia National Laboratories, Albuquerque, NM.

Notz, P.K., Subia, S.R., Hopkins, M.M., Moffat, H.K., & Noble D.R. 2007. Aria 1.5: User Manual. SAND2007-2734, Sandia National Laboratories, Albuquerque, NM.

Prij, J., Jansen, D., Klerks, W., Luyten, G.B., de Ruiter, A., Vons, L.H. 1986. Measurements in the 300-metre deep dry-drilled borehole and feasibility study on the dry-drilling of a 600-metre deep borehole in the Asse II salt-mine. EUR 10737, Commission of the European

Communities, Nuclear Science and Technology, Netherlands Energy Research Foundation ECN, Petten.

SIERRA Solid Mechanics Team. 2010. Adagio 4.18 User's Guide. SAND2010-6313, Sandia National Laboratories, Albuquerque, NM.

Scherzinger, W.A., & Hammerand, D.C. 2007. "Constitutive Models in LAME," SAND2007-5873, Sandia National Laboratories: Albuquerque, NM.

Stone, C.M., Holland, J.F., Bean, J.E., & Argüello, J.G. 2010. Coupled Thermal- Mechanical Analyses of a Generic Salt Repository for High-Level Waste (ARMA-10-180). *Proc. American Rock Mechanics Association (ARMA) 44th US Rock Mechanics Symposium*, 27-30 June 2010. Salt Lake City: American Rock Mechanics Association.

APPENDIX A: SPECIFICATION OF BENCHMARK PROBLEMS

Information and specifications for all project partners regarding the benchmark calculation models of the ECN borehole experiments IFC and HFCP in the Asse Mine

author: K. Herchen (TUC), revised and completed by A. Hampel und R.-M. Günther,
Date: 24.08.2011, translated for Sandia by A. Hampel, 26.01.2012

1.) IFC (isothermal free convergence benchmark)

Calculation model:
quarter disc or wedge-shaped model with outside radius of 20 m,
initial borehole diameter: 315 mm (radius 15.75 cm).

Discretizations with different fineness in radial direction

optional: different vertical discretizations: 1 layer / 10 layer model with different model heights, among them 1 m model height for comparisons with partner results.

Model center in vertical direction at depth z = -1042 m (borehole depth: 292 m),
rock temperature: 42 °C, constant over entire model height,
initial stress: 24 MPa (isotrop).

The simulation results shall be compared at z = -1042 m with following measured data (COSA II report, p. 48):

Time (days)	Radial Displacement (mm)	Time (days)	Radial Displacement (mm)
3.5	0.38	301.1	4.82
5.5	0.54	321.5	5.00
7.6	0.66	340.6	5.16
10.7	0.83	360.2	5.31
12.8	0.92	380.1	5.48
14.9	1.00	406.6	5.70
16.5	1.07	420.2	5.82
18.6	1.15	441.0	5.74
20.5	1.21	461.6	5.88
22.4	1.27	480.9	6.02
36.6	1.65	501.0	6.16
41.1	1.75	522.1	6.30
46.6	1.86	541.7	6.45
50.4	1.94	554.6	6.54
55.4	2.04	580.6	6.97
61.5	2.14	602.0	7.09
71.6	2.32	638.4	7.34
121.4	3.00	661.1	7.48
131.2	3.11	682.2	7.62
140.9	3.23	701.5	7.75
150.8	3.34	723.7	7.89
171.4	3.57	737.6	7.98
202.2	3.88	760.0	8.12
221.2	4.07	780.2	8.25
240.0	4.25	800.4	8.38
263.2	4.50	834.3	8.59
280.1	4.64		

Table 6.1 A Selection of IFC Convergence Measurements at 292 metres depth

Main objective of IFC calculation is the optimal parameter determination for each constitutive model.

In the following calculations of the HFCP these parameter values for the constitutive models shall be applied. Please do not change the parameter values anymore!!

2.) HFCP (heated free convergence probe benchmark)

COSA II report, p. 57

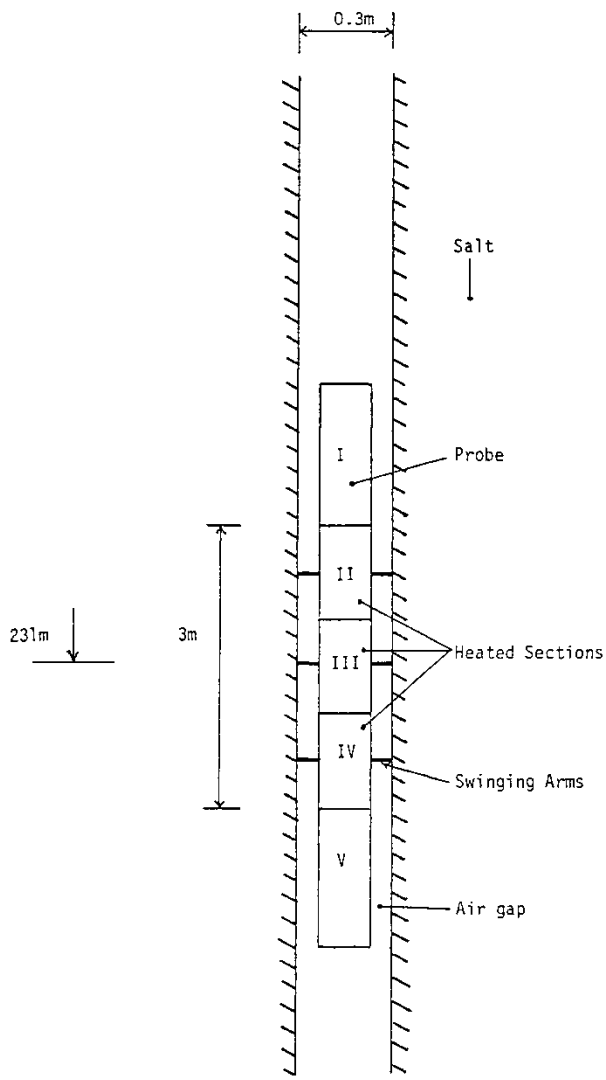

Figure 6.6 Illustration of Heated Free Convergence Probe (HFCP)

Calculation model:
quarter disc or wedge-shaped model with outside radius 20 m (min. 15 m),
total model height: 20 m,
model center and center of heated zone in vertical direction at depth z = -981 m ((borehole depth: 231 m),
initial borehole diameter: 315 mm (radius 15.75 cm),

initial rock temperature: 40.8 °C (T = 313.95 K) corresponding to depth z = -981 with 0.02 K/m compared to 42 °C at -292 m (IFC); constant over entire model height.

Calculation of equilibrium of the compact model (borehole still filled):
initial stress 23 MPa (isotrop) at depth z = -981 m,

calculation with gravitation. stress gradient corresponding to model height.
Then: "Excavation" of the borehole and free convergence for 1309 days at constant rock temperature of 313,95 K.

Then: **Thermomechanically coupled calculation**
Start of the heater (temperature curve applied at borehole wall as direct boundary condition), temperature evolution of the heater (after COSA II report, p. 51, Fig. on p. 58):

Δt d	t (abs) d	ΔT °C	T (abs) K	KfK-prognosis (with ASYTE-KA) (optional)
0	1309	40.8	313.95	313.95
0.1	1309.1	94	367.15	327.05
0.5	1309.5	153	426.15	382.35
1	1310	173	446.15	407.75
2	1311	185	458.15	432.45
3	1312	191	464.15	446.15
5	1314	199	472.15	460.75
10	1319	213	486.15	479.95
15	1324	223	496.15	488.15
19	1328	229	502.15	495.85

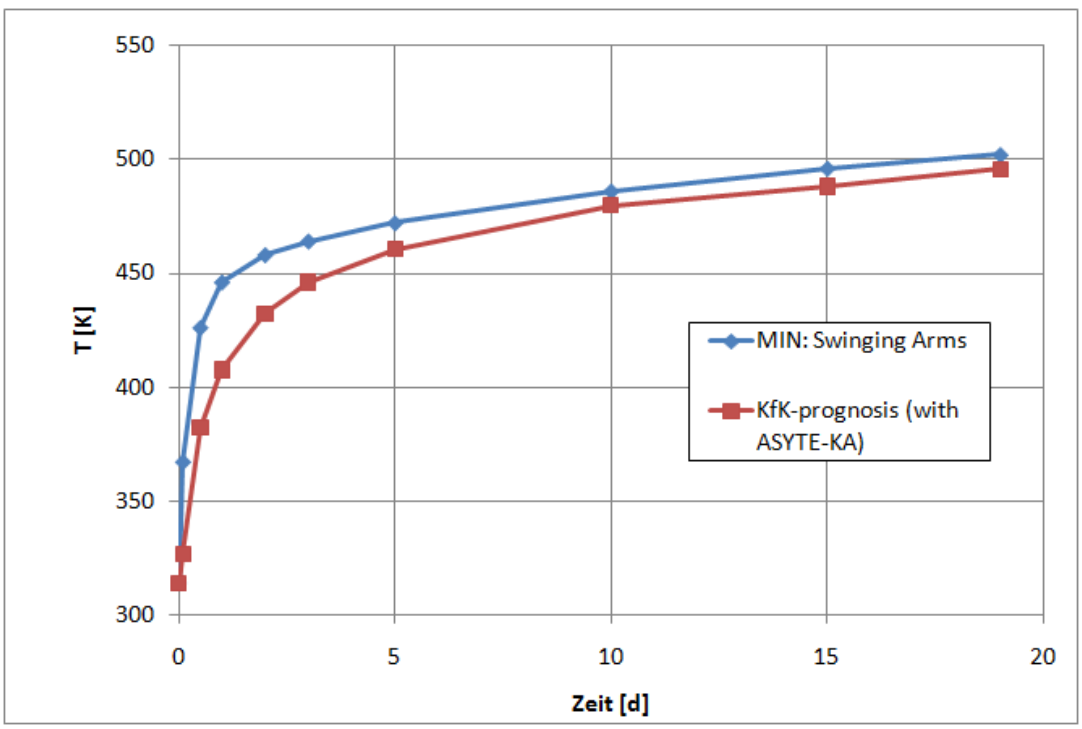

(*Zeit* = time)

Remark: The blue column is mandatory for all partners. It corresponds to the minimal measured temperatures (except after 1 day: 173 °C – this is the mean value of all 3 temperatures, because otherwise (with 163 °C) the T-curve would have an ugly kink.

The temperature evolution after the KfK prognosis is optional. It corresponds to a representative average of the calculation results of the COSA partners. Since the swinging arms have probably heated up faster then the air gap, the mismatch in the temperature measurements will be largest in the first days. Therefore, the KfK prognosis might yield more realistic values in the first days (later both curves converge).

The temperature evolution shall be assumed as equal for all three heater segments (upper, middle und lower), i.e. over the total heater height of 3.0 m. The upper and lower adjoining heater ranges shall thermally not be taken into account (set free, not applied).

The temperature evolution shall be applied directly to the salt contour as a thermal boundary condition for a time period of 19 days in the depth range from z = -979.5 m to z = -982.5 m.

After that, the temperature shall be set free, and the coupled calculation (cool-down) shall be continued until day 22.

The calculation results of the partners shall be compared. Therefore, please do not fit the model to the measured data of HFCP – take the model parameter values from the IFC fit.
The comparison with the measured convergence data of HFCP serve only as a check of the right order of magnitude of the calculation results.

Material parameters for rock salt:
Defaults according to Fig. 3 on p. 324 (COSA II report):

Thermal parameters: coefficient of thermal expansion, coefficient of thermal conductivity, specific heat capacity

Mechanical parameters: density, Young's modulus, Poisson's ratio.

The unit of the specific heat capacity is given in the COSA II report in J/(°C m³).
→ For transformation into Flac3D unit J/(°C kg) use the given density.

Density

$\rho = 2187 \ Kg/m^3$

Coefficient of thermal expansion

$\alpha = 4.2 \times 10^{-5} \quad /^0C$

Young's modulus

$E = 24 \ GPa$

Poisson's ratio

$\nu = 0.27$

Coefficient of thermal conductivity

$\lambda = a_0 + a_1T + a_2T^2 + a_3T^3 \quad W/(^0C \ m)$

$a_0 = 5.734$
$a_1 = -1.838 \times 10^{-2}$
$a_2 = 2.86 \times 10^{-5}$
$a_3 = -1.51 \times 10^{-8}$
T = Temperature in ^0C

Specific Heat Capacity

$Cp = b_0 + b_1T \quad J/(^0C \ m^3)$

$b_0 = 1.8705 \times 10^6$
$b_1 = 3.8772 \times 10^2$
T = Temperature in ^0C

Figure 3. Material data for salt

Start phase of simulation:
Defaults according to COSA II report, pp. 52 and 318:

Start of simulation at borehole excavation (18.12.1979), i.e. the free convergence in the first 3.5 years (1309 days) shall be simulated without heater influence (before start of heating).

Plots of results, quantities for evaluation:

1.) Horizontal (radial) trace outwards at z = -981 m, and vertical trace at borehole contour (over total model height), both at selected points in time: t = 0, 1, 2, 4, 8, 15, 19 and 22 days: principal stress components, displacements, creep rate, creep strain, and temperature.

2.) History variables at the borehole wall (salt contour, height: center of heated zone): displacements (borehole convergence), temperature (as a check), principal stress components.

3.) Comparison of the borehole profile with measured data, s. Fig. 6.9, COSA II report, p. 60.

(Additional remark: Take plots from presentation of Hampel at workshop 5 in Braunschweig as examples.)

APPENDIX B: DESCRIPTION ASSE SPEISESALZ LAB DATA

Comparison of Constitutive Models

Joint project I (2004-2006)

Tables and figures (translated for Sandia) taken from

A. Hampel (2006): Final scientific report to joint project I, Essenheim.

Determination of one unique salt-type specific set of model parameter values and (re-)calculation of all tests with this unique set

File number	temperature [C]	stress difference [MPa]	confining stress [MPa]
04141	30	11	0
95015	22	14.1	0
04139	30	14 / 16	20
94097	27	20	25
04138	50	20 / 15 / 20 /18 / 20	20
95008	30	37.2	15
TUC-313	30	38	3

File number	temperature [C]	deformation rate [1/s]	confining stress [MPa]
99073	30	$1*10^{-5}$	0.2
99071	30	$1*10^{-5}$	0.5
99086 + 04131	30	$1*10^{-5}$	1
99070 + 04132	30	$1*10^{-5}$	2
99088	30	$1*10^{-5}$	3
04140	*30*	$1*10^{-6}$	*1*

Creep tests (top) and strength tests (bottom) from the BGR and TUC (test 313) laboratory with rock salt of type “Speisesalz” (z2Sp) from the Asse mine in Germany. The tests were

selected and (re-)calculated by each project partner with his own constitutive model and with <u>one unique set of model parameter values</u> for this salt type. The set was determined with these calculations, see fig. 1 – 5.

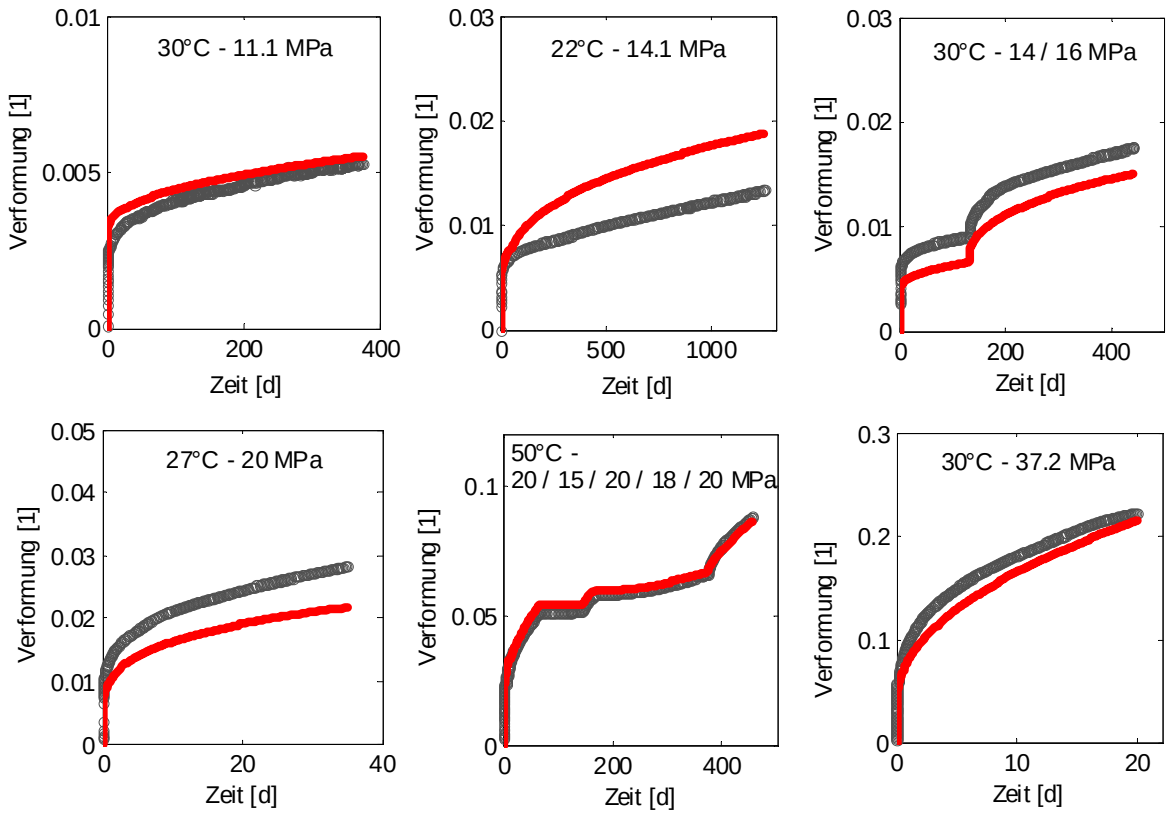

(Re-)calculations of six BGR creep tests with Asse-Speisesalz from tab. 1 with the CDM of Hampel and one unique set of CDM parameter values (red) in comparison with the test data (black). With this set of parameter values, also the tests in fig. 2 to fig. 5 were calculated. (*Verformung* = strain, *Zeit* = time)

<u>General remark:</u>

An almost perfect agreement of each simulated curve (red) with the corresponding experimental data (black) could have been achieved individually if specific parameter values would have been used for each test. However, around underground openings different and changing boundary conditions occur in different sections at the same time. Therefore, the constitutive model and the used set of parameter values must be valid for all possible boundary conditions that might occur during the simulation. Thus, it had to be shown in the project by all partners that all the different creep and strength tests can be modeled with one unique salt-type specific set of model parameter values. This is a much bigger challenge and a more crucial test of the constitutive models.

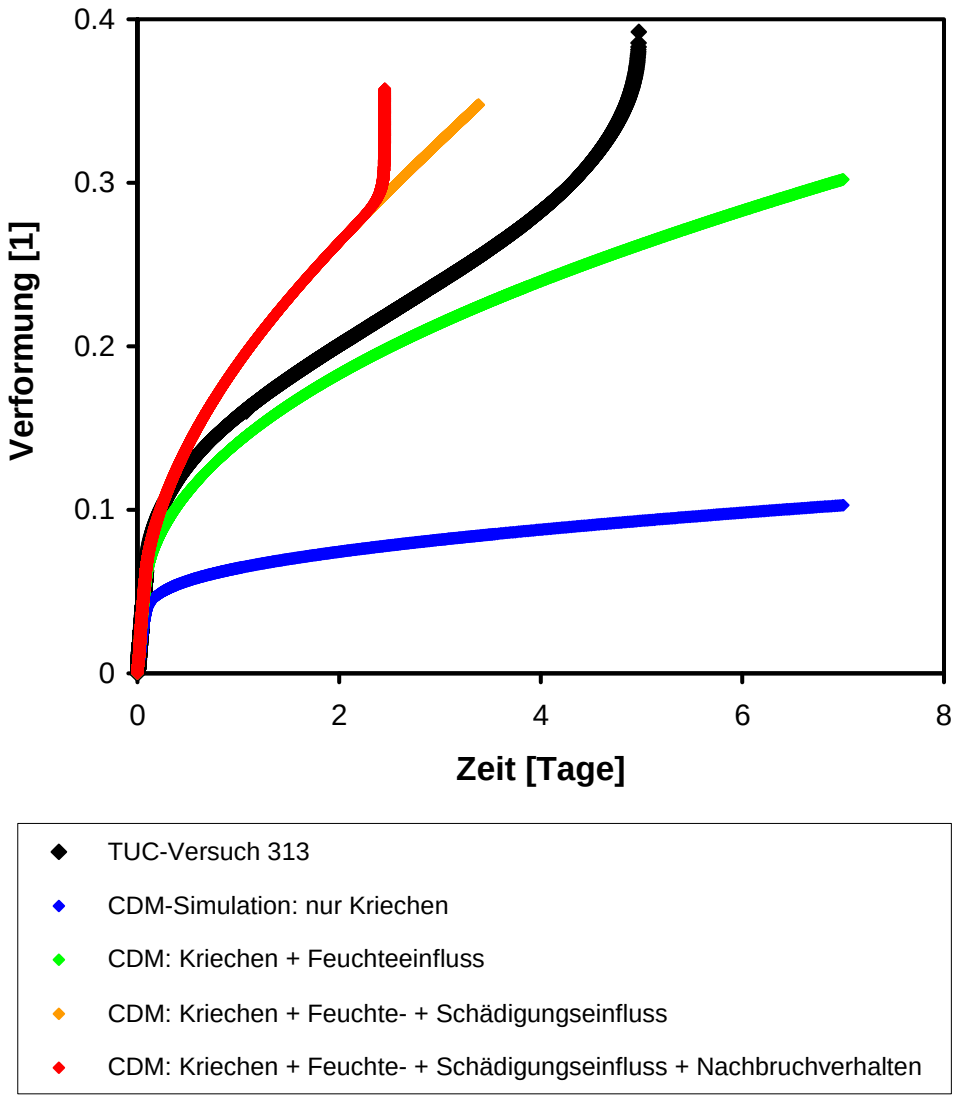

Different re-calculations of the creep failure test TUC-313 with Asse-Speisesalz (see tab. 1) with the CDM of Hampel and the unique set of CDM parameter values for this salt type (colored) in comparison with the test data (black). Blue: only creep, green: creep + humidity influence, orange: creep + humidity influence + damage influence, red: creep + humidity influence + damage influence + post-failure behavior (complete model). (*Verformung* = strain, *Zeit* = time, *Tage* = days)

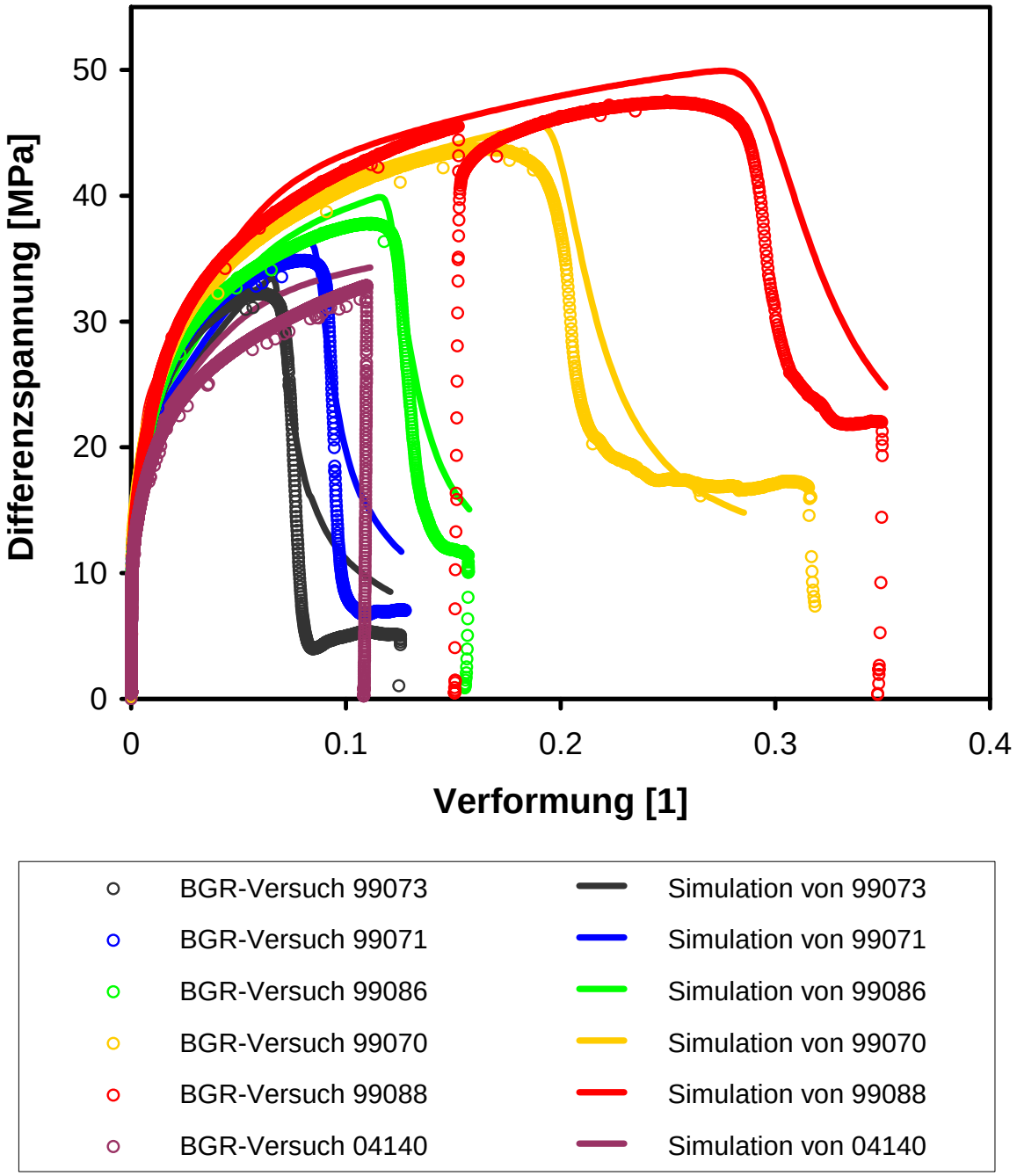

Re-calculation of six strength tests with Asse-Speisesalz with the CDM of Hampel and the unique set of CDM parameter values (lines) in comparison with the test data (symbols). The tests were performed and calculated with a different confining pressure, see tab. 1. In addition, test 04140 was performed and calculated with a different applied strain rate. (*Differenzspannung* = stress difference, *Verformung* = strain, *Versuch* = test, *von* = of)

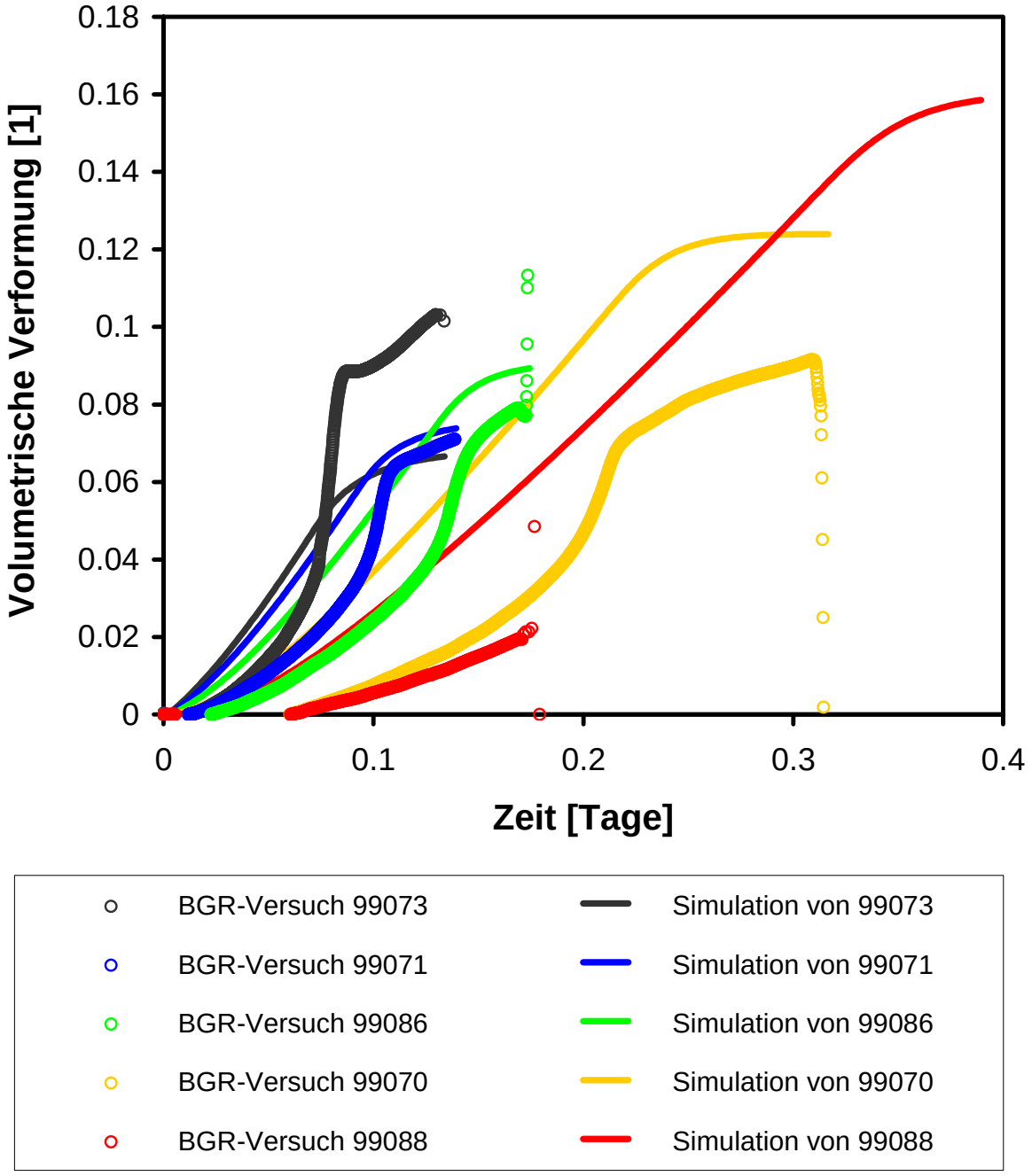

Evolution of dilatancy in the calculations with the CDM and the unique set of parameter values (lines) and in the tests with an applied strain rate of **10^{-5} 1/s** (symbols) of fig. 3. (*Volumetrische Verformung* = volumetric strain = dilatancy, *Zeit* = time, *Tage* = days)

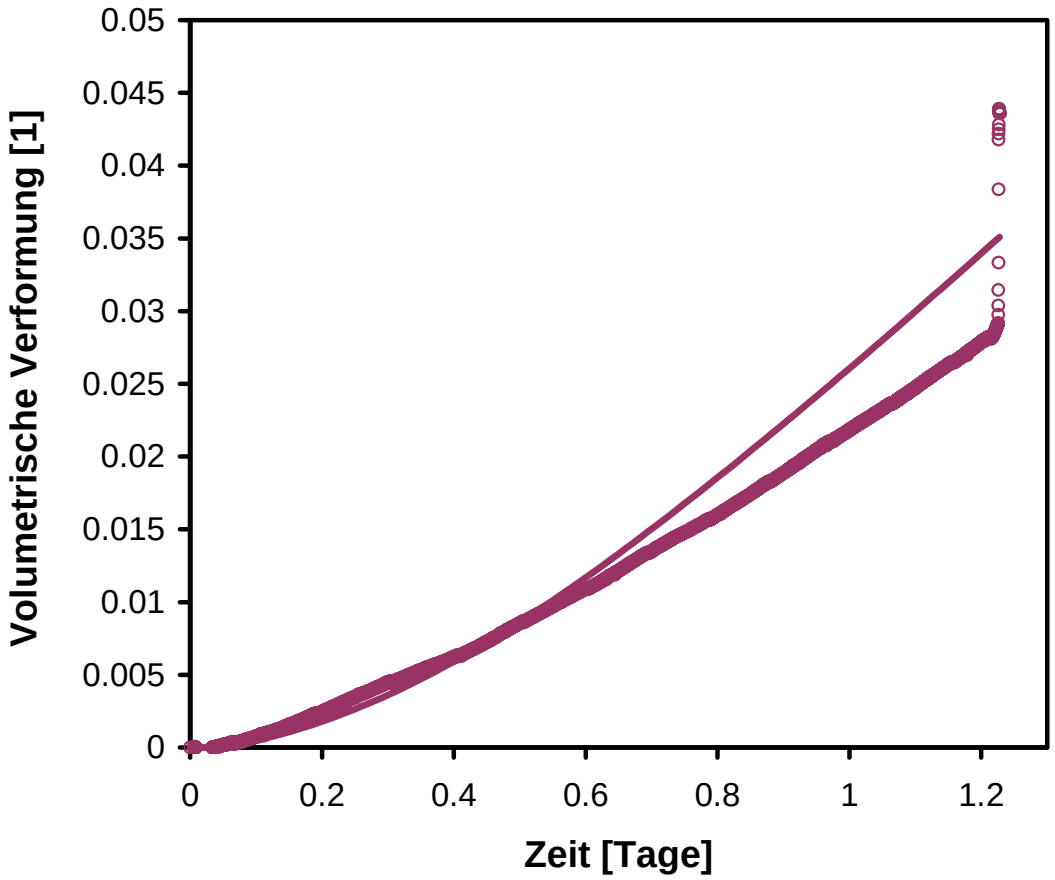

Evolution of dilatancy in the calculation with the CDM and the unique set of parameter values (line) and in the test with an applied strain rate of **10^{-6} 1/s** (symbols) of fig. 3.

File number	temperature [C]	stress difference [MPa]	confining stress [MPa]
210-01	22	16 / 19	0.5
210-02	22	16 / 22	2.5
210-03	22	16 / 25	5
210-04	22	16 / 28	10

File number	temperature [C]	strain rate [1/s]	confining stress [MPa]
210-10	22	$1*10^{-5}$	0
210-13	22	$1*10^{-5}$	0.5
210-11	22	$1*10^{-5}$	1
210-08	22	$1*10^{-5}$	2.5
210-09	22	$1*10^{-5}$	4
210-14	22	$1*10^{-5}$	7
210-15	22	$1*10^{-5}$	10
210-21	22	$1*10^{-5}$	15
210-22	22	$1*10^{-5}$	20

Creep tests (top) and strength tests (bottom) from the IfG laboratory with rock salt from the drift "EU1" in the Sondershausen mine in Germany. The tests were (re-) calculated by each project partner with his own constitutive model and with one unique set of model parameter values for this salt type that was determined with these calculations, see fig. 6 – 8.

Re-calculations of four creep tests with rock salt from the drift “EU1” in the Sondershausen

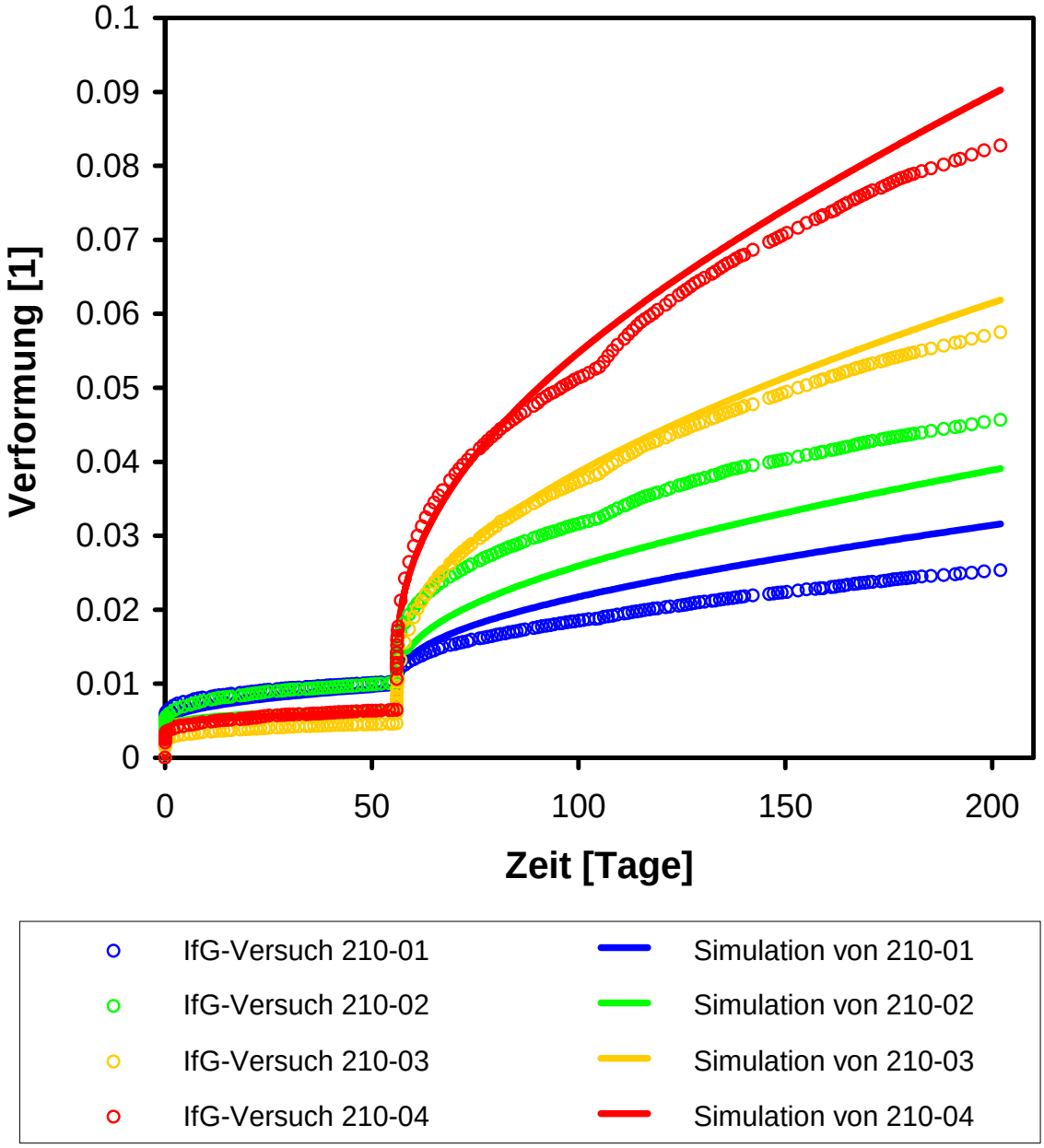

mine, see tab. 2, with the CDM of Hampel and one unique set of CDM parameter values for this salt type (lines) in comparison with the test data (symbols). (*Verformung* = strain, *Zeit* = time, *Tage* = days, *Versuch* = test, *von* = of)

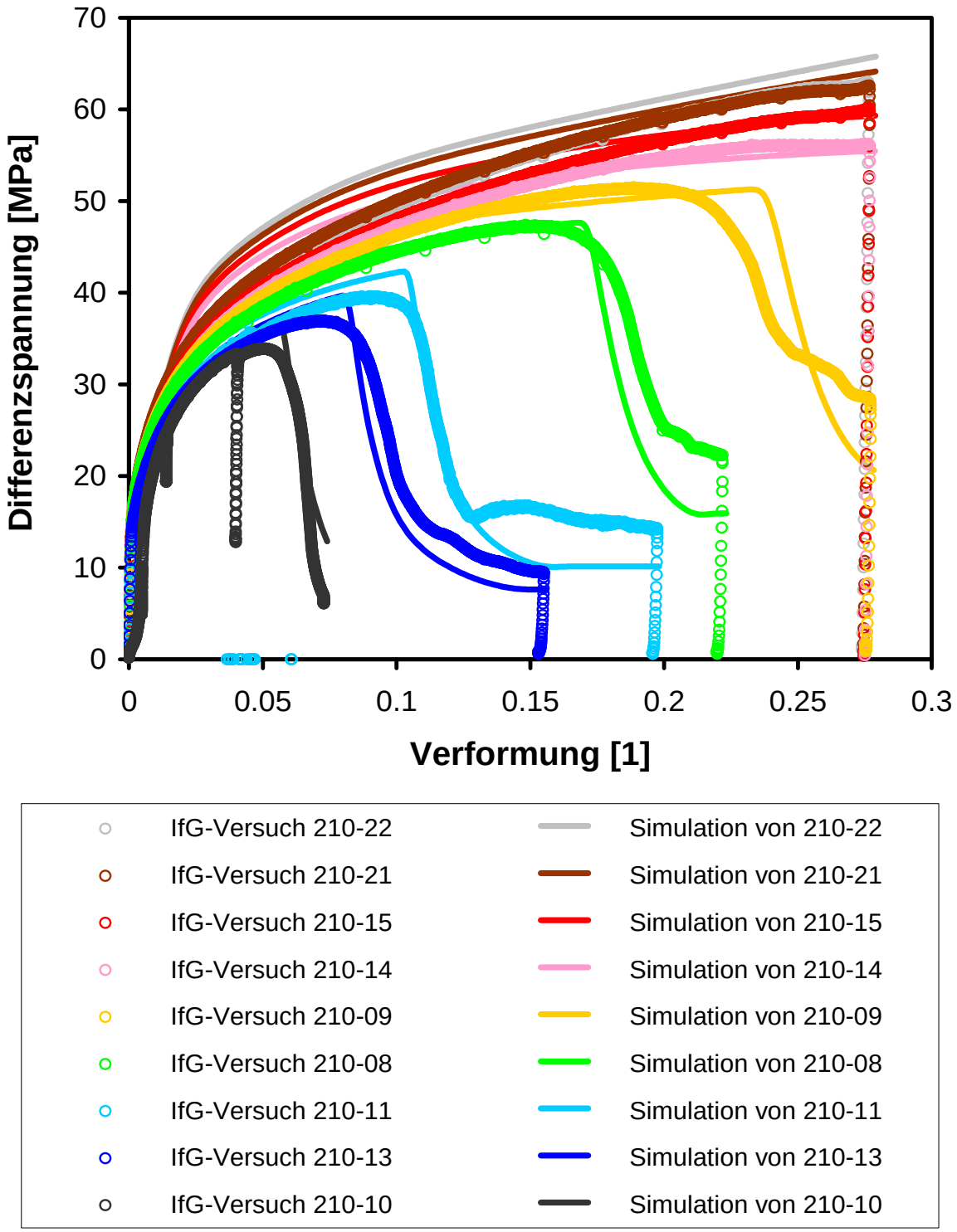

Re-calculations of nine strength tests with rock salt from the drift "EU1" in the Sondershausen mine, see tab. 2, with the CDM of Hampel and the unique set of CDM parameter values for this salt type (lines) in comparison with the test data (symbols). (*Differenzspannung* = stress difference, *Verformung* = strain, *Versuch* = test, *von* = of)

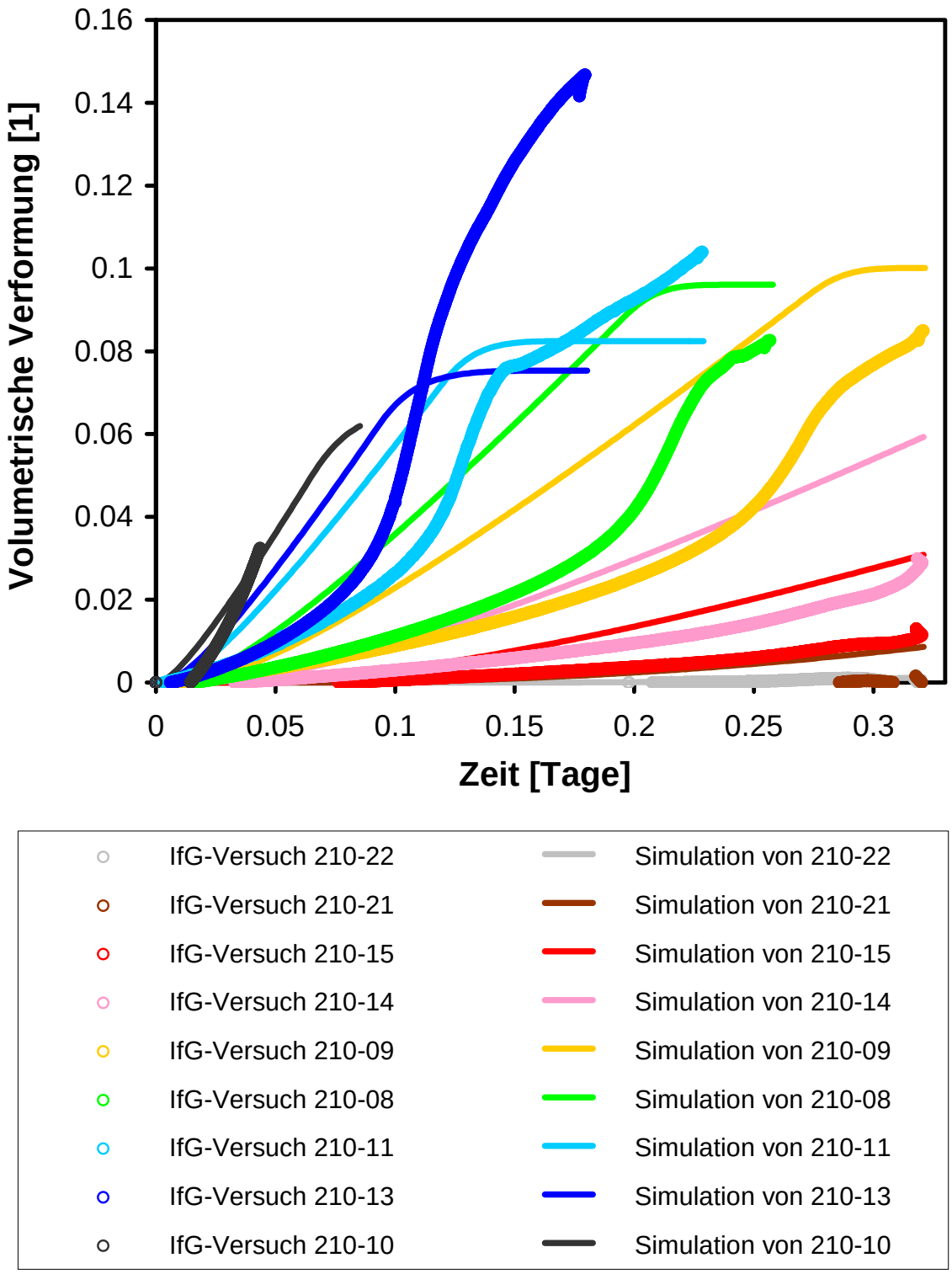

Evolution of dilatancy in the calculations with the CDM and the unique set of parameter values (lines) and in the tests (symbols) of fig. 7. (*Volumetrische Verformung* = volumetric strain = dilatancy, *Zeit* = time, *Tage* = days, *Versuch* = test, *von* = of)

APPENDIX C: RESPEC MEMORANDUM ON MD CREEP MODEL PARAMETER ESTIMATION

January 25, 2011

Mr. Tom W. Pfeifle
Sandia National Laboratories
Geomechanics Org. 06914
MS 0751
P.O. Box 5800
Albuquerque, NM 87185-5800

Dear Mr. Pfeifle:

RE: Munson-Dawson Model Parameter Estimation of Sondershausen and Asse Salt

Sandia National Laboratories (SNL), as a partner in a Joint Project with various German collaborators, is engaged in modeling the thermomechanical behavior of natural rock salt for several site-specific salt benchmark programs. Goals of the benchmarking project are to evaluate the adequacy of various salt constitutive models as well as assess the computational capabilities of the participating partners. RESPEC is assisting SNL in defining parameter estimates for the Munson-Dawson (M-D) constitutive model [Munson et al., 1989] as part of the benchmark program. Specifically, RESPEC is responsible for determining the creep constitutive model parameters to the extent possible for salt at the Asse and Sondershausen Mines. This letter describes the experimental data and results of a least-squares fitting effort performed to determine the M-D model parameters. Separate sections are provided for the evaluation of the Sondershausen (Staβfurt) and Asse (Speisesalz) rock salt following a brief introduction.

INTRODUCTION

In addition to the elastic properties, the M-D model contains 17 model parameters that must be determined before the benchmark calculations can be performed. The goal of the parameter evaluation is to determine values for the parameters of the M-D model that accurately describe the creep behavior of the salt. Brittle behavior is not described by the M-D model; hence, those tests that include brittle deformations (inelastic volumetric strains) cannot be expected to be described accurately if the brittle deformation contributes significantly to the total deformation. Further, those tests believed to exhibit significant brittle deformations cannot be used during the model fitting effort or must be given less importance.

Because the M-D model contains numerous parameters, it is not practical to determine all the parameters simultaneously using the entire database of laboratory test results. In fact, the test database is insufficient to determine all of the parameter values because of an inadequate range in test conditions to determine the change in the dependent variables with respect to the independent variables. Therefore, the technical approach used separated the problem into a few smaller and more manageable least-squares analyses; wherein, only a few parameters had to be determined from any single analysis. Parameter values are determined based on the

3824 Jet Drive, PO Box 725, Rapid City, South Dakota 57709-0725 Phone: 605.394.6400 Fax: 605.394.6456 www.respec.com

result that produces the lowest sum-of-squares error between the measured and predicted responses (either stress or strain). The steps followed to determine parameter values of the M-D model include:

1. Fit individual creep tests to determine approximate estimates for the steady-state strain rate, transient strain limit, and work-hardening/recovery parameters for each test.
2. Determine estimates for the steady-state parameters A_1, A_2, B_1, B_2, q, σ_0, n_1, and n_2 and temperature-dependent parameters Q_1 and Q_2 based on a combination of deterministic analysis, engineering experience, and least-squares fits.
3. Determine estimates for the M-D model parameters that describe the transient creep behavior based on a combination of deterministic analysis, engineering experience, and least-squares fits (α_h, β_h, α_r, β_r, K_0, c, and m).
4. Refine the model predictions through graphical and least-squares fits to the combined creep and constant strain-rate data.

The aforementioned procedure provides the general approach used to determine a set of parameters that provides a reasonable reproduction of the laboratory measurements. The final step of the processes is as much subjective as it is objective. The goal of the final step was to determine a final set of parameters with improved agreement to the data that did not deviate significantly from the trends and magnitudes for steady-state rates, transient strain limits, and rate of work-hardening and recovery established during the first three steps.

EVALUATION OF SONDERSHAUSEN SALT

SNL provided RESPEC with data from four long-term creep tests and nine constant strain-rate tests to be used in the evaluation of the Sondershausen salt. The creep data were obtained from tests performed in two stages at a constant temperature of 22° Celsius (C). During the first stage of the tests, an effective stress (difference between the axial stress and confining pressure) of 16 MPa was specified for all four tests having durations of approximately 56 days. Following completion of the first stage, the effective stresses specified were increased to either 19, 22, 25, or 28 MPa for approximately 140 days. Confining pressures were maintained constant throughout the duration of the tests and varied from 0.5 to 10.0 MPa, as identified in Table 1.

Table 1. IfG Creep Tests Conducted on Sondershausen Salt

File Number	Temperature (C)	Stress Difference (MPa)	Confining Stress (MPa)
210-01	22	16/19	0.5
210-02	22	16/22	2.5
210-03	22	16/25	5
210-04	22	16/28	10

The nine constant strain-rate tests were conducted at 22°C and an axial strain rate of 10^{-5} s^{-1}. Confining pressures ranged from a minimum of 0 MPa to a maximum of 20 MPa, as identified in Table 2. In general, the constant strain-rate tests were either terminated when the specimen failed or at an axial strain of approximately 27 percent. The postpeak response was recorded for five of the tests performed at low confining pressures (4 MPa or less). A reduction in load-bearing capacity was not evident for the four tests performed at confining pressures of 7, 10, 15, and 20 MPa.

Table 2. IfG Constant Strain-Rate Tests Conducted on Sondershausen Salt

File Number	Temperature (C)	Strain Rate (1/s)	Confining Stress (MPa)
210-10	22	1×10^{-5}	0
210-13	22	1×10^{-5}	0.5
210-11	22	1×10^{-5}	1
210-08	22	1×10^{-5}	2.5
210-09	22	1×10^{-5}	4
210-14	22	1×10^{-5}	7
210-15	22	1×10^{-5}	10
210-21	22	1×10^{-5}	15
210-22	22	1×10^{-5}	20

Because the Sondershausen salt tests were performed at a constant temperature, the M-D model parameters that define temperature dependency cannot be determined. Therefore, those parameters that define temperature dependency of the M-D model (c, Q_1, and Q_2) were assumed to have the same value as that determined for Waste Isolation Pilot Plant (WIPP) salt given by Munson et al. [1989]. Additionally, no data are available to determine recovery of work-hardened salt. Thus the M-D model recovery parameters α_r and β_r were also assumed to be the same as those of WIPP salt.

Individual fits to the creep tests were performed after subtracting elastic strains from the total strains measured in the laboratory. The elastic constants could not be readily determined from the laboratory data; therefore, the elastic properties of Sondershausen salt reported by Günther and Salzer [2007] were assumed. The first data measurement of each creep test was taken before the effective stress was applied to the Sondershausen test specimens. The second data point recorded in each data file indicated that the full axial stress difference of 16 MPa had been applied. The time entered for the second data point of each test is 1 hour. For the M-D model predictions, it was assumed that the load was applied instantaneously at time zero. Similarly, it was assumed that the effective stress was applied instantaneously when transitioning from the first stage to the second stage of the test. The recorded data provided

indicated that the desired stress level for the second stage of the creep tests was reached within 6 minutes.

Results of individual fits to the creep tests are shown in Figure 1. Based on the individual fits, estimates for steady-state strain rates, transient strain limits, and work-hardening parameters (Δ) were derived. Figure 2a illustrates the steady-state rates as a function of stress. The steady-state rates determined from the individual fits to each stage of the creep tests are in reasonable agreement with the strain rates at the end of each test stage. The steady-state creep rates are relatively slow compared to those from many other salt formations throughout the world. For example, Munson [1998] evaluated M-D model parameters for several domal salts used for the Strategic Petroleum Reserve. Munson [1998] classified the creep of domal salts as forming two distinct groups, either "soft" (fast creeping) or "hard" (slow creeping), where the difference is roughly a factor of ten for the creep rate between the two groups. The creep rate of Sondershausen salt is roughly 20 percent of "hard" salt or about 2 percent of "soft" salt.

Evaluation of the transient strain limit response as a function of stress is illustrated in Figure 2b. In general, nearly half of the transient strain exhibited during the first stage of Sondershausen creep tests occurred during the first 2 hours of the test. The initial rapid accumulation of transient strain followed by an abrupt decrease in the accumulation rate is an extremely difficult response to reproduce using the M-D model. To capture this response, the hardening parameter, Δ, is necessarily greater than commonly determined for other salts. The strain-rate change parameter, Δ, is presented as a function of stress in Figure 2c. Because no apparent trend is observed for the hardening parameter as a function of stress, the value of β_h determined for WIPP salt was assumed. The value of α_h was determined from least-squares fitting excluding the tests performed at 0.5 and 2.5 MPa confining pressures.

The data presented in Figure 1 and Figure 2 do not provide definitive information for determining both the stress dependency parameter, q, and the stress cutoff parameter, σ_0. Therefore, the stress cutoff parameter was considered deterministic and assigned the value determined for WIPP (20.57 MPa). Following the example of Munson [1998], a single scaling factor was initially applied to the leading coefficients A_1, A_2, B_1, and B_2. The scaling factor was applied to M-D parameters estimates for "hard" salt reported by Munson [1998] because of the slow creep rate exhibited by Sondershausen salt.

Further evaluation of the model led to adjustments to several of the M-D parameters with the most notable changes realized for the third mechanism. The creep rate of the third mechanism is instrumental in predicting the constant strain-rate tests. The maximum effective stress conditions of the constant strain-rate tests are considerably greater than those of the creep tests and the stress cutoff value of 20.57 MPa. The resultant parameter set determined from the evaluation is provided in Table 3. Predictions of the creep and constant strain-rate tests using the parameter estimates given in Table 3 are provided in Figures 3 and 4, respectively. In general, the M-D model predicts slower strain rates than those measured during the early minutes of each test. Nevertheless, the model provides reasonable agreement with the measured data after considering the model-predicted strains do not include the influence of dilation, damage, or humidity on the creep of salt.

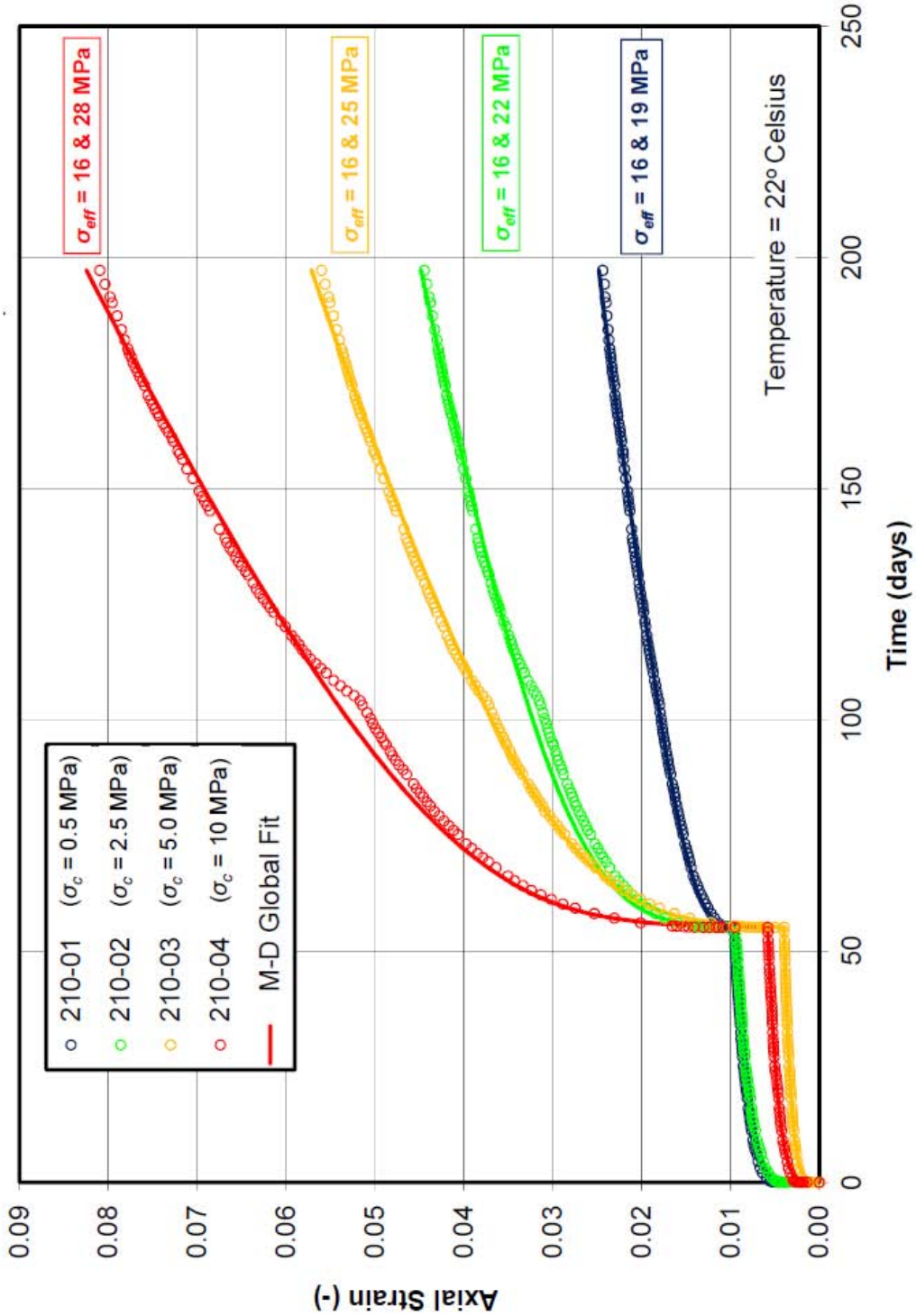

Figure 1. Comparison of Individual Fits of the M-D Model to the Creep Tests Performed on Sondershausen Salt.

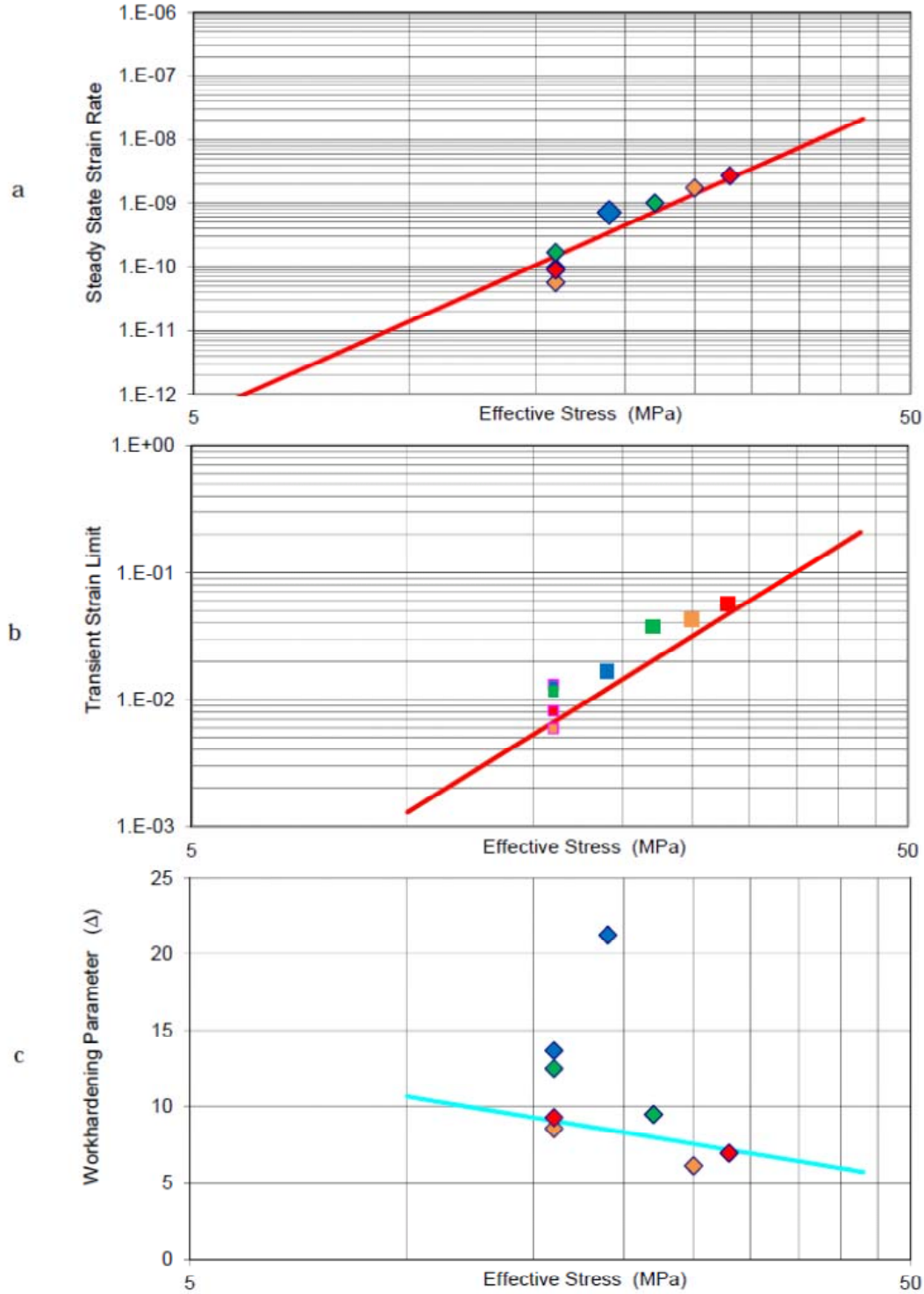

Figure 2. Stress Dependence of the Steady-State Creep Rates, Transient Strain Limit, and Work-Hardening Transient Strain-Rate Change Parameter for Sondershausen Salt.

Table 3. M-D Parameter Values for Sondershausen and Asse Salt

Parameter	Units	Sondershausen	Asse
A_1	sec^{-1}	3.020×10^{21}	5.741×10^{17}
A_2	sec^{-1}	3.480×10^{11}	2.353×10^{11}
B_1	sec^{-1}	2.230×10^{9}	1.180×10^{5}
B_2	sec^{-1}	9.890×10^{-4}	5.881×10^{-4}
Q_1/R	K	12,589	12,589
Q_2/R	K	5035.5	5035.5
n_1		5.5	5.5
n_2		5.0	5.0
q		1,500	4,450
σ_0	MPa	20.57	20.57
m		3.49	3.0
K_0		2.480×10^{6}	925
c	K^{-1}	0.009198	2.706×10^{-2}
α_h		–10.88	–12.293
β_h		–7.738	–8.518
α_r		0.58	0.58
β_r		0.0	0.0
Elastic Properties	**Units**	**Sondershausen**	**Asse**
E	MPa	24,900	25,000
ν		0.25	0.27
μ	MPa	9,960	9,850

EVALUATION OF ASSE SALT

The dataset to be used for the fitting effort of the Asse salt provided to RESPEC by SNL included seven creep tests and six constant deformation rate tests. Five single-stage and two multistage creep tests at temperatures ranging from 22 to 50°C were performed on the "Asse-Speisesalz" salt. Two of the single-stage creep tests were unconfined and a third test was subjected to a 3 MPa confining pressure. These three single-stage tests had limited value and were used with reservation in the fitting effort because they were performed at confining pressures too low to suppress dilation. The other two single-stage creep tests were performed at nominally the same temperature (27°C and 30°C) with the effective stress of the lower

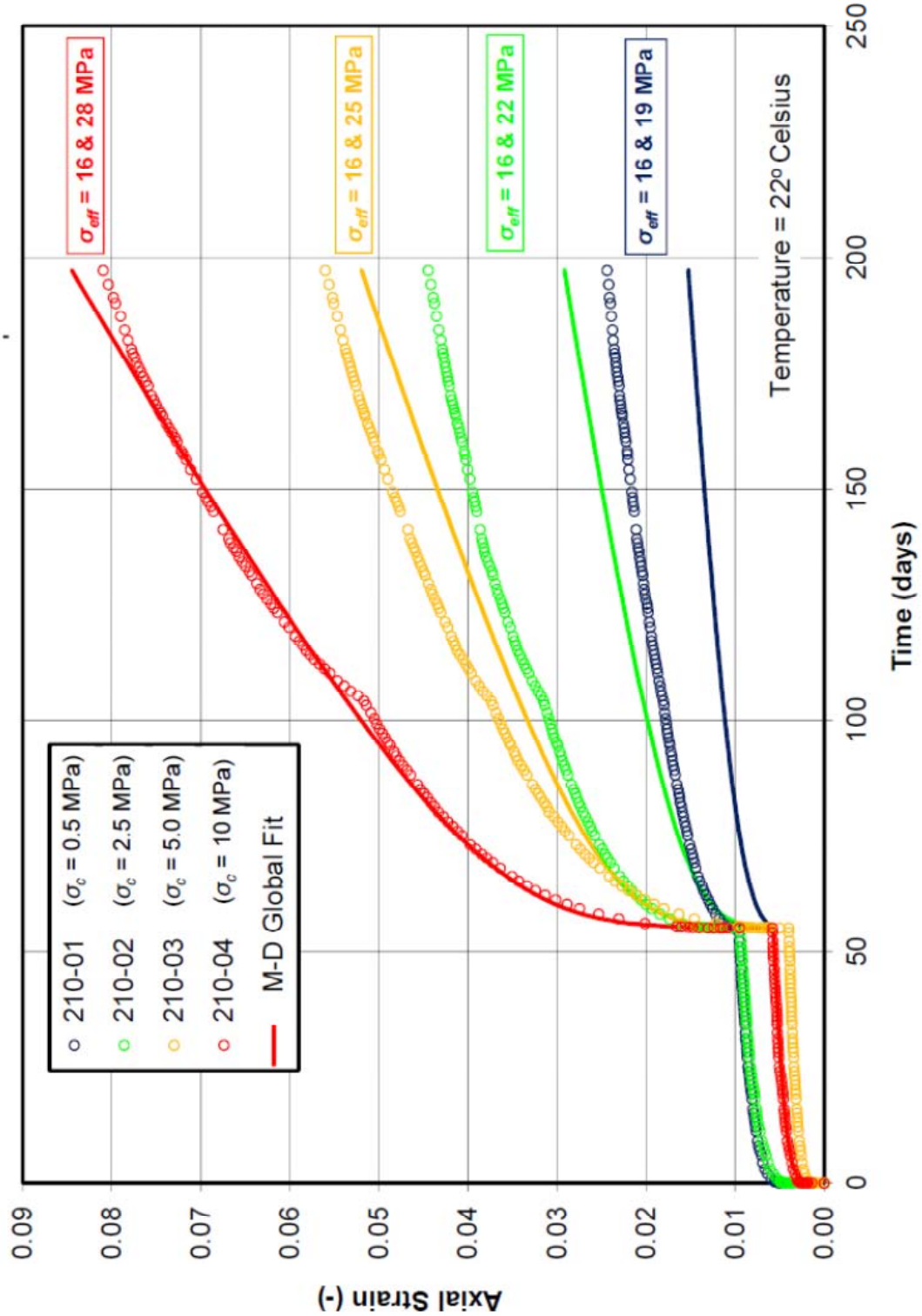

Figure 3. M-D Model Global Fit Predictions of Creep Tests Performed on Sondershausen Salt.

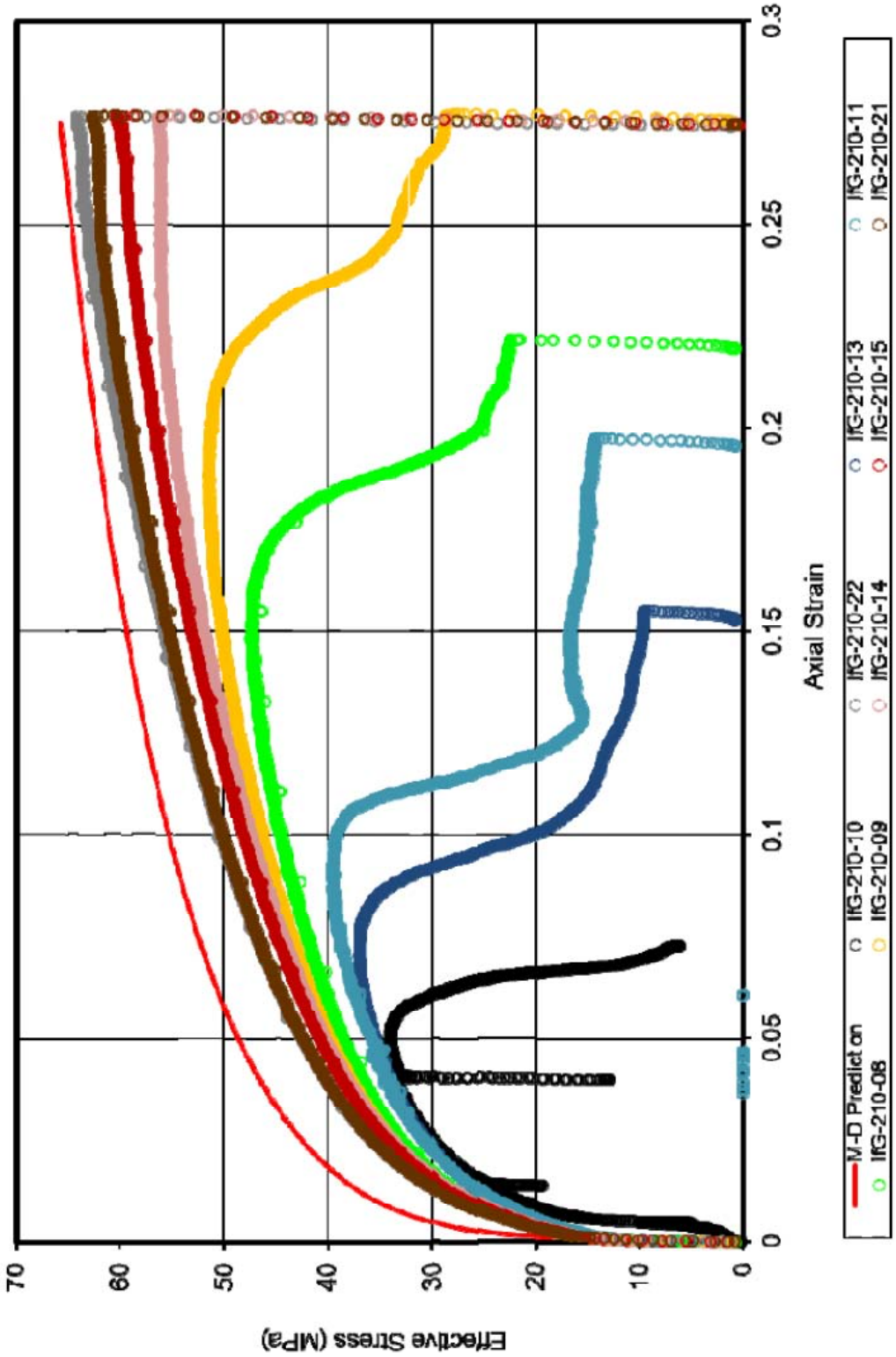

Figure 4. M-D Model Global Fit Prediction of Constant Strain-Rate Tests on Sondershausen Salt.

temperature test performed at 14.1 MPa and the higher temperature test performed at 37.2 MPa. One of the multistage creep tests included five stages with three stress increases and two stress drops at 50°C. The other multistage test was performed at 30°C and included a stress increase from 14 MPa to 16 MPa. Table 4 identifies the conditions of the creep tests performed on Asse salt which ranged in duration between 5 and 1,250 days.

Table 4. BGR and TUC Creep Tests Conducted on Asse Salt

File Number	Temperature (C)	Stress Difference (MPa)	Confining Stress (MPa)
04141	30	11	0
95015	22	14.1	0
04139	30	14/16	20
94097	27	20	25
04138	50	20/15/20/18/20	20
95008	30	37.2	15
TUC-313	30	41	3

The six constant strain-rate tests were conducted at 30°C with five of the tests conducted using an axial strain rate of 10^{-5} s^{-1} and one using a strain rate of 10^{-6} s^{-1}. Confining pressures ranged from a minimum of 0.2 MPa to a maximum of 3.0 MPa, as identified in Table 5. Because of the low confining pressures used for these tests, they were not included in the fitting effort but aided in definition of the creep rate of salt at high effective stresses. The constant strain-rate tests appear to have been terminated when the specimens failed.

Table 5. BGR Constant Strain-Rate Tests Conducted on Asse Salt

File Number	Temperature (°C)	Deformation Rate (1/s)	Confining Stress (MPa)
99073	30	1×10^{-5}	0.2
99071	30	1×10^{-5}	0.5
99086 + 04131	30	1×10^{-5}	1
99070 + 04132	30	1×10^{-5}	2
99088	30	1×10^{-5}	3
04140	30	1×10^{-6}	1

Individual fits to all the creep tests, as well as individual fits to each stage of the multistage tests, were performed after subtracting elastic strains from the total strains measured in the

laboratory. Because the elastic constants could not be readily determined from the laboratory data, the elastic properties of Asse salt reported by Lux and Eberth [2007] were assumed. All of the creep data included frequent measurements during the load application that was simulated by the M-D model during the fitting effort with the exception of Test *09015*. Test *09015* did not include load application data but the second measurement recorded in the data file indicates that the full axial load had been applied within 15 minutes of the start of the test. For the M-D model predictions of this test, it was assumed that the load was applied instantaneously at time zero. Irregularities were apparent during the load application of the test identified as *04139*. This test was held at an effective stress of about 0.5 MPa for about 5 days before the stress was increased to 14 MPa. During this 5-day period, an anomalous increase of about 0.25 percent strain was recorded. This strain was included in the total strain during the fitting effort for consistency. Results of individual fits to the creep tests are shown in Figure 5. Individual estimates for steady-state strain rates, transient strain limit, and the hardening parameter are provided in Figure 6.

Least-squares fitting to the steady-state rates indicated that the Asse salt creeps at about 15 percent the rate of "hard" salt. Further, the initial parameters determined for the fitting process indicated that the values for the parameters n_2, and m, did not deviate significantly from those of WIPP salt. Therefore, the WIPP values were retained for these two parameters. Because of the limited temperature and stress range of the tests, the temperature dependency parameters Q_1 and Q_2 as well as the stress exponent parameter n_1, could not be uniquely identified and were assumed to have the same values as that determined for WIPP salt.

Efforts to evaluate the recovery parameters α_r and β_r using the strain data from the five-stage creep test with stress drops were unsuccessful. The M-D model did not predict that the salt was sufficiently hardened before the stress drops and/or the recovery is predicted to be more rapid than the data indicate. As a result, the M-D model predicts a relatively rapid transition to the steady-state strain rate at the reduced effective stresses of 15 and 18 MPa, as illustrated in Figure 5.

The parameters A_1, A_2, B_1, B_2 q, c, K_0, α_h and β_h were determined from graphical and least-squares fitting. In addition to the constraints discussed above, a scaling factor was applied to the M-D parameters estimates for "hard" salt to maintain the same proportionality between the parameters A_1 and A_2. A separate scaling factor was applied to B_1 and B_2 to increase the contribution of the third mechanism and provide a better prediction of constant strain-rate tests and creep tests performed at effective stresses of 37.2 MPa and 41 MPa.

The resultant parameter set determined from the evaluation of the Asse salt is provided in Table 3. Predictions of the creep and constant strain-rate tests using the parameter estimates given in Table 3 are provided in Figures 7 and 8, respectively. The model predictions of the test that exhibited tertiary behavior (TUC-313) are provided in Figure 9. In general, the M-D model predicts slower strain rates than those measured during the early minutes of each test. Nevertheless, the model provides reasonable agreement with the measured data after considering the model-predicted strains do not include the influence of dilation, damage, or humidity on the creep of salt.

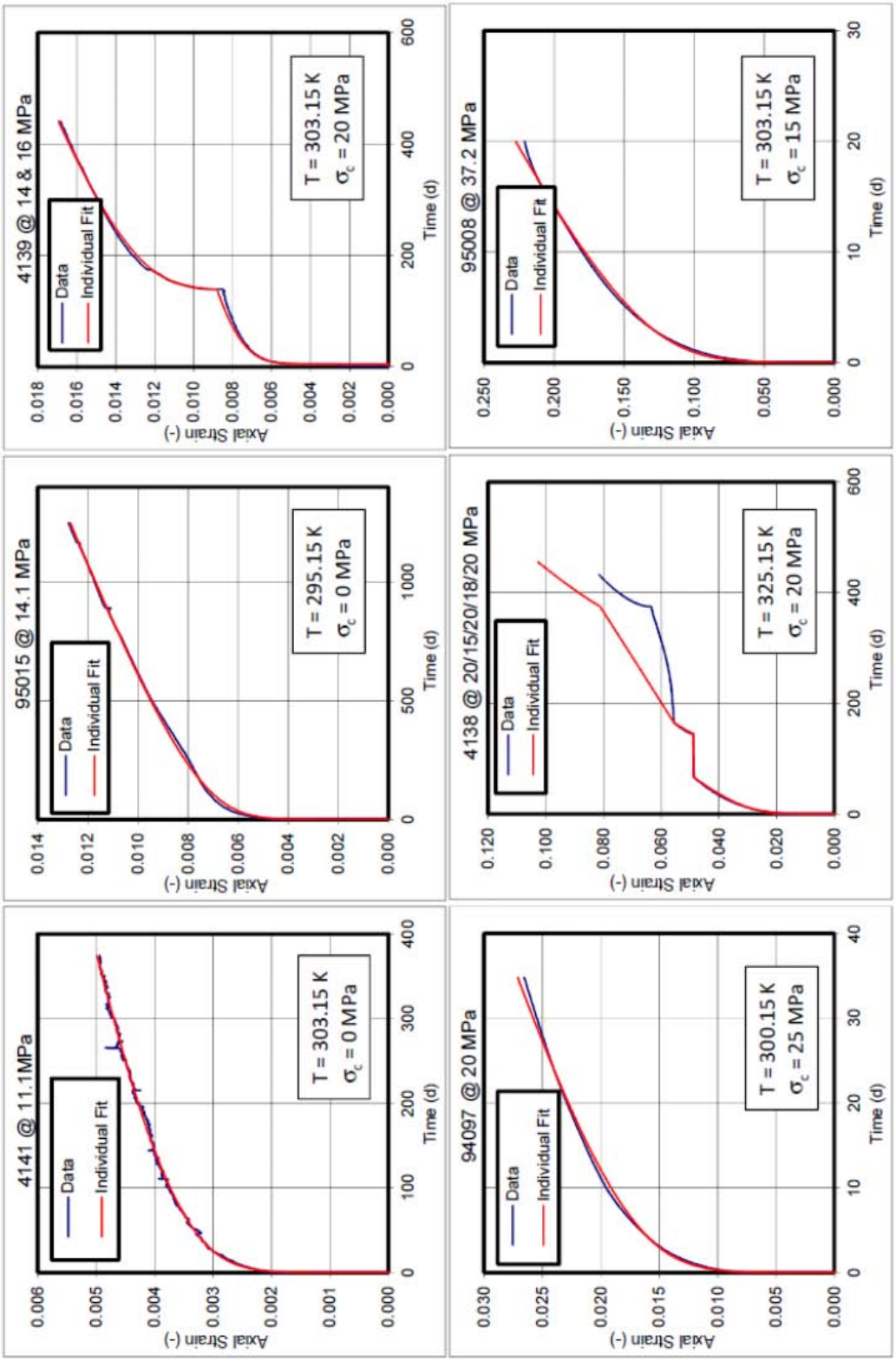

Figure 5. Comparison of Individual Fits of the M-D Model to the Creep Tests Performed on Asse Salt.

RSI-1989-11-006

a

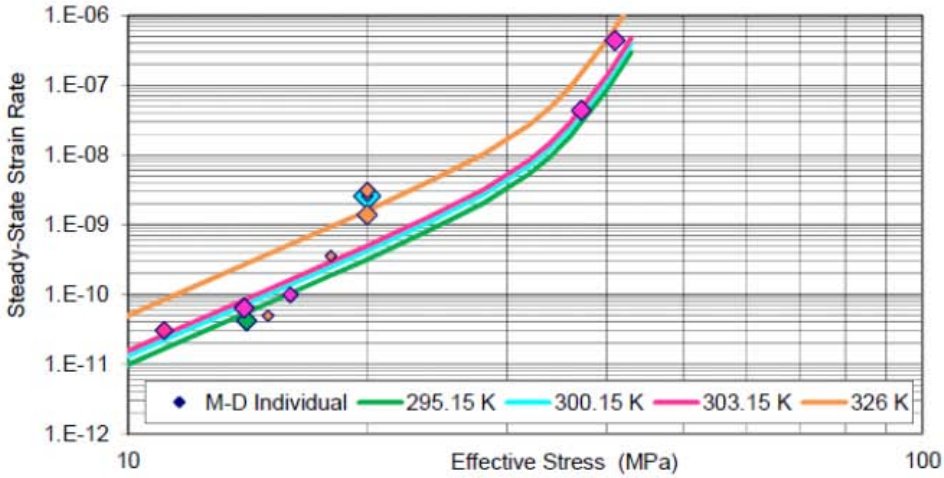

b

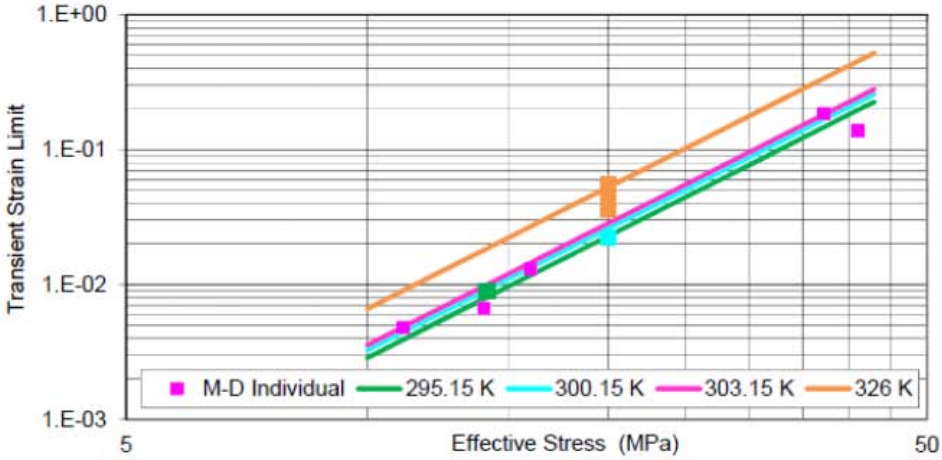

c

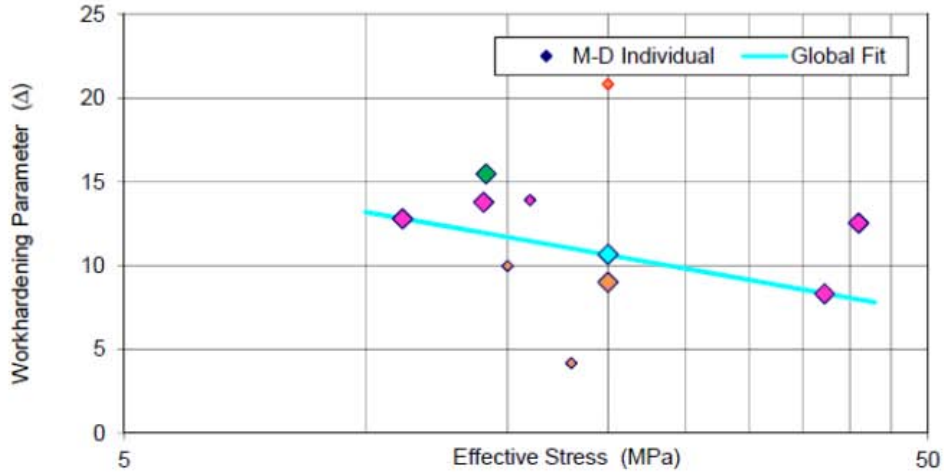

Figure 6. Stress Dependence of the Steady-State Creep Rates, Transient Strain Limit, and Work-Hardening Transient Strain-Rate Change Parameter for Asse Salt.

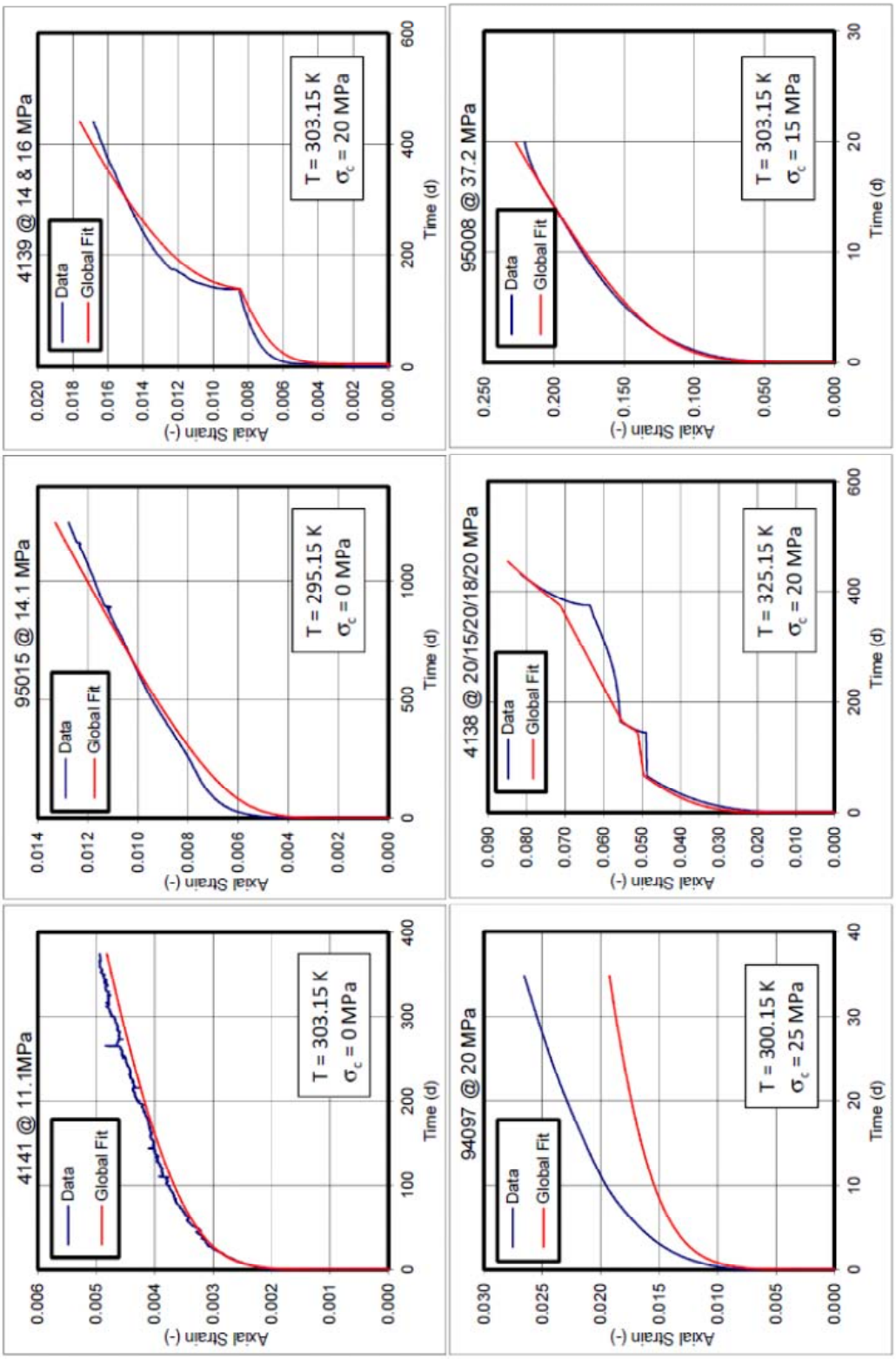

Figure 7. M-D Model Global Fit Predictions of Creep Tests Performed on Asse Salt.

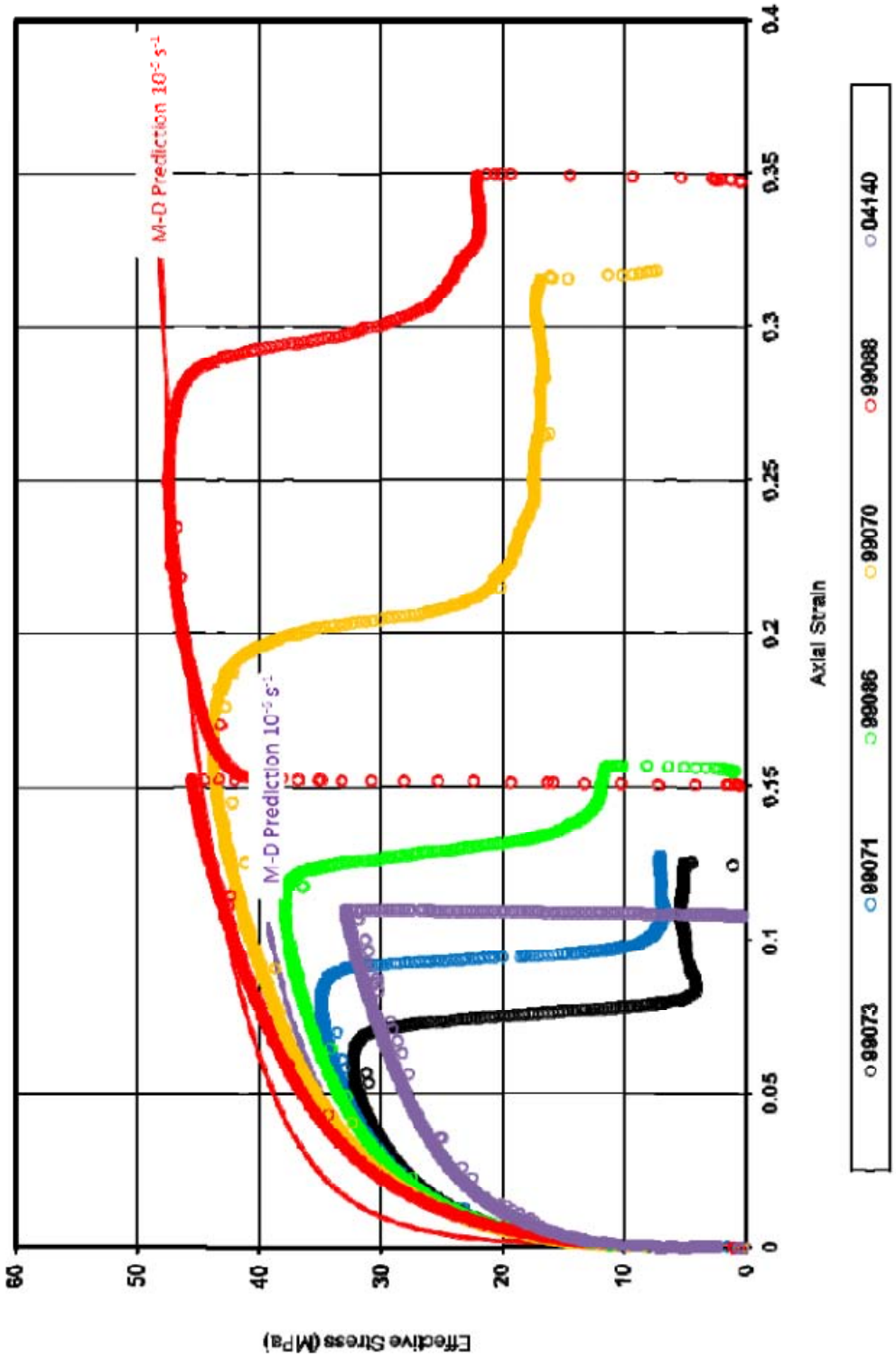

Figure 8. M-D Model Global Fit Prediction of Constant Strain-Rate Tests on Asse Salt.

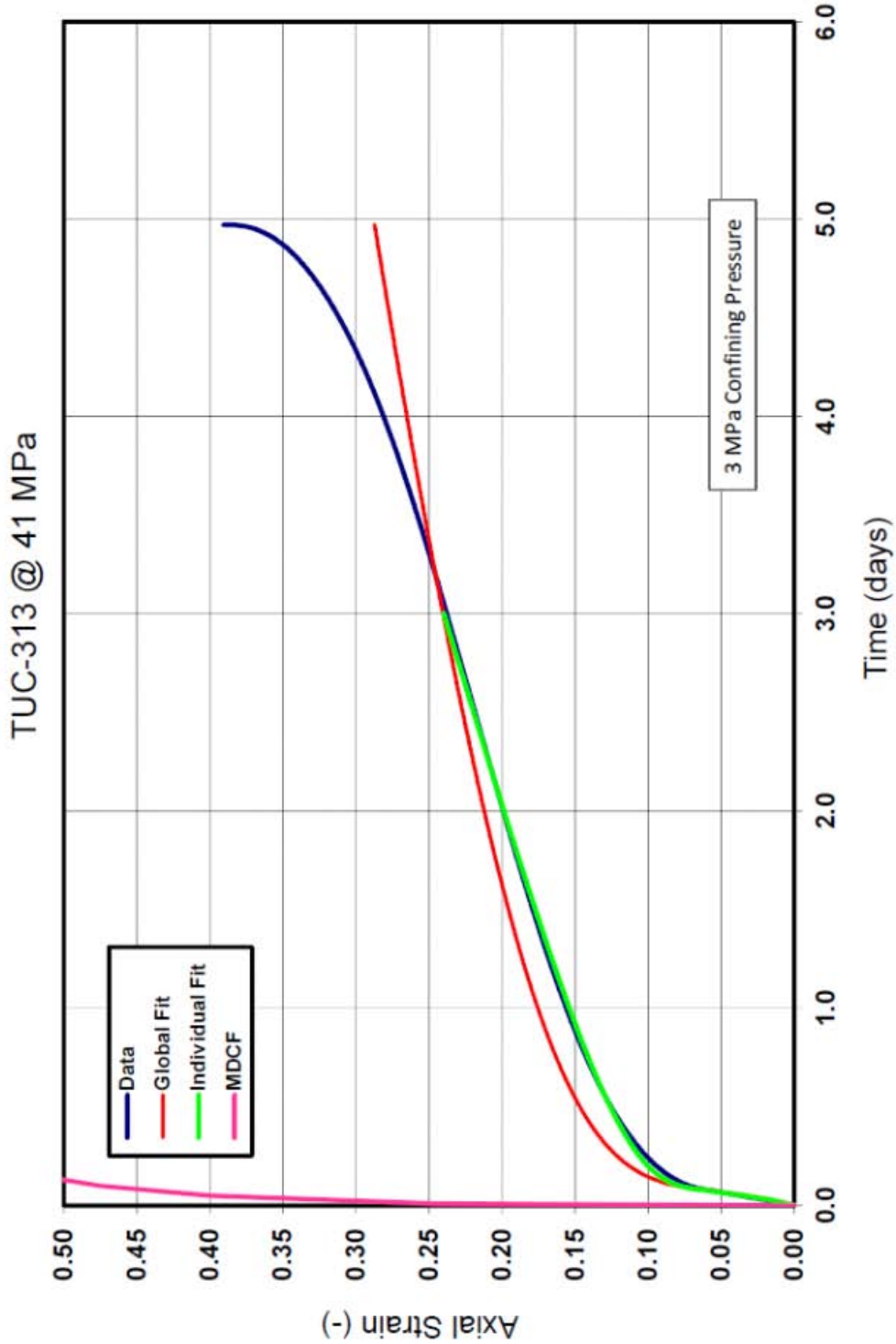

Figure 9. M-D and MDCF Model Predictions of Test TUC-313 on Asse Salt.

MULTIMECHANISM COUPLED FRACTURE (MDCF) CONTINUM DAMAGE MODEL PREDICTIONS

Following determination of the material parameters of the M-D model, they were combined with Multimechanism Coupled Fracture (MDCF) model parameters determined for the WIPP site [Chan, 1996]. The prediction of the creep tests using the MDCF model was not very favorable, as illustrated in Figures 10 and 11 for the Sondershausen salt and Asse salt, respectively. Hence, model fitting and perhaps model revision are recommended before the MDCF model can be used for the benchmark problem.

REFERENCES

Chan, K. S., 1996. *Final Development of the Multimechanism Deformation Coupled Fracture (MDCF) Constitutive Model*, Monthly Technical Report No. FY '96–2, Monthly Progress Report for Southwest Research Institute, Contract AQ-1458 with Sandia National Laboratories, February.

Munson, D. E., 1998. *Analysis of Multistage and Other Creep Data for Domal Salt,* SAND98-2276, Sandia National Laboratories, Albuquerque, NM.

Munson, D. E., A. F. Fossum, and P. E. Senseny, 1989. *Advances in Resolution of Discrepancies Between Predicted and Measured In Situ WIPP Room Closures,* SAND88-2948, Sandia National Laboratories, Albuquerque, NM.

Günther, R.-M. and K. Salzer, 2007. "A Model for Rock Salt, Describing Transient, Stationary, and Accelerated Creep and Dilatancy," *Proceedings, 6th Conference on the Mechanical Behavior of Salt*, Hannover, Germany, May 22–25, M. Wallner; K. H. Lux; W. Minkley; and H. R. Hardy, Jr. (eds.), Taylor & Francis Group, London, England, pp. 109–117.

Lux, K.-H. and S. Eberth, 2007. "Fundamental and First Application of a New Healing Model for Rock Salt," *Proceedings, 6th Conference on the Mechanical Behavior of Salt*, Hannover, Germany, May 22–25, M. Wallner; K. H. Lux; W. Minkley; and H. R. Hardy, Jr. (eds.), Taylor & Francis Group, London, England, pp. 129–138.

Sincerely,

Kerry L. DeVries

Kerry L. DeVries
Manager, Geomechanics

KLD:krl

cc: Project Central File 1989 — Category A

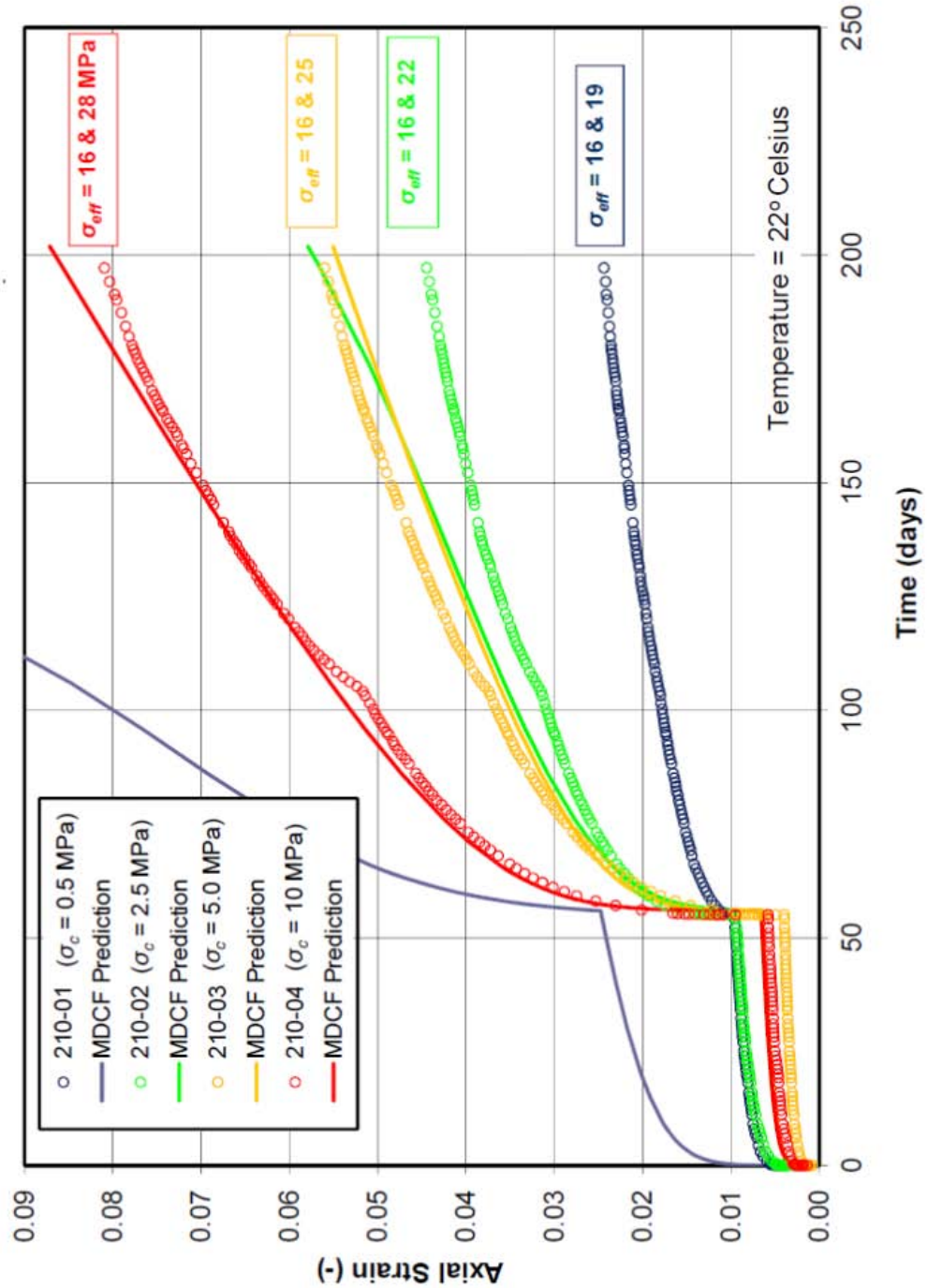

Figure 10. MDCF Model Prediction of Creep Tests on Sondershausen Salt.

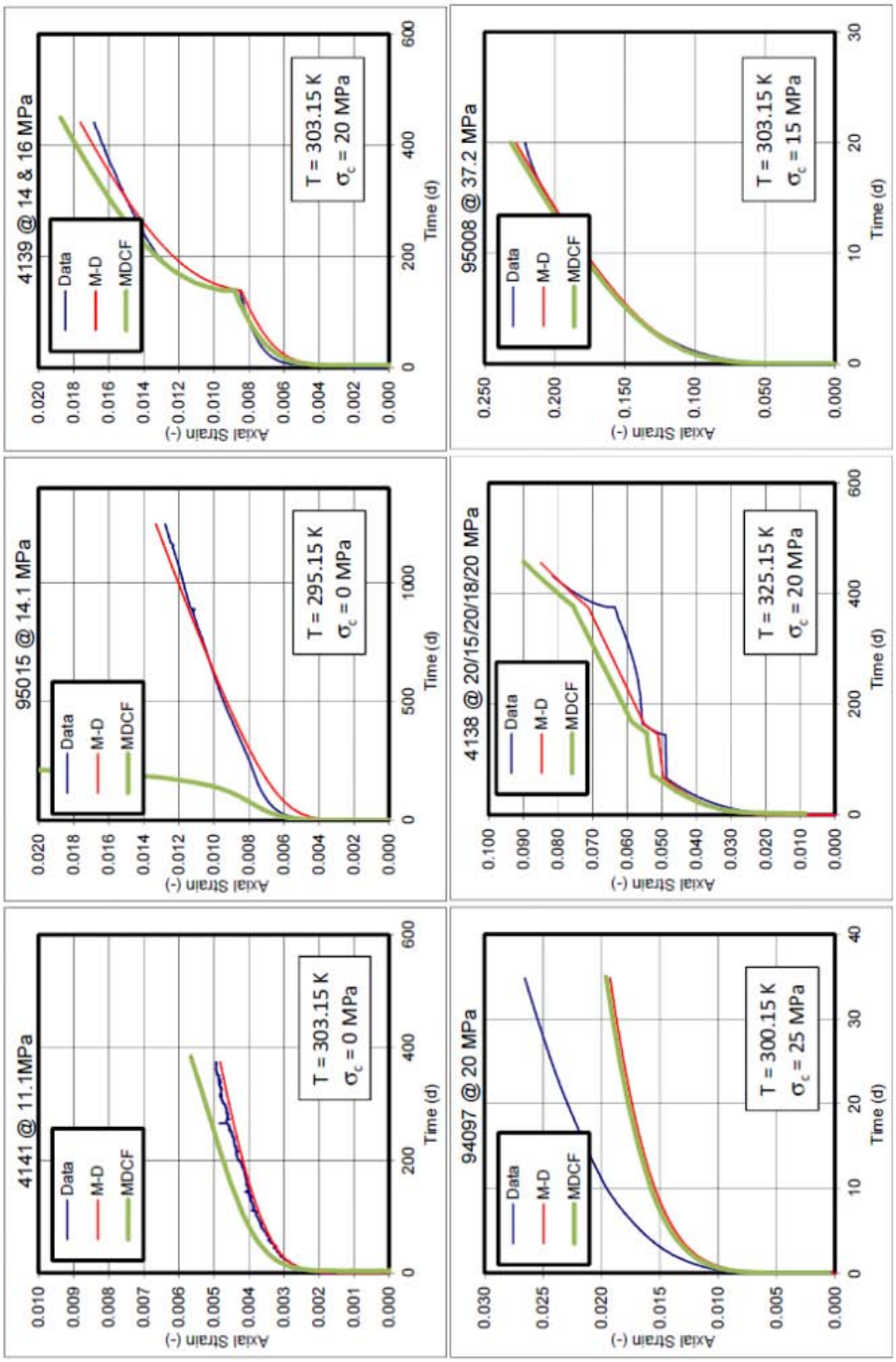

Figure 11. MDCF Model Prediction of Creep Tests on Asse Salt.

DISTRIBUTION

Federal Agencies

1 US Department of Energy
Office of Fuel Cycle Research and Development
Attn: Jeffrey R Williams
NE-52/Forrestal Building
1000 Independence Ave. SW
Washington DC 20585

3 US Department of Energy
Attn: William Boyle
Prasad Nair
Tim Gunter
DOE-NE
232 Energy Way
North Las Vegas, NV 89030

1 Waste Isolation Pilot Plant
Attn: Roger Nelson
U.S. Department of Energy
4021 National Parks Highway
Carlsbad, NM 88220

Laboratories/Corporations

2 Argonne National Laboratory
Attn: M. Nutt
9700 S. Cass Avenue
Argonne, IL 60439

1 Los Alamos National Laboratory
Attn: Ned Elkins
115 N. Main
Carlsbad, NM 88221

1 Chandrika Manepally
Center for Nuclear Waste Regulatory Analyses
Geosciences and Engineering Division
Southwest Research Institute
6220 Culebra Road
San Antonio, TX 78238

Foreign Addresses

1 Dr. Andreas Hampel
Grünberger Str. 56
DE – 55129 Mainz
Germany

4 Institut für Gebirgsmechanik GmbH
Attn: Dr Wolfgang Minkley
Dr Till Popp
Dr Ralf-Michael Günther
Dr Klaus Salzer
Friederikenstrasse 60
DE – 4279 Leipzig
Germany

1 Forschungszentrum Karlsruhe (FZK) GmbH
Attn: Mrs Alexandra Pudewills
Institut für Nukleare Entsorgung (INE)
Weberstrasse 5
DE – 76021 Karlsruhe
Germany

1 Forschungszentrum Karlsruhe (FZK) GmbH
(PTKA-WTE)
Attn: Dr Walter Steininger
Postfach 3640
DE – 76344 Eggenstein-Leopoldshafen
Germany

1 Karlsruhe Institute of Technology (KIT)
Attn: Mr Michael Bühler
Hermann-von-Helmhotz-Platz 1
DE – 76344 Eggenstein-Leopoldshafen
Germany

5 Leibniz Universität Hannover
Institut für Geotechnik
Attn: Dr Reinhard Rokahr
Mr Kurt Staudtmeister
Mr Dirk Zapf
Mr Bastian Leuger
Mr Savas Yildirim
Welfengarten 1
DE – 30167 Hannover
Germany

3 Technische Universität Braunschweig
Institut für Grundbau und Bodenmechanik
Attn: Dr Joachim Stahlmann
Mr Christian Missal
Mr Andreas Gährken
Beethovenstraße 51b
DE – 38106 Braunschweig
Germany

5 Clausthal University of Technology
Institut for Mineral and Waste Processing, Waste Disposal and Geomechanics
Attn: Dr Karl-Heinz Lux
Dr Uwe Düsterloh
Mr Oleksandr Dyogtyev
Mr Kai Herchen
Mr Ralf WOLTERS
Adolph-Roemer-Straße
DE – 38678 Clausthal-Zellerfeld
Germany

Internal

5	MS0840	J. G. Argüello	01525	
1	MS0840	J. Pott	01525	(electronic copy)
1	MS0824	J. E. Bean	01525	(electronic copy)
1	MS0840	J. E. Bishop	01525	(electronic copy)
1	MS0824	J. F. Holland	01525	(electronic copy)
1	MS0840	P. Newell	01525	(electronic copy)
1	MS0828	J.S. Rath	01525	(electronic copy)
1	MS0380	J. Jung	01542	(electronic copy)
1	MS0380	M. W. Heinstein	01542	(electronic copy)
1	MS1395	C. D. Leigh	06212	(electronic copy)
1	MS0747	D. J. Clayton	06223	(electronic copy)
1	MS1370	R. J. MacKinnon	06224	(electronic copy)
1	MS0701	M. C. Walck	06900	(electronic copy)
1	MS0751	F. D. Hansen	06910	(electronic copy)
1	MS0751	B.Y. Park	06914	(electronic copy)
1	MS0751	S. R. Sobolik	06914	(electronic copy)
1	MS0899	Technical Library	09536	(electronic copy)

Sandia National Laboratories